Reaction Dynamics of Some Pendant Arm Macrocycles

by

Jeremy Lucas B. Sc. (Hons.) (Adelaide)

Thesis submitted for the degree of

Doctor of Philosophy

in

The University of Adelaide

(Faculty of Science)

Department of Chemistry

December, 1994

Contents

ERRATA

Page 29, line 14 - comma required after 'solvents'

Page 30, line -11 - comma required after 'however'

Page 75, Table 4.6 - within the table there should be footnotes ***a***, ***b*** and ***c*** after $[Na(TMEC14)]^+$, $[Na(TMEC12)]^+$ and $[Na(THEC14)]^+$, respectively. The caption at the bottom of the table should then read: '^{a}This work. ^{b}Ref. 17. ^{c}Ref. 18.'

Page 78 - reference 18 has been omitted and should read:

'18 S. Whitbread and S. F. Lincoln, unpublished material.'

Page 94, Table 5.5 - footnote ***a*** should be removed, and footnotes ***b***, ***c*** and ***d*** should become footnotes ***a***, ***b*** and ***c***, respectively.

Page 109, Figure 7.2 - in the caption, precipitation of $Cu(OH)_2$ occurs at about 0.43 cm^3 (as per graph) and not 4.3 cm^3.

Statement

To the best of my knowledge and belief this thesis contains no material which has been submitted for any other degree or diploma in any university, nor any material previously published or written by another author except where due reference is made in the text.

I consent to making this thesis available for copying or loan.

Signed

Jeremy Lucas

December, 1994

Acknowledgements

I would like to extend my very sincere gratitude to my supervisor, Professor Stephen Lincoln for his inestimable help, support and encouragement throughout this project.

I would also like to thank my fellow co-workers, Phil Clarke, Ramesh Dhillon, Samer Madbak and especially my good friend and co-worker Ashley Stephens, for their invaluable advice, help and support throughout.

Finally, I would like to thank my parents for their constant interest and encouragement, not only during the course of this study, but throughout the last twenty five years.

Abbreviations

The following abbreviations have been used in this study:

18-crown-6	1,4,7,10,13,16-hexaoxacyclooctadecane
dibenzo-18-crown-6	2,3,11,12-dibenzo-1,4,7,10,13,16-hexaoxacyclo-octadeca-2,11-diene
C21	4,7,13-trioxa-1,10-diazacyclopentadecane
C22	4,7,13,16-tetraoxa-1,10-diazacyclooctadecane
C221	4,7,13,16,21-pentaoxa-1,10-diazabicyclo[8.8.5]tricosane
C222	4,7,13,16,21,24-hexaoxa-1,10-diazabicyclo[8.8.8]-hexacosane
BME-C21	1,7-bis(2-methoxyethyl)-4,10,13-trioxa-1,7-diazacyclo-pentadecane
BME-C22	7,16-bis(2-methoxyethyl)-1,4,10,13-tetraoxa-7,16-diaza-cyclooctadecane
BHE-C21	1,7-bis(2-hydroxyethyl)-4,10,13-trioxa-1,7-diazacyclo-pentadecane
BHE-C22	7,16-bis(2-hydroxyethyl)-1,4,10,13-tetraoxa-7,16-diaza-cyclooctadecane
cyclen	1,4,7,10-tetraazacyclododecane
THEC12	1,4,7,10-tetrakis-(2-hydroxyethyl)-1,4,7,10-tetraaza-cyclododecane
TMEC12	1,4,7,10-tetrakis-(2-methoxyethyl)-1,4,7,10-tetraaza-cyclododecane
THPC12	1,4,7,10-tetrakis-((*S*)-2-hydroxypropyl)-1,4,7,10-tetra-azacyclododecane
cyclam	1,4,8,11-tetraazacyclotetradecane
TMC	1,4,8,11-tetrakis-(methyl)-1,4,8,11-tetraaza-cyclotetradecane
THEC14	1,4,8,11-tetrakis-(2-hydroxyethyl)-1,4,8,11-tetraaza-cyclotetradecane
TMEC14	1,4,8,11-tetrakis-(2-methoxyethyl)-1,4,8,11-tetraaza-cyclotetradecane
THPC14	1,4,8,11-tetrakis-((*S*)-2-hydroxypropyl)-1,4,8,11-tetra-azacyclotetradecane

dimethyl-formamide	N,N-dimethylformamide
propylene-carbonate	1,2-propanediol cyclic carbonate
NEt_4ClO_4	tetraethylammonium perchlorate
NEt_4OH	tetraethylammonium hydroxide
NEt_4Cl	tetraethylammonium chloride
NEt_4Br	tetraethylammonium bromide
tosyl	*p*-toluene sulfonyl
tosylate	*p*-toluene sulfonate
triflic acid	trifluoromethane sulfonic acid
triflate	trifluoromethane sulfonate
CFSE	Crystal Field Stabilisation Energy
L	unspecified ligand
M	mol dm^{-3}
ε	dielectric constant
Å	angstrom (10^{-10} m)
D_N	Gutmann donor number
d_n	n-deuterated
Conc.	concentration (mol dm^{-3})
Expt	experimental
Calc	calculated
ln	logarithm (base e)
log	logarithm (base 10)
Torr	mm Hg
mm Hg	1 mm Hg = 101325 kg m^{-1} s^{-2}
ms	milliseconds (10^{-3} s)
mV	millivolts (10^{-3} volts)
EMF	potential (volts)
E	electrode potential (volts)
E_O	standard electrode potential (volts)
F	Faraday's constant, 9.6487 x 10^4 (C mol^{-1})
pH	$-\log_{10}[H^+]$
K_W	equilibrium constant for the self ionisation of water
pK_W	$-\log_{10}[K_W]$
K_a	acid dissociation constant
pK_a	$-\log_{10}[K_a]$
T	temperature (K)
R	universal gas constant, 8.314 (J K^{-1} mol^{-1})

k_B	Boltzmann's constant, 1.381×10^{-23} (J K^{-1})
h	Planck's constant, 6.603×10^{-34} (J s)
$\Delta H^{\ddagger}$	enthalpy of activation (kJ mol^{-1})
$\Delta S^{\ddagger}$	entropy of activation (J K^{-1} mol^{-1})
K	equilibrium (stability) constant
k	rate constant (s^{-1})
τ	mean lifetime (s)
NMR	Nuclear Magnetic Resonance (spectroscopy)
NOE	Nuclear Overhauser Effect
Hz	hertz (s^{-1})
MHz	megahertz (10^6 s^{-1})
ppm	parts per million
δ	chemical shift (ppm)
χ	mole fraction
ω	frequency (rad s^{-1})
ν	frequency (s^{-1})
v	absorption mode lineshape
$w_{\frac{1}{2}}$	half-height width at maximum intensity
T_1	longitudinal relaxation time (s)
T_2	transverse relaxation time (s)
γ	gyromagnetic ratio

Abstract

In the first part of this study the complexation characteristics of the lariat ethers, BME-C21 and BME-C22, with the alkali metal ions and silver(I) have been investigated in a range of non-aqueous solvents. The stability constants were determined by potentiometric titrations using silver wire and sodium selective electrodes. In addition, the protonation constants of the ligands, BME-C21 and BME-C22 and the stability constants of their complexes with a range of alkaline earth, transition and heavy metal ions in aqueous solution have been determined by potentiometric titration using a pH electrode. The potentiometric titration results are discussed by comparison with those of the corresponding complexes of the crown ethers, C21 and C22, the cryptands, C221 and C222, and the lariat ethers, BHE-C21 and BME-C22.

The complexation characteristics of the tetraaza macrocyclic ligands, TMEC14 and (*S*)-THPC14 with the alkali metal ions and silver(I) in a range of non-aqueous solvents are also investigated. These results are compared with those of the corresponding metal complexes of TMEC12 and (*S*)-THPC12. In addition, the protonation constants of the tetraaza macrocycle, TMEC14 and the stability constants of the complexes of TMEC14 with a range of alkaline earth, transition and heavy metal ions in aqueous solution were determined and are compared with those of the related ligands, cyclam, TMEC12 and THEC14.

These potentiometric titration results are discussed in terms of the size of the metal ion, the solvation energy of the metal ion, the size and flexibility of the complexing ligand, and the influence of different types of pendant arms on the stability of the complexes formed.

The second part of this study investigates the exchange of Li^+ and Na^+ on $[M(BME\text{-}C21)]^+$, $[M(BME\text{-}C22)]^+$ and $[M(TMEC14)]^+$ using variable temperature ^7Li and ^{23}Na NMR, respectively. The kinetic parameters for these systems were determined by complete lineshape analysis of the NMR spectra. The results are discussed in terms of the size of the metal ion, the solvation energy of the metal ion, the size and flexibility of the complexing ligand, and the influence of different types of pendant arms on the lability of the complexes formed. In addition, these

results are correlated with those of the non-aqueous potentiometric titrations above.

Finally, this study involves the investigation of an intramolecular exchange process between isomers of some alkali and heavy metal complexes of the tetraaza macrocyclic ligands, TMEC14 and (*S*)-THPC14 using variable temperature ^{13}C NMR in ^{12}C-d_4 methanol. From these results the solution structures of these complexes were able to be determined. In addition, the kinetic parameters for the intramolecular exchange process occurring within the $[Cd(TMEC14)]^{2+}$ and $[Hg(TMEC14)]^{2+}$ complexes were derived by complete lineshape analysis of their variable temperature ^{13}C NMR spectra. A comparison of these solution structures is made with those of the heavy metal complexes of the smaller TMEC12 and THPC12.

1. Introduction

1.1 Crown Ethers, Cryptands and Lariat Ethers

C. J. Pedersen, in 1967, was the first to recognise the complexation of alkali metal ions by macrocyclic crown ethers (or coronands) [1-2]. While reacting catechol with bis(2-chloroethyl)ether in the presence of sodium hydroxide in the solvent *n*-butanol some white fibrous crystals were formed (Figure 1.1). This crystalline product was found to be 2,3,11,12-dibenzo-1,4,7,10,13,16-hexaoxacyclooctadeca-2,11-diene or dibenzo-18-crown-6 and had the unusual property of becoming more soluble in methanol with the addition of sodium salts due to the formation of a sodium complex. The trivial name of dibenzo-18-crown-6 denotes an 18-membered ring with 6 oxygens and 2 benzo substituents, with the '*crown*' label coming from the ligands ability to '*crown*' a metal ion [2-3]. This was the first of a family of crown ethers, and lead to a large expansion in the field of inclusion or host-guest chemistry due to the ability of the crown ethers to selectively complex alkali and alkaline earth metal ions. The general structure and trivial nomenclature of some crown and diaza crown ethers are shown in Figures 1.2 and 1.3, respectively.

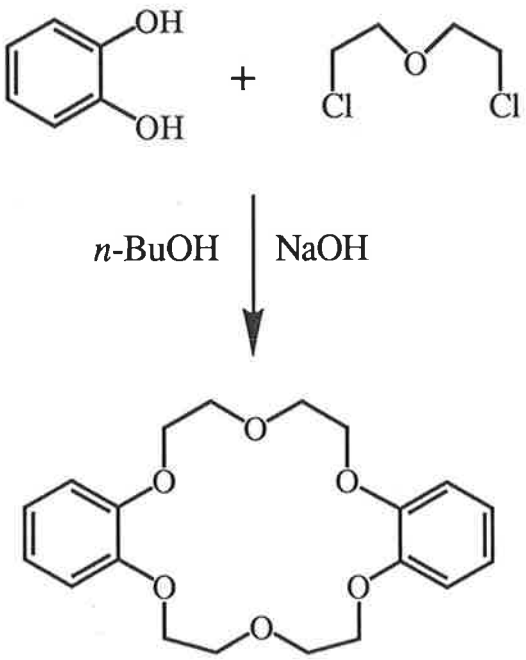

Figure 1.1 Formation of the crown ether, dibenzo-18-crown-6.

Following the work of Pedersen, J.-M. Lehn developed a range of three-dimensional bicyclic ligands which he named cryptands (Greek: *cryptos* = *cave*) in 1969 [4-7]. It was envisaged by Lehn that cryptands, with rigid three-dimensional cavities, would form more stable complexes (*cryptates*) with metal ions than the two-dimensional crown ethers. The first cryptand synthesised by Lehn was 4,7,13,16,21,24-hexaoxa-1,10-diazabicyclo[8.8.8]hexacosane or C222 [4]. The trivial nomenclature of the ligand C222 indicates that there are two oxygen atoms in each of the three polyether chains. The general structure and trivial nomenclature of the cryptands are shown in Figure 1.4.

The cryptands are part of a larger area of molecular recognition chemistry which Lehn named '*supramolecular chemistry*' [8-10], a field which generated considerable interest with the earlier discovery of the metal ion selectivity of a number of naturally occurring macrocyclic compounds such as nonactin, monactin, enniatin and valinomycin [11-15].

In 1979, D. J. Cram designed and demonstrated the selectivity of a group of ligands known as spherands [16-18] and in 1987, Pedersen, Lehn and Cram were awarded the Nobel Prize in chemistry for their work in supramolecular chemistry.

In an effort to study and mimic valinomycin, G. W. Gokel synthesised a group of compounds which he named the '*lariat ethers*' [19-20]. Gokel decided that the cryptands had the desired three-dimensional structure, but formed cryptates which were not very labile, whereas the crown ethers formed complexes which were labile, but lacked the ability to encapsulate a metal ion resulting in complexes of low stability, particularly in water. His solution was to explore crown ethers with sidearms or pendant arms with one or more donor atoms which may aid in the complexation of the metal ion. Gokel named these pendant armed ligands, lariat ethers, with the '*lariat*' label coming from the ligands ability to '*lasso*' a metal ion, aiding in the complexation [21].

Two families of lariat ethers were prepared by Gokel, the carbon-pivot (C-pivot) and the nitrogen-pivot (N-pivot) lariat ethers. The C-pivot lariat ethers had the pendant arm(s) attached to a carbon of the ring, whereas the N-pivot lariat ethers had the pendant arm(s) attached to the nitrogen atoms. The C-pivot lariat ethers were found to form more stable complexes with metal ions compared with those formed by the N-pivot

lariat ethers. However, the C-pivot lariat ether complexes were also less labile than their N-pivot analogues. This was attributed to the facile inversion of the nitrogen atom, a property not shared by carbon [22-23]. The lariat ethers generated considerable interest as they occupy a niche between the crown ethers and cryptands, forming more labile complexes than the cryptates, and more able to encapsulate a metal ion than the crown ethers. Examples of C-pivot, N-pivot and bibracchial lariat ethers are shown in Figure 1.5.

A major aim of this study is to investigate the complexation properties of the bibracchial lariat ethers, 1,7-bis(2-methoxyethyl)-4,10,13-trioxa-1,7-diazacyclopentadecane (BME-C21) and 7,16-bis(2-methoxyethyl)-1,4,10,13-tetraoxa-7,16-diazacyclooctadecane (BME-C22) with the alkali metal ions and silver(I) in a range of non-aqueous solvents, and with the alkaline earth, transition and heavy metal cations in aqueous solution. The lariat ethers, BME-C21 and BME-C22 both possess two methoxyethyl pendant arms which can facilitate the complexation of metal ions. The lariat ether, BME-C21 has a smaller 15-membered ring and one less ether oxygen donor atom than BME-C22 which has an 18-membered ring.

Structurally, BME-C21 and BME-C22 are similar to the lariat ethers, BHE-C21 and BHE-C22 (with the replacement of the methoxyethyl pendant arms by hydroxyethyl pendant arms), the cryptands, C221 and C222 (with the same number of oxygen and nitrogen donor atoms, respectively) and the crown ethers, C21 and C22 (with the methoxyethyl pendant arms replaced by protons). A comparison of the complexation properties of these related ligands with those of BME-C21 and BME-C22 will be made. The structures of the crown ethers, C21 and C22, the cryptands, C221 and C222 and the lariat ethers, BME-C21, BME-C22, BHE-C21 and BHE-C22 are shown in Figure 1.6.

In addition, a number of factors which effect the stability and lability of the metal ion complexes studied will be investigated including: (i) the flexibility of the ligand, (ii) the effect of pendant arms on the complexation of metal ions, (iii) the size of the ring cavity, (iv) the number and type of donor groups including those on any pendant arms, (v) the nature of the metal ion being complexed and (vi) the effect of solvent.

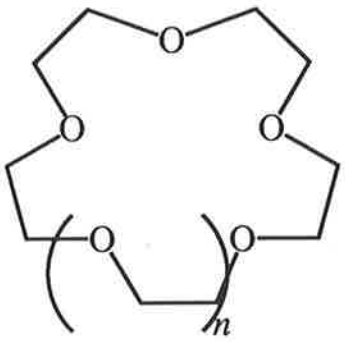

n	*crown*
0	12-crown-4
1	15-crown-5
2	18-crown-6
	etc

Figure 1.2 General structure and trivial nomenclature of some crown ethers.

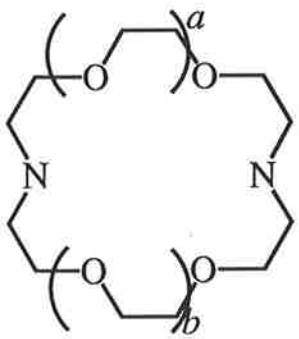

a	*b*	*crown*
0	0	C11
1	0	C21
1	1	C22
		etc

Figure 1.3 General structure and trivial nomenclature of some diaza crown ethers.

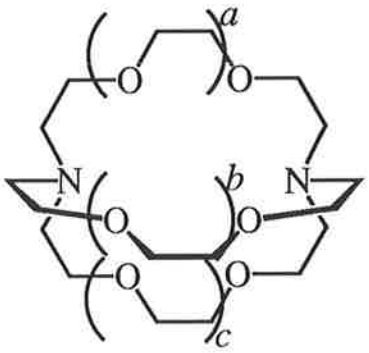

a	*b*	*c*	*cryptand*
0	0	0	C111
1	0	0	C211
1	1	0	C221
1	1	1	C222
			etc

Figure 1.4 General structure and trivial nomenclature of some cryptands.

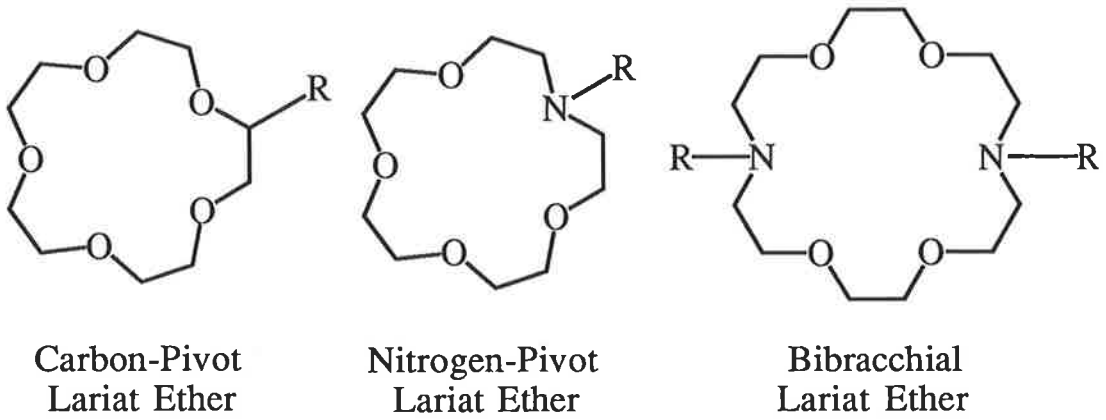

Figure 1.5 General structure of some carbon and nitrogen-pivot lariat ethers.

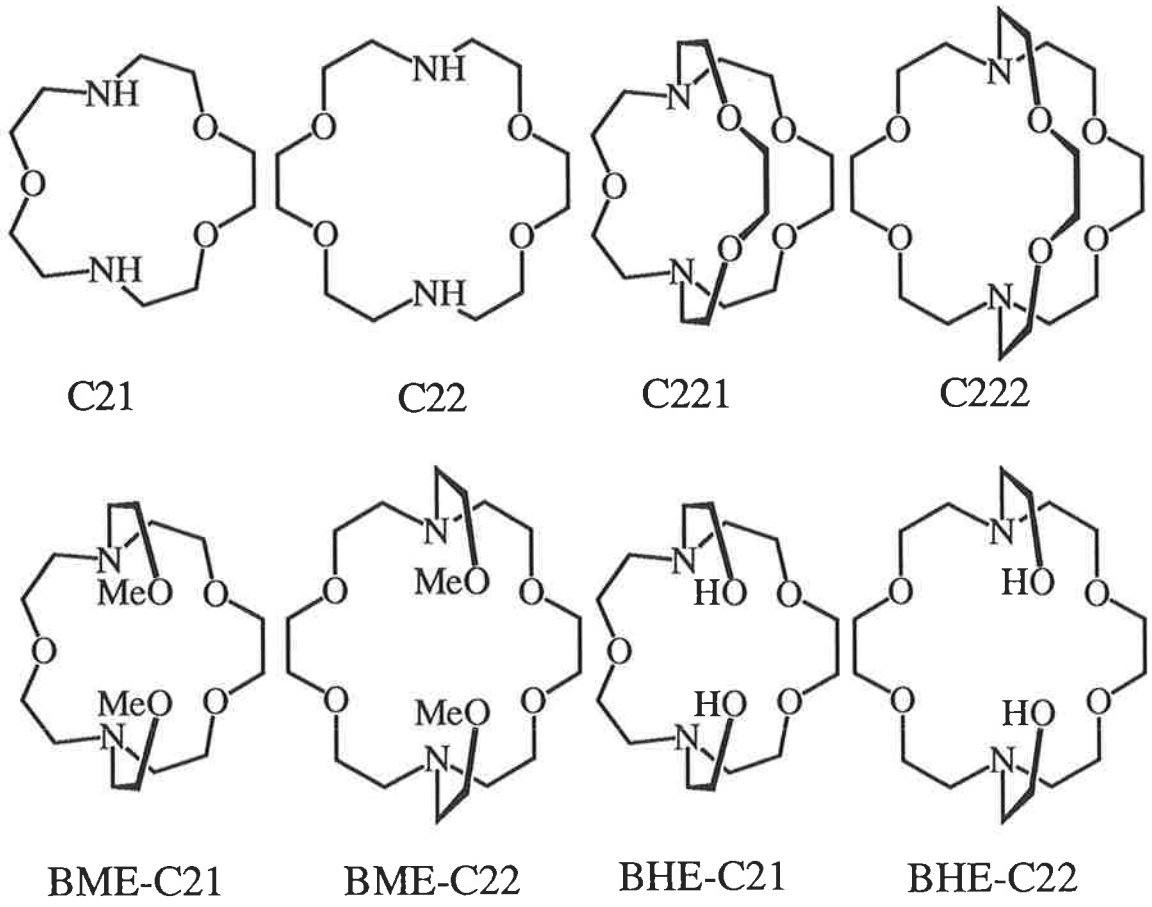

Figure 1.6 General structure of the crown ethers, C21 and C22, the cryptands, C221 and C222, and the lariat ethers BME-C21, BME-C22, BHE-C21 and BHE-C22.

1.2 Tetraaza Macrocyclic Ligands

In contrast to the large amount of research carried out on the crown ethers, lariat ethers and cryptands, a relatively small amount of research has been performed on the alkali metal complexes of the tetraaza macrocyclic ligands. The interest in tetraaza macrocyclic ligands has stemmed from the study of some naturally occurring tetraaza macrocycles such as the porphyrin ring of the iron-containing haem proteins, the related chlorin complex of magnesium observed in chlorophyll, and the corrin ring from vitamin B_{12} [24-27]. These tetraaza macrocyclic ring systems, contained in a number of naturally occurring compounds, are responsible for the complexation of metal ions necessary for a variety of biological processes.

Although most naturally occurring polyaza macrocycles are unsaturated, a number of saturated polyaza macrocyclic ligands have been synthesised, some with pendant arms, leading to a number of applications for these ligands. Examples of some useful polyaza macrocyclic ligands include tris(2,3-dihydroxybenzoyl)-1,5,9-triazacyclotridecane synthesised by Raymond which selectively binds Fe^{3+} [28] and 2-dodecyl-1,5,8,12-tetraazacyclotetradecane (cyclam with a long aliphatic side chain -$C_{12}H_{25}$) which makes the ligand and its metal complexes soluble in organic solvents and can be used to extract metal ions from aqueous solution into the organic phase [29].

In the search for metal ion selective ligands the polyaza macrocyclic ligands have attracted substantial interest, with the stabilities of the complexes formed depending on a number of factors, including the nature of the pendant arms, the nature of the complexing metal ion, and the size and number of donor groups for the macrocyclic ring [30-46]. In particular, the nature of the pendant arms can have a substantial effect on the complexation of metal ions. This is clearly demonstrated for the case when the rates of complexation of divalent transition metal ions change from hours for the parent macrocycle, 1,4,8,11-tetraazacyclotetradecane (cyclam), to seconds for the 2-hydroxyethyl pendant armed ligand, 1,4,8,11-tetrakis-(2-hydroxyethyl)-1,4,8,11-tetraazacyclotetradecane (THEC14) [33,47]. The increase in the rate of complexation for THEC14 may be attributed to a fast initial coordination of the metal ion by the flexible hydroxyethyl pendant arms, followed by coordination of the tetraaza ring.

The second major aim of this study (see Section 1.1) is to investigate the complexation properties of the tetraaza macrocyclic ligands, 1,4,8,11-tetrakis-(2-methoxyethyl)-1,4,8,11-tetraazacyclotetradecane (TMEC14) and 1,4,8,11-tetrakis-((*S*)-2-hydroxypropyl)-1,4,8,11-tetraazacyclotetradecane (THPC14) with the alkali metal ions and silver(I) in a range of non-aqueous solvents. In addition, the complexation properties of TMEC14 with some of the alkaline earth, transition and heavy metal ions in aqueous solution will be investigated. The tetraaza macrocyclic ligands, TMEC14 and THPC14 both possess 14-membered rings, with methoxyethyl and (*S*)-2-hydroxypropyl pendant arms, respectively. It was expected that the presence of these pendant arms would facilitate the complexation of metal ions in comparison with the parent macrocycle, 1,4,8,11-tetraazacyclotetradecane (cyclam).

Structurally, the tetraaza macrocyclic ligands, TMEC14 and THPC14 are similar to TMEC12 and THPC12, respectively, with the 14-membered ring replaced by a 12-membered ring, and a comparison of the complexation properties of these related ligands will be made. The structures of the ligands, TMEC14 and THPC14 along with the parent macrocycle, cyclam and the related ligands, TMEC12, THPC12 and THEC14 used in this study appear in Figure 1.7.

In addition, a number of factors which affect the stability and lability of the metal ion complexes studied will be investigated including: (i) the flexibility of the ligand, (ii) the effect of pendant arms on the complexation of metal ions, (iii) the size of the ring cavity, (iv) the number and type of donor groups including those on any pendant arms, (v) the nature of the metal ion being complexed and (vi) the effect of solvent.

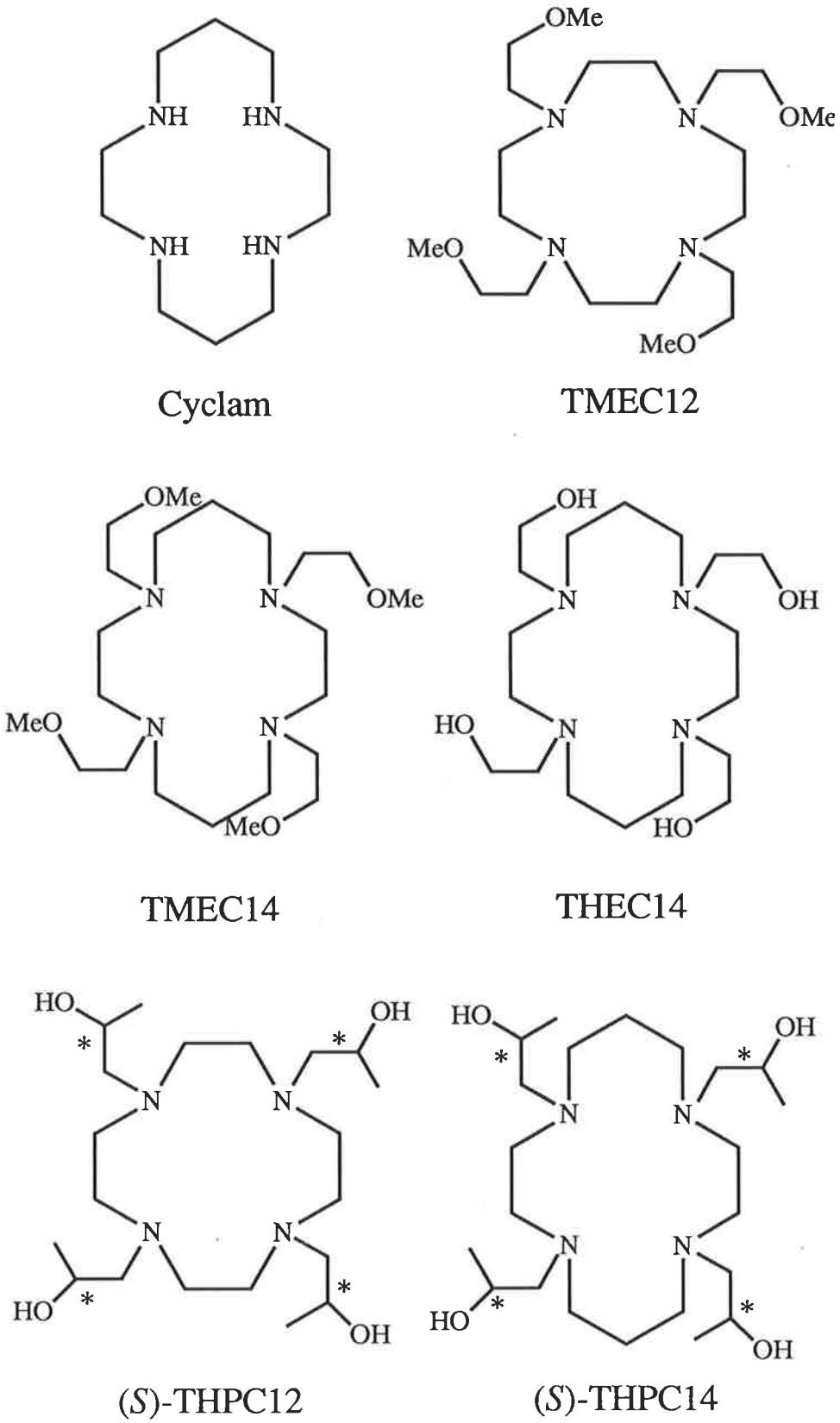

Figure 1.7 General structure of TMEC14 and (*S*)-THPC14, and the related ligands, cyclam, TMEC12, (*S*)-THPC12 and THEC14 (* indicates the chiral carbons which are in the (*S*)-configuration).

1.3 Applications of Macrocyclic Ligands

Macrocyclic ligands have many applications in a number of fields, including analytical, biological, chemical and industrial. Some of the many applications are listed below:

(i) Alkalides

Macrocyclic ligands can be used for the stabilisation of a number of anionic species such as alkalides, electrides and polymetallic anions [10]. Alkalides, or negatively charged alkali metal ions can behave as intrinsic semiconductors and have possible applications in solid-state devices and as aprotic reducing agents [9,48-50].

(ii) Anion Activation

Activation of an anion by removal of the cation into a macrocyclic ligands yields a number of applications. These include, solid-liquid and liquid-liquid phase transfer catalysis [19], the solubilisation of inorganic salts in organic solvents [1-2,19,29,51], and reactive anions for use in industrial polymerisation processes [9].

(iii) Anion Recognition

The selective coordination of anionic species is possible in certain macrocyclic compounds [52]. Anionic species are important in both chemical and biological processes. These anion selective macrocycles may act as anchoring sites for various biological substrates or as a mimic for biological receptors [7].

(iv) Binding and Removal of Toxic Heavy Metal Ions

The detection and treatment of heavy metal poisoning with heavy metal ions such as Cd^{2+}, Pb^{2+} and Hg^{2+} is of great importance for use in industrial smelters and environmental chemistry [53-59].

(v) Catalysis

The macrocycles act as receptors containing specialised reactive groups. The substrate is bound by the macrocycle, reacts with the specialised group, and is finally decomplexed as the product(s) [7,53].

(vi) **Chiral Recognition**

The ability for macrocyclic ligands containing chiral centres to separate racemic mixtures into their enantiomers yields a number of important applications [18-19,60-64] and is currently used for the resolution of amino acids [62].

(vii) **Fluorescent Probes**

Certain macrocycles have an enhanced fluorescence upon complexation of cations such as Zn^{2+}. They can be used as fluorescent probes in membrane studies [65] and cation detection (including heavy metal ion detection (iv)) [66-71].

(viii) **Ion Chromatography**

Resin bound macrocycles can be used for the selective separation of alkali and alkaline earth metal ions [19,55,60,72].

(ix) **Ion-selective Electrodes**

The macrocyclic ligand can be used as the ion carrier [60,73-75].

(x) **Isotope Separation**

The separation of isotopes using macrocyclic ligands has important applications [9-10,76] and has been used to purify ^{137}Cs [9] and for the separation of ^{22}Na / ^{24}Na [77], ^{6}Li / ^{7}Li and ^{40}Ca / ^{44}Ca [78].

(xi) **Membrane Transport**

The macrocycles act as the carrier molecules which transport the lipophilic substrates (such as cations) across the membrane [7,19,79-85].

(xii) **Molecular Devices**

Macrocycles may be used for light conversion molecular devices in which the ultraviolet light is absorbed by the macrocycle and transferred to the complexed lanthanide (by intramolecular energy transfer) which then re-emits the energy as visible light [7,86].

References

1 C. J. Pedersen, *Angew. Chem., Int. Ed. Engl.*, 1988, **27**, 1021.
2 C. J. Pedersen, *J. Am. Chem. Soc.*, 1967, **89**, 7017.
3 C. J. Pedersen, *J. Am. Chem. Soc.*, 1967, **89**, 2495.
4 B. Dietrich, J.-M. Lehn and J.-P. Sauvage, *Tetrahedron Lett.*, 1969, 2885.
5 B. Dietrich, J.-M. Lehn and J.-P. Sauvage, *Tetrahedron Lett.*, 1969, 2889.
6 J.-M. Lehn, *Struct. Bonding (Berlin)*, 1973, **16**, 1.
7 J.-M. Lehn, *J. Inclusion Phenom.*, 1988, **6**, 351.
8 J.-M. Lehn, *Pure Appl. Chem.*, 1979, **51**, 979.
9 J.-M. Lehn, *Acc. Chem. Res.*, 1978, **11**, 49.
10 B. Dietrich, P. Viout and J.-M. Lehn, *"Macrocyclic Chemistry"*, VCH (New York), 1993.
11 C. Moore and B. C. Pressman, *Biochem. Biophys. Res. Commun.*, 1964, **15**, 562.
12 L. A. R. Pioda, H. A. Wachter, R. E. Dohner and W. Simon, *Helv. Chim. Acta*, 1967, **50**, 1373.
13 B. T. Kilbourn, J. D. Dunitz, L. A. R. Pioda and W. Simon, *J. Mol. Biol.*, 1967, **30**, 559.
14 M. Dobler, J. D. Dunitz and B. T. Kilbourn, *Helv. Chim. Acta*, 1969, **52**, 2573.
15 K. Neupert-Laves and M. Dobler, *Helv. Chim. Acta*, 1975, **58**, 432.
16 D. J. Cram, T. Kaneda, R. C. Helgeson and G. M. Lein, *J. Am. Chem. Soc.*, 1979, **101**, 6752.
17 D. J. Cram, T. Kaneda, R. C. Helgeson, S. B. Brown, C. B. Knobler, E. Maverick and K. N. Trueblood, *J. Am. Chem. Soc.*, 1985, **107**, 3645.
18 D. J. Cram, *J. Inclusion Phenom.*, 1988, **6**, 397.
19 G. W. Gokel, *"Crown Ethers and Cryptands"*, The Royal Society of Chemistry (Cambridge), 1991.
20 G. W. Gokel, *Chem. Soc. Rev.*, 1992, 39.
21 G. W. Gokel, D. M. Dishong and C. J. Diamond, *J. Chem. Soc., Chem. Commun.*, 1980, 1053.
22 D. M. Dishong, C. J. Diamond, M. I. Cinoman and G. W. Gokel, *J. Am. Chem. Soc.*, 1983, **105**, 586.
23 R. A. Shultz, B. D. White, D. M. Dishong, K. A. Arnold and G. W. Gokel, *J. Am. Chem. Soc.*, 1985, **107**, 6659.

24 L. F. Lindoy, *"The Chemistry of Macrocyclic Ligand Complexes"*, University Press (Cambridge), 1989.

25 R. M. Izatt and J. J. Christensen, *"The Design of Selective Complexing Agents"* -in *"Synthesis of Macrocycles"*, Wiley (New York), 1987.

26 A. I. Popov and J.-M. Lehn: in G. A. Melson (Ed.), *"Coordination Chemistry of Macrocyclic Compounds"*, Plenum Press (New York), 1979.

27 T. A. Kaden, *Topp. Curr. Chem.*, 1984, **121**, 157.

28 F. Weitl and K. Raymond, *J. Am. Chem. Soc.*, 1979, **101**, 2728.

29 F. R. Muller and H. Handel, *Tetrahedron Lett.*, 1982, **23**, 2769.

30 H. Stetter and W. Frank, *Angew. Chem., Int. Ed. Engl.*, 1976, **15**, 686.

31 H. Hafliger and T. A. Kaden, *Helv. Chim. Acta*, 1979, **62**, 683.

32 K. P. Wainwright, *J. Chem. Soc., Dalton Trans.*, 1980, 2117.

33 C. M. Madeyski, J. P. Michael and R. D. Hancock, *Inorg. Chem.*, 1984, **23**, 1487.

34 I. Murase, M. Mikuriya, H. Sonoda and S. Kida, *J. Chem. Soc., Chem. Commun.*, 1984, 692.

35 I. Murase, M. Mikuriya, H. Sonoda, Y. Fukada and S. Kida, *J. Chem. Soc., Dalton Trans.*, 1986, 953.

36 I. Murase, I. Ueda, N. Marubayashi, S. Kida, N. Matsumoto, M. Kudo, M. Toyohara, K. Hiate and M. Mikuriya, *J. Chem. Soc., Dalton Trans.*, 1990, 2763.

37 N. W. Alcock, K. P. Balakrishnan and P. Moore, *J. Chem. Soc., Dalton Trans.*, 1986, 1743.

38 C.-M. Che, W.-T. Tang and T. C. W. Mak, *J. Chem. Soc., Dalton Trans.*, 1988, 2879.

39 A. Reison, M. Zehnder, T. A. Kaden, *Acta Crystallogr., Sect. C: Cryst. Struct. Commun.*, 1988, **C44**, 1740.

40 E. Asato, H. Toftlind, S. Kida, M. Mikurita and K. S. Murray, *Inorg. Chim. Acta*, 1989, **165**, 207.

41 E. Asato, S. Kida and I. Murase, *Inorg. Chem.*, 1989, **28**, 800.

42 G. Vukovic, E. Asato, N. Matsumoto and S. Kida, *Inorg. Chim. Acta*, 1990, **171**, 45.

43 M. K. Moi, M. Yanuck, S. V. Deshpande, H. Hope, S. J. DeNardo and C. F. Meares, *Inorg. Chem.*, 1987, **26**, 3458.

44 A. Bencini, A. Bianchi, M. Castello, M. Di Vaira, J. Faus, E. Garcia-Espana, M. Micheloni and P. Paoletti, *Inorg. Chem.*, 1989, **28**, 347.

45 R. D. Hancock, M. S. Shaikjee, S. M. Dobson and J. C. A. Boeyens, *Inorg. Chim. Acta*, 1988, **154**, 229.

46 D. Parker, J. R. Morphy, K. Jankowski and J. Cox, *Pure Appl. Chem.*, 1989, **61**, 1637.

47 R. W. Hay, M. P. Pujari, W. T. Moodie, S. Craig, D. T. Richens, A. Perotti and L. Ungaretti, *J. Chem. Soc., Dalton Trans.*, 1987, 2605.

48 J. L. Dye, *Pure Appl. Chem.*, 1989, **61**, 1555.

49 J. L. Dye and R.-H. Huang, *Chem. Br.*, 1990, 240.

50 R. S. Bannwart, S. A. Solin, M. G. DeBacker and J. L. Dye, *J. Am. Chem. Soc.*, 1989, **111**, 5552.

51 T. Taura, *Inorg. Chim. Acta*, 1989, **162**, 105.

52 B. Dietrich, J.-M. Lehn, J. Guilhem and C. Pascard, *Tetrahedron Lett.*, 1989, **30**, 4125.

53 J.-M. Lehn, *Pure Appl. Chem.*, 1978, **50**, 871.

54 S. Kulstad and L. A. Malmsten, *J. Inorg. Nucl. Chem.*, 1981, **43**, 1299.

55 J. S. Bradshaw, K. E. Krakowiak, B. J. Tarbet, R. L. Breuning, J. F. Biernat, M. Bochenska, R. M. Izatt and J. J. Christensen, *Pure Appl. Chem.*, 1989, **61**, 1619.

56 F. Arnaud-Neu, B. Spiess and M.-J. Schwing-Weill, *Helv. Chim. Acta*, 1977, **60**, 2633.

57 B. Spiess, F. Arnaud-Neu and M.-J. Schwing-Weill, *Helv. Chim. Acta*, 1980, **63**, 2287.

58 F. Arnaud-Neu, B. Spiess and M.-J. Schwing-Weill, *J. Am. Chem. Soc.*, 1982, **104**, 5641.

59 G. Wu, W. Jiang, J. D. Lamb, J. S. Bradshaw and R. M. Izatt, *J. Am. Chem. Soc.*, 1991, **113**, 6538.

60 M. Takagi and N. Nakamura, *J. Coord. Chem.*, 1986, **15**, 53.

61 J. S. Bradshaw, R. M. Izatt, J. J. Christensen, K. E. Krakowiak, B. J. Tarbet and R. L. Breuning, *J. Inclusion Phenom.*, 1989, **7**, 127.

62 J.-P. Joly and B. Gross, *Tetrahedron Lett.*, 1989, **30**, 4231.

63 K. Yamamoto, T. Ikeda, T. Kitsuki, Y. Okamoto, H. Chikamatsu and N. Nakazaki, *J. Chem. Soc., Perkin Trans. 1*, 1990, 271.

64 P. Huszthy, J. S. Bradshaw, C. Y. Zhu and R. M. Izatt, *J. Org. Chem.*, 1991, **56**, 3330.

65 U. Herrmann, B. Tummler, G. Maass, P. K. T. Mew and F. Vogtle, *Biochemistry*, 1984, **23**, 4059.

66 F. Fages, J.-P. Desvergne, H. Bouas-Laurent, J.-M. Lehn, J. P. Konopelski, P. Marsau and Y. Barrans, *J. Chem. Soc., Chem. Commun.*, 1990, 655.

67 A. P. DeSilva, N. Gunaratne and K. R. A. S. Sandanayake, *Tetrahedron Lett.*, 1990, **31**, 5193.

68 F. Fages, J.-P. Desvergne, H. Bouas-Laurent, P. Marsau, J.-M. Lehn, F. Kotzyba-Hibert, A.-M. Albrecht-Gary and M. Al-Joubbeh, *J. Am. Chem. Soc.*, 1989, **111**, 8672.

69 J. P. Konopelski, F. Kotzyba-Hibert, J.-M. Lehn, J.-P. Desvergne, F. Fages, A. Castellan and H. Bouas-Laurent, *J. Chem. Soc., Chem. Commun.*, 1985, 433.

70 F. Fages, J.-P. Desvergne, H. Bouas-Laurent, J. Hinschberger and P. Marsau, *New J. Chem.*, 1988, **12**, 95.

71 A. P. DeSilva and K. R. A. S. Sandanayake, *Tetrahedron Lett.*, 1991, **32**, 421.

72 Y. Frere and P. Gramain, *Makromol. Chem.*, 1982, **183**, 2163.

73 E. Luboch, A. Cygan and J. F. Biernat, *Tetrahedron*, 1990, **46**, 2461.

74 E. Luboch, A. Cygan and J. F. Biernat, *Tetrahedron*, 1991, **47**, 4101.

75 R. Kataky, P. E. Nicholson, D. Parker and A. K. Covington, *Analyst*, 1991, **116**, 135.

76 S. Munoz and L. Echegoyen, *J. Chem. Soc., Perkin Trans. II*, 1991, 1735.

77 A. Knochel and R. D. Wilken, *J. Radioanal. Chem.*, 1976, **32**, 345.

78 K. G. Heumann, *Top. Curr. Chem.*, 1985, **127**, 77.

79 G. W. Gokel and L. Echegoyen, *Bioorg. Chem. Frontiers*, 1990, **1**, 115.

80 T. M. Fyles, *Bioorg. Chem. Frontiers*, 1990, **1**, 71.

81 H. Tsukube, *J. Coord. Chem.*, 1987, **16**, 101.

82 B. Sesta and A. D'Aprano, *J. Solution Chem.*, 1989, **18**, 1163.

83 H. Tsukube, K. Yamashita, T. Iwachido and M. Zenki, *J. Org. Chem.*, 1991, **56**, 268.

84 H. Tsukube, K. Takagi, T. Higashiyama, T. Iwachido and N. Hayama, *J. Chem. Soc., Perkin Trans. 1*, 1986, 1033.

85 H. Tsukube, H. Adachi and S. Morosawa, *J. Chem. Soc., Perkin Trans. 1*, 1989, 1537.

86 B. Alpha, J.-M. Lehn and G. Mathis, *Angew. Chem., Int. Ed. Engl.*, 1987, **26**, 266.

2. Non-Aqueous Titrations

2.1 Introduction

For metal ions and macrocyclic ligands in non-aqueous solution there exists an equilibrium between the solvated metal ion, M^+, the macrocyclic ligand, L, and the metal complex, $[ML]^+$, as defined by:

$$L + M^+ \underset{}{\overset{K_S}{\rightleftharpoons}} [ML]^+ \qquad \textbf{2.1}$$

where K_S, the stability constant, is defined as:

$$K_S = \frac{[ML^+]}{[M^+][L]} \qquad \textbf{2.2}$$

The factors that affect the magnitude of K_S are:

(i) The effective size of the cavity of the macrocyclic ligand, (ii) the flexibility of the ligand, (iii) the number of ligand binding sites, (iv) the size of M^+ (Table 2.1), (v) the solvation energy of M^+ and (vi) the number and type of pendant arms present.

In the next two chapters, these factors will be investigated and some conclusions drawn about the relative influence of each of these factors, in particular the effect on the stabilities of the complexes of attaching coordinating pendant arms to crown ethers and tetraaza macrocycles to form lariat ethers and pendant armed tetraaza macrocycles, respectively.

Table 2.1 The ionic radii of the alkali metal ions and Ag^+ [1]

Coordination	Ionic Radii (Å)					
	Li^+	Na^+	K^+	Rb^+	Cs^+	Ag^+
6-coordinate	0.76	1.02	1.38	1.52	1.67	1.19
7-coordinate		1.12	1.46	1.56		1.22
8-coordinate	0.92	1.18	1.51	1.61	1.74	1.28

2.2 Crystal Structures of Lariat Ether Complexes

Although no solid state structures of $[M(BME\text{-}C21)]^+$ and $[M(BHE\text{-}C21)]^+$ appear to have been reported in the literature, X-ray crystallographic studies of the complexes, $[Na(BME\text{-}C22)]^+$, $[K(BME\text{-}C22)]^+$, $[Na(BHE\text{-}C22)]^+$ and $[K(BHE\text{-}C22)]^+$ have been published [2-4]. The crystal structures of the Na^+ and K^+ complexes of BME-C22 show that both methoxyethyl pendant arms are coordinated to M^+ from above the plane of the C22 ring in the Na^+ complex (the *syn* conformation), and from opposite sides of the ring in the K^+ complex (the *anti* conformation). However, the crystal structures of $[Na(BHE\text{-}C22)]^+$ and $[K(BHE\text{-}C22)]^+$ show that both complexes adopt the *syn* conformation (Figure 2.1).

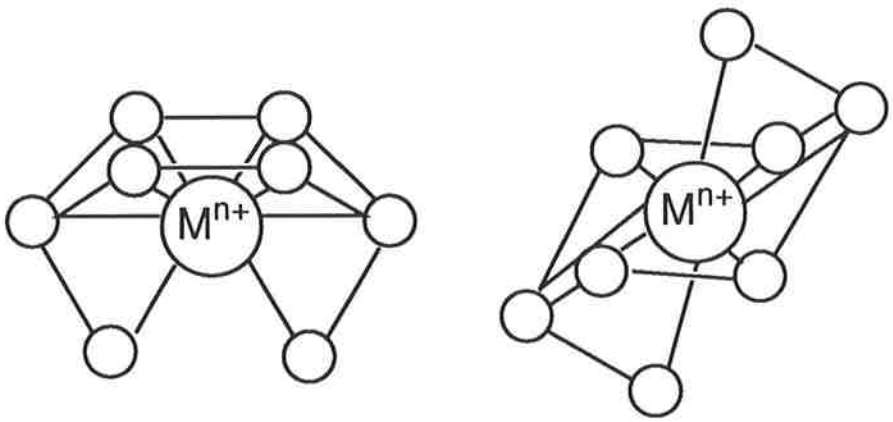

syn *anti*

Figure 2.1 Diagram showing the *syn* and *anti* conformations for a bibracchial lariat ether.

2.3 Stability Constants of the Complexes of the Lariat Ethers BME-C21 and BME-C22 in Non-Aqueous Solution

Schematic diagrams of the lariat ethers BME-C21 and BME-C22 studied, and some related ligands, C21, C22, C221, C222, BHE-C21 and BHE-C22 appear in Figure 2.2.

2.3.1 Stability Constants of the Complexes of the Lariat Ether BME-C21 in Non-Aqueous Solution

The stability constants of the complexes of BME-C21 with the alkali metal ions and Ag^+ in acetonitrile, propylene carbonate, methanol, dimethylformamide and pyridine determined in this study are given in Table 2.2.

The variations in the selectivity patterns observed for the ligand BME-C21 arise from a changing balance between the binding energy of L, the formation of a cavity to accommodate M^+ and minimise strain, the solvation energy of M^+ and the solvating power of the solvent. From Table 2.2, $[Na(BME\text{-}C21)]^+$ is seen to be the most stable of the alkali metal ion complexes, except in the weaker electron donating solvents, acetonitrile and propylene carbonate.

It has been shown for the cryptands that the most stable complex (or cryptate) is formed when the cavity size most closely matches the ionic radii of the metal ion [5]. The cryptand C221, with a cavity size of 1.1 Å [6-7] is Na^+ selective as a result of Na^+ (having a 7-coordinate ionic radius of 1.12 Å [1]) most closely matching the cavity size of C221. In the solvents methanol and dimethylformamide the Na^+ complex of BME-C21 is the most stable which suggests that BME-C21 forms a cavity of approximately 1.1 Å if it adopts the *syn* conformation.

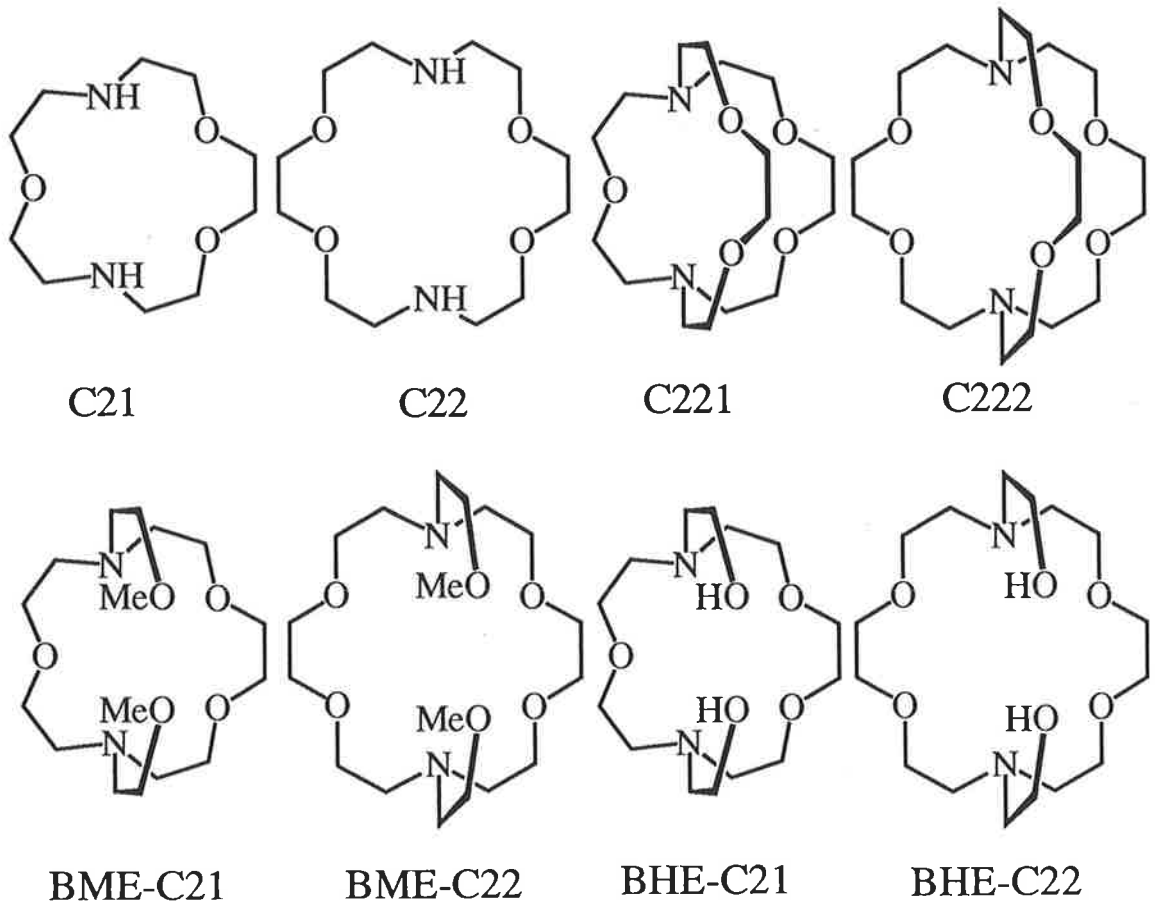

Figure 2.2 The diaza crown ethers, C21 and C22, the cryptands, C221 and C222, and the lariat ethers, BME-C21, BME-C22, BHE-C21 and BHE-C22.

Table 2.2 Non-aqueous stability constants for BME-C21 at 298.2 K with an ionic strength of 0.05 M NEt_4ClO_4.

		$\log(K_S / dm^3\ mol^{-1})$					
Solvent	D_N[a]	Li^+	Na^+	K^+	Rb^+	Cs^+	Ag^+
acetonitrile	14.1	9.13[c]	8.17[c]	5.24[c]	4.39[c]	3.77[c]	7.08[c]
propylene carbonate	15.1	7.0[d]	7.1[d]	5.0[d]	4.2[d]	3.6[d]	12.2[d]
methanol	23.5[b]	3.01[c]	4.89[c]	4.69[c]	3.97[c]	3.46[c]	9.86[c]
dimethyl-formamide	26.6	2.23[c]	3.50[c]	3.31[c]	2.84[c]	2.31[c]	8.37[c]
pyridine	33.1	5.08[c]	6.17[c]				1.8[d]

[a]Gutmann donor numbers from reference 10. [b]Gutmann donor number from references 11 and 12. [c]Error ± 0.05. [d]Error ± 0.1.

Thus, Na^+ (1.02 and 1.12 Å for the 6 and 7-coordinate geometries, respectively) minimises the strain within the BME-C21 cavity and hence produces the most stable complex in the solvents methanol and dimethylformamide but not in the lower electron donating solvents, acetonitrile and propylene carbonate, as is explained below (Section 2.3.2). In addition, although the $[Na(BME\text{-}C21)]^+$ complex is the most stable in methanol and dimethylformamide, the $[Li(BME\text{-}C21)]^+$ and $[K(BME\text{-}C21)]^+$ complexes are of similar stability which implies that the ligand, BME-C21 is able to undergo considerable variation in cavity size before the strain significantly destabilises the $[M(BME\text{-}C21)]^+$ complex.

2.3.2 Variation of Stability Constants with Solvent for the Complexes of the Lariat Ether BME-C21

For the alkali metal complexes of BME-C21 in Table 2.2, K_S varies substantially with the nature of the solvent. Firstly, the stability constants, K_S, decrease as the Gutmann donor number, D_N (Appendix i [8-12]) increases, except for pyridine. This is consistent with an increase in the solvation energy of M^+ (with increasing D_N) resulting in a decrease in the stability of the complex, $[ML]^+$. Thus, as D_N increases the solvent is able to compete more favourably with the ligand for the metal ion with a

concomitant decrease in the stability of the complex. Pyridine, which is a borderline soft base as a result of the nitrogen lone pair being delocalised into the aromatic ring, may not solvate the hard acid alkali metal ions as strongly as expected on the basis of a Gutmann donor number, D_N of 33.1. In addition, there is a steric crowding effect due to the large size of the pyridine molecules. These two effects lead to pyridine poorly solvating the alkali metal ions and hence the ligand is able to compete more favourably for the metal ions than would be anticipated from a D_N of 33.1 for pyridine.

In the oxygen donor solvents, dimethylformamide, methanol and propylene carbonate, the stability constants of the Ag^+ complexes are much greater than those of their alkali metal analogues. This is a result of the soft acid Ag^+ having a greater affinity for the nitrogen donor atoms of the ligand than do the alkali metal ions. However, upon going to the nitrogen donor solvents, acetonitrile and pyridine, Ag^+ is more strongly solvated and the stability of the Ag^+ complexes decrease in comparison with the stabilities of the alkali metal complexes.

The second major effect of solvent, is that for the alkali metal ions the relative stabilities of $[M(BME\text{-}C21)]^+$ change as the Gutmann donor number, D_N, increases from acetonitrile to dimethylformamide. Thus, in acetonitrile, the stability sequence $Li^+ > Na^+ > K^+ > Rb^+ > Cs^+$ is observed, with Li^+ forming the most stable complex. This sequence changes to $Li^+ \approx Na^+ > K^+ > Rb^+ > Cs^+$ for propylene carbonate, and finally for methanol and dimethylformamide the sequence $Li^+ < Na^+ > K^+ > Rb^+ > Cs^+$ is observed, with $[Na(BME\text{-}C21)]^+$ becoming the most stable complex. This effect is consistent with the weaker electron donating solvents competing less effectively for Li^+ relative to Na^+ and K^+, in comparison with the stronger donor solvents. Thus, although $[Na(BME\text{-}C21)]^+$ is the most stable complex in methanol and dimethylformamide, the decrease in solvating power of the solvents, acetonitrile and propylene carbonate leads to $[Li(BME\text{-}C21)]^+$ becoming the most stable complex. The data for the alkali metal complexes in pyridine also follows this pattern, with $[Na(BME\text{-}C21)]^+$ being more stable than $[Li(BME\text{-}C21)]^+$. Unfortunately, the complexes of BME-C21 with K^+, Rb^+ and Cs^+ were not amenable to our competitive stability constant determination method due to the low stability of the Ag^+ complex in pyridine.

2.3.3 Stability Constants of the Complexes of the Lariat Ether BME-C22 in Non-Aqueous Solution

The apparent stability constants of BME-C22 with the alkali metal ions and Ag^+ in acetonitrile, propylene carbonate, methanol, dimethylformamide and pyridine are shown in Table 2.3.

The cryptand, C222, with a cavity size of 1.4 Å [6-7], is K^+ selective as a result of K^+ (having an 8-coordinate ionic radius of 1.51 Å [1]) most closely matching the cavity size of C222. In the solvents methanol and dimethylformamide, the K^+ complex of BME-C22 is the most stable which suggests that BME-C22 forms a cavity of approximately 1.4 Å if it adopts the *syn* conformation. Thus, K^+ minimises the strain within the BME-C22 cavity and produces the most stable complex in the solvents, methanol and dimethylformamide, but not in the lower electron donating solvents, acetonitrile and propylene carbonate, as explained below. However, similar to the case for BME-C21 (Section 2.3.1), the ligand BME-C22 is able to accommodate Na^+ and Rb^+ quite well in comparison with K^+ which implies the ligand BME-C22 is able to undergo considerable variation in cavity size before the strain significantly destabilises the $[M(BME\text{-}C22)]^+$ complex.

Table 2.3 Non-aqueous stability constants for BME-C22 at 298.2 K with an ionic strength of 0.05 M NEt_4ClO_4.

		$\log(K_S / dm^3\ mol^{-1})$					
Solvent	D_N[a]	Li^+	Na^+	K^+	Rb^+	Cs^+	Ag^+
acetonitrile	14.1	5.80[c]	7.91[c]	6.19[c]	5.24[c]	4.41[c]	6.90[c]
propylene carbonate	15.1	5.1[d]	6.8[d]	6.0[d]	4.7[d]	4.0[d]	11.7[d]
methanol	23.5[b]	2.47[c]	4.57[c]	5.30[c]	4.44[c]	3.66[c]	9.39[c]
dimethyl-formamide	26.6	1.93[c]	3.31[c]	3.82[c]	3.08[c]	2.38[c]	8.28[c]
pyridine	33.1	2.79[c]	6.55[c]				1.7[d]

[a]Gutmann donor numbers from reference 10. [b]Gutmann donor number from references 11 and 12. [c]Error ± 0.05. [d]Error ± 0.1.

For BME-C22, a similar variation in complex stability with solvent is observed, with the stability constants, K_S, decreasing with increasing Gutmann donor number, D_N, except for pyridine, due to its soft base properties and large size as discussed previously for the ligand, BME-C21 (Section 2.3.2). Similarly, the $[Ag(BME\text{-}C22)]^+$ complexes are more stable than their alkali metal analogues, except in the nitrogen donor solvents, acetonitrile and pyridine, as observed for BME-C21 previously (Section 2.3.2). This is a result of Ag^+ having a much higher solvation energy in the nitrogen donor solvents in comparison with the oxygen donor solvents due to its soft acid nature, leading to a decrease in stability of the Ag^+ complexes in acetonitrile and pyridine. In contrast, the stability of the alkali metal complexes in acetonitrile and pyridine increase relative to Ag^+ due to the hard acid nature of the alkali metal ions.

The other major effect of solvent is the change in the selectivity of BME-C22 for M^+ as the Gutmann donor number, D_N, increases from acetonitrile to dimethylformamide. Thus, in acetonitrile and propylene carbonate the stability sequence $Li^+ < Na^+ > K^+ > Rb^+ > Cs^+$ is observed, with Na^+ forming the most stable complex. This sequence changes to $Li^+ < Na^+ < K^+ > Rb^+ > Cs^+$ in methanol and dimethylformamide with the K^+ complex becoming the most stable. This is consistent with the lower electron donating solvents, acetonitrile and propylene carbonate, competing less effectively for Na^+ relative to K^+ when compared with the stronger donor solvents.

2.3.4 A Comparison between the Stability Constants of the Complexes of the Lariat Ethers BME-C21 and BME-C22

The stabilities of the alkali metal complexes of BME-C22 are less than those of BME-C21, except for the larger cations K^+, Rb^+ and Cs^+. Thus, as the size of the ligand increases from BME-C21 to BME-C22 it is more able to accommodate the larger alkali metal ions, with the selectivity changing from Na^+ for BME-C21 to the larger K^+ for BME-C22.

The lower selectivity of BME-C22 compared to BME-C21 can be attributed to the higher flexibility of the ligand, BME-C22. For the $[Li(BME\text{-}C22)]^+$ complex, however, the larger cavity of BME-C22 is unable to effectively coordinate the smaller Li^+ ion without inducing considerable strain, and hence the Li^+ complex is generally much lower in stability that the other alkali metal complexes.

For the Ag^+ complexes there is a slight decrease in stability in going from BME-C21 to BME-C22 as a result of Ag^+ being too small for the larger cavity of BME-C22. The cavity of BME-C21 was found to be of optimal size for Na^+ (Section 2.3.1) and since Ag^+ and Na^+ have similar ionic radii (1.22 and 1.28, and 1.12 and 1.18 Å for the 7 and 8-coordinate geometries of Ag^+ and Na^+, respectively [1]) BME-C21 would be expected to provide a more optimal fit for Ag^+ in comparison with BME-C22 with a concomitant increase in stability of the Ag^+ complex. However, the Ag^+ ion binds very strongly to the ring nitrogens of both ligands as a result of its soft acid nature, leading to similarly high stabilities for the $[Ag(BME\text{-}C21)]^+$ and $[Ag(BME\text{-}C22)]^+$ complexes.

2.3.5 Effect of the Pendant Arms on the Stabilities of the Lariat Ether Complexes

The stability constants of the complexes of the lariat ethers BME-C21 and BME-C22 together with those of BHE-C21, BHE-C22, C211, C222, C21 and C22, in acetonitrile, methanol and dimethylformamide are given in Table 2.4.

Upon varying the methoxyethyl pendant arms of the lariat ethers BME-C21 and BME-C22, to the hydroxyethyl pendant arms of BHE-C21 and BHE-C22, there is little variation in complex stability. This implies that the stronger inductive effect of the methoxy donor groups over the hydroxy donor groups is counterbalanced by the greater steric hindrance of the methoxy pendant arms over the hydroxy pendant arms. In comparing the alkali metal complexes of BME-C21 with those of BHE-C21 in dimethylformamide, an increase in stability is observed for BME-C21. This may be a result of the two methoxyethyl pendant arms binding the alkali metal ions from opposite sides of the diaza crown ring in the *anti* conformation (Section 2.2) reducing the effect of steric hindrance.

The cryptands C221 and C222 have the same number and type of donor atoms as the lariat ethers BME-C21 and BME-C22, respectively, but possess rigid three-dimensional cavities, and hence are far less flexible than the lariat ethers. From Table 2.4, it is observed that the stability constants of the cryptates of the alkali metal ions and Ag^+ are greater in all three solvents, acetonitrile, methanol and dimethylformamide, by comparison with those of the complexes of the lariat ethers BME-C21 and BME-C22. The greater stability of the cryptates may be attributed to the macrobicyclic effect [5], with the three dimensional cavity of the cryptand able to

encapsulate the metal ion and generate more stable complexes by comparison with those of the monocyclic lariat ethers, which, although forming a three dimensional cavity when the two pendant arms bind the metal ion, do not possess the structural rigidity of the cryptand cavity. A number of examples of the macrobicyclic effect are reported in the literature [5,13-14]. Another result of the macrobicyclic effect is the greater selectivity exhibited by the cryptands, which leads to a greater difference between the stabilities of the alkali metal complexes. This is consistent with the rigid cavity of the cryptands being unable to accommodate smaller or larger metal ions as readily as the more flexible diaza crown and lariat ethers.

The diaza crown ethers C21 and C22 differ from the lariat ethers, BME-C21 and BME-C22, respectively, by the replacement of the amine protons by methoxyethyl pendant arms. The stability constants for the alkali metal complexes of C21 and C22 are substantially lower in acetonitrile, dimethylformamide and methanol (Table 2.4) than those of the lariat ethers BME-C21 and BME-C22. This can largely be attributed to the higher number of binding sites of the lariat ethers. Another effect of the pendant arms on the diaza crown ethers C21 and C22 is that the lariat ethers BME-C21 and BME-C22 are more selective. This implies that the addition of pendant arms on the diaza crown ethers to form lariat ethers leads to a decrease in flexibility and a greater discrimination in matching metal ion and cavity size. The more flexible C21 and C22 are able to accommodate larger and smaller alkali metal ions more readily than the lariat ethers and hence are less selective.

Table 2.4 Stability constants for the alkali metal ions and Ag^+ with a range of ligands, C21, C22, C221, C222, BME-C21, BME-C22, BHE-C21 and BME-C22 in acetonitrile, methanol and dimethylformamide.

	log(K_S / dm^3 mol^{-1})					
Ligand	Li^+	Na^+	K^+	Rb^+	Cs^+	Ag^+
			acetonitrile			
BME-C21[a]	9.13	8.17	5.24	4.39	3.77	7.08
BME-C22[a]	5.80	7.91	6.19	5.24	4.41	6.90
BHE-C21[b]	8.61	7.00				6.24
C221	10.33[c]	12.4[d]	9.5[c]	7.27[c]	5.15[c]	11.24[c]
C222[c]	6.97	9.63	11.3	9.50	4.57	8.99
C21[e]			2.11			6.55
C22	4.39[f]	4.49[g]	4.35[g]	3.37[h]	2.25[g]	7.94[i]
			methanol			
BME-C21[a]	3.01	4.89	4.69	3.97	3.46	9.86
BME-C22[a]	2.47	4.57	5.30	4.44	3.66	9.39
BHE-C21[b]	2.85	4.71				9.36
BHE-C22[b]		4.87				
C221	5.38[j]	9.65[j]	8.54[j]	6.74[j]	4.33[k]	14.64[l]
C222	2.6[k]	7.9[j]	10.4[j]	8.98[j]	4.4[m]	12.29[l]
C21		< 1.5[n]	< 1.5[n]			7.63[o]
C22		1.0[p]	2.0[p]	1.2[p]		9.99[i]
			dimethylformamide			
BME-C21[a]	2.23	3.50	3.31	2.84	2.31	8.37
BME-C22[a]	1.93	3.31	3.82	3.08	2.38	8.28
BHE-C21[b]	2.36	3.93	3.08	2.50	2.11	9.34
BHE-C22[b]	2.29	3.65	4.66	3.56	3.36	9.13
C221[c]	3.58	7.93	6.66	5.35	3.61	12.41
C222[c]		6.17	7.98	6.78	2.16	10.07
C21		2.1[q]				
C22	~ 0[f]	< 2[r]	<2[r]		0.61[f]	9.91[i]

[a]This work. [b]Ref. 15. [c]Ref. 16. 0.1 M Et_4NClO_4 [d]Ref. 17. 0.1 M Bu_4NClO_4 [e]Ref. 18. [f]Ref. 19. [g]Ref. 20. [h]Ref. 21. [i]Ref. 22. [j]Ref. 23. [k]Ref. 23. 0.01 M Et_4NBr [l]Ref. 23. 0.1 M Et_4NClO_4. [m]Ref. 5. 0.01 M Et_4NBr. [n]Ref. 23, 24. [o]Ref. 25. [p]Ref. 26. [q]Ref. 27. [r]Ref. 28.

2.4 Stability Constants of the Complexes of the Tetraaza Macrocyclic Ligands TMEC14 and (*S*)-THPC14 in Non-Aqueous Solution

A diagram showing the ligands TMEC14 and (*S*)-THPC14, with related ligands TMEC12 and (*S*)-THPC12 appears in Figure 2.3.

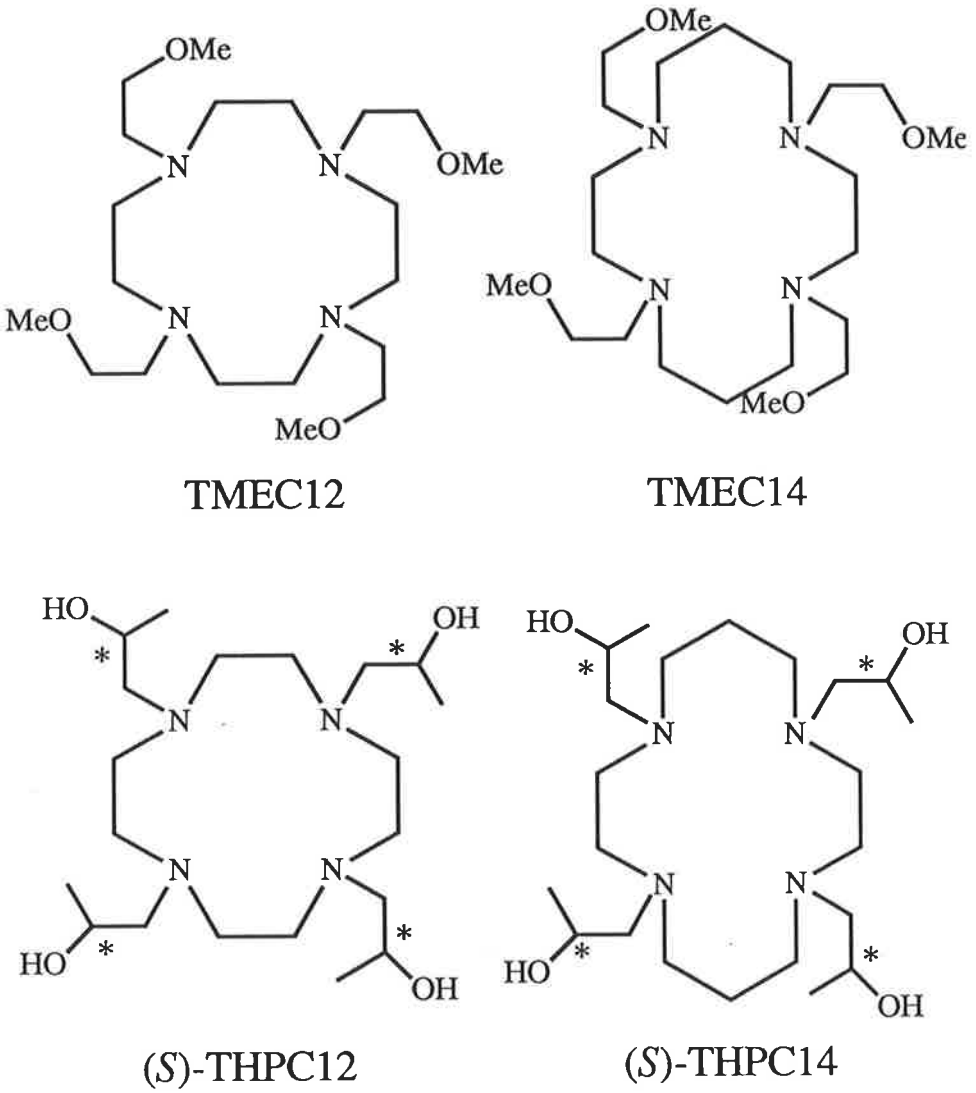

Figure 2.3 The tetraaza macrocyclic ligands TMEC12, TMEC14, (*S*)-THPC12 and (*S*)-THPC14 (* indicates chiral carbons are in the (*S*) configuration).

2.4.1 Stability Constants of the Complexes of the Tetraaza Macrocyclic Ligands TMEC14 and (*S*)-THPC14

The stability constants of TMEC14 and THPC14 with the alkali metal ions and Ag^+ in acetonitrile, dimethylformamide and methanol determined in this study are given in Table 2.5.

For the stability constants of TMEC14 and THPC14 from Table 2.5 there are a number of trends evident. Firstly, in the oxygen donor solvents methanol and dimethylformamide, the K^+ complexes of TMEC14 and THPC14 are the most stable, consistent with the K^+ ion being of optimum size for the 14-membered ring of the two ligands. In acetonitrile, however, the selectivity changes, with the Li^+ complex becoming the most stable, as discussed below (Section 2.4.2). The other notable aspect of the large 14-membered ring is the poor selectivity shown by TMEC14 and THPC14 for the complexes of M^+ in Table 2.5 in all three solvents, acetonitrile, dimethylformamide and methanol, consistent with the high flexibility of the 14-membered macrocyclic ring.

2.4.2 Variation of Stability Constants with Solvent for the Complexes of the Tetraaza Macrocyclic Ligands TMEC14 and THPC14

For the alkali metal complexes of TMEC14 and THPC14 in Table 2.5, K_S varies substantially with the nature of the solvent. Firstly, it is observed that the stability constants, K_S, decrease as the Gutmann donor number, D_N, increases for all three solvents. Hence, the stability constants decrease along the series acetonitrile, methanol and dimethylformamide, consistent with the stronger donor solvents competing more effectively with the ligand for the alkali metal ions. The stabilities of the Ag^+ complexes of TMEC14 and THPC14 also decrease with increasing D_N except in acetonitrile, which is a nitrogen donor solvent and hence strongly solvates the Ag^+ ion leading to a decrease in the stability of the Ag^+ complex.

The stability constants of the Ag^+ complexes of TMEC14 and THPC14 from Table 2.5 are substantially higher than their alkali metal analogues in all three solvents. The tetraaza macrocyclic ligands, TMEC14 and THPC14, each have four nitrogen donor atoms, so that the soft Ag^+ ion will bind very strongly to these soft nitrogen groups, even in the presence of a strong nitrogen donor solvent, such as acetonitrile, in which the Ag^+ ion is highly solvated. This leads to the Ag^+ complex being more stable that the alkali metal complexes in all three solvents, acetonitrile, dimethylformamide and methanol.

Table 2.5 Non-aqueous stability constants for TMEC14 and THPC14 at 298.2 K with an ionic strength of 0.05 M NEt_4ClO_4.

		TMEC14 $\log(K_S / dm^3\ mol^{-1})$					
Solvent	D_N[a]	Li^+	Na^+	K^+	Rb^+	Cs^+	Ag^+
acetonitrile	14.1	4.64[c]	4.03[c]	3.37[c]	3.32[c]	3.25[c]	8.48[c]
methanol	23.5[b]	2.65[c]	2.82[c]	3.02[c]	2.91[c]	2.69[c]	10.32[c]
dimethyl-formamide	26.6	2.37[c]	2.42[c]	2.48[c]	2.45[c]	2.40[c]	9.70[c]
		THPC14					
acetonitrile	14.1	3.72[c]	3.15[c]	3.03[c]	2.99[c]	2.93[c]	5.43[c]
methanol	23.5[b]	2.54[c]	2.65[c]	2.76[c]	2.74[c]	2.60[c]	7.84[c]
dimethyl-formamide	26.6	2.14[c]	2.19[c]	2.24[c]	2.20[c]	2.16[c]	7.29[c]

[a]Gutmann donor numbers from reference 10. [b]Gutmann donor number from references 11 and 12. [c]Error ± 0.05.

Another major effect of solvent is the change in selectivity for the complexes of TMEC14 and THPC14 with increasing D_N. The sequence $Li^+ > Na^+ > K^+ > Rb^+ > Cs^+$ is observed in acetonitrile, with the Li^+ complex the most stable, however, in the higher electron donor solvents, methanol and dimethylformamide the sequence $Li^+ < Na^+ < K^+ > Rb^+ > Cs^+$ is observed with the K^+ complex being marginally the most stable. The change in selectivity from K^+ to Li^+ upon changing solvent is consistent with the ligand competing more effectively for Li^+ and Na^+ than for K^+ in the weak donor solvent, acetonitrile. This contrasts with the situation in methanol and dimethylformamide and can be attributed to the high flexibility of the ligands, TMEC14 and THPC14, which leads to a poor selectivity for K^+.

2.4.3 The Size Effect of the 12- and 14-Membered Rings on the Stabilities of the Complexes Formed

The stability constants of the alkali metal complexes of TMEC14 and THPC14 in the solvents, acetonitrile, methanol and dimethylformamide are given in Table 2.6, along with those for the related ligands, TMEC12 and THPC12.

The stability constants of the Ag^+ complexes of TMEC12 and THPC12 are approximately four orders of magnitude higher than those of their 14-membered analogues, TMEC14 and THPC14, respectively, regardless of solvent. This implies that the smaller 12-membered ring ligands, TMEC12 and THPC12 with four equal ($-CH_2CH_2-$) moieties between the nitrogen groups are able to optimise the bonding distances for the formation of the Ag^+ complexes. The ligands, TMEC12 and THPC12 are Na^+ selective in the solvents, methanol and dimethylformamide (Table 2.6). As Na^+ and Ag^+ have similar ionic radii (1.18 and 1.28 Å, respectively, for the 8-coordinate geometries [1]) TMEC12 and THPC12 would be expected to form Ag^+ complexes of higher stability by comparison with those of the larger TMEC14 and THPC14. In addition, a study by Hancock [32] shows the lowest energy configuration for 12-membered macrocyclic ligands is *trans*-I (Chapter 5, Figure 5.3) with the four pendant arms above the plane of the ring. This suggests that the Ag^+ complexes of TMEC12 and THPC12 are 8-coordinate *trans*-I, and is further supported by the characterisation of a range of alkali and heavy metal complexes of TMEC12 and THPC12 which are 8-coordinate *trans*-I [30,31]. In contrast, the lowest energy configuration for 14-membered macrocyclic ligands is *trans*-III (Chapter 5, Figure 5.3) with two pendant arms above the plane of the ring, and two below. This suggests that the Ag^+ complexes of TMEC14 and THPC14 are 6-coordinate *trans*-III. This is further supported by the characterisation of a range of alkali and heavy metal complexes of TMEC14 and THPC14 which are 6-coordinate *trans*-III (although some were found to be 6-coordinate *cis*-V - see Chapter 5). Thus, the higher coordination of the Ag^+ complexes of TMEC12 and THPC12 by comparison with those of their 14-membered analogues, TMEC14 and THPC14 results in more stable complexes.

Similarly, the stabilities of the alkali metal complexes of TMEC12 and THPC12 are greater than those of TMEC14 and THPC14, respectively, except for some of the Cs^+ complexes. The smaller 12-membered ring ligands, TMEC12 and THPC12 are less flexible than their 14-membered ring analogues, and have a more optimal size and positioning of donor atoms for the formation of 8-coordinate complexes as explained above. The 14-membered ring ligands, TMEC14 and THPC14 are simply too large for optimal coordination, except for the larger alkali metal ions such as Cs^+, and would probably form 6-coordinate complexes as for their Ag^+ analogues above.

2.4.4 Effect of the Pendant Arms on the Stabilities of the Complexes of the Tetraaza Macrocyclic Ligands

It is seen from Table 2.6 that the stability constants of the Ag^+ complexes of TMEC14 and THPC14 differ by two to three orders of magnitude in all three solvents, acetonitrile, methanol and dimethylformamide, with TMEC14 forming the most stable complexes of the two ligands. Similarly, the alkali metal complexes of TMEC14 are slightly greater in stability than those of THPC14.

The methoxyethyl pendant arms of TMEC14 have a stronger inductive effect than the 2-hydroxypropyl pendant arms of THPC14, however this is often counterbalanced by the greater steric hindrance induced by the bulkier methoxy groups, particularly when there are four pendant arms on a relatively small 14-membered ring. For THPC14, the pendant arms are (*S*)-2-hydroxypropyl, with methyl groups on the chiral carbon, and hence there may be considerable steric hindrance between these groups upon complexation. This implies that the lower stability of the alkali metal and Ag^+ complexes of THPC14 by comparison with those of TMEC14 results from a combination of the weaker inductive effect of the hydroxy groups in THPC14 and differing steric hindrance within the complexes formed with respect to the methoxy and methyl groups of TMEC14 and THPC14, respectively.

Table 2.6 Complexes of the alkali metal ions and Ag^+ with a range of ligands, TMEC12, TMEC14, THPC12 and THPC14 in acetonitrile, methanol and dimethylformamide.

	log(K_S / dm^3 mol^{-1})					
Ligand	Li^+	Na^+	K^+	Rb^+	Cs^+	Ag^+
			acetonitrile			
TMEC12[a]	9.34	9.13	6.07	4.85	3.55	12.30
TMEC14[b]	4.64	4.03	3.37	3.32	3.25	8.48
THPC12[c]	7.65	5.98	3.20	3.16	3.10	8.51
THPC14[b]	3.72	3.15	3.03	2.99	2.93	5.43
			methanol			
TMEC12[a]	4.1	6.2	3.9	3.0	2.5	14.2
TMEC14[b]	2.65	2.82	3.02	2.91	2.69	10.32
THPC12[c]	4.0	4.8	3.5	3.4	3.2	12.80
THPC14[b]	2.54	2.65	2.76	2.74	2.60	7.84
			dimethylformamide			
TMEC12[a]	3.60	5.68	3.62	2.72	2.20	13.73
TMEC14[b]	2.37	2.42	2.48	2.45	2.40	9.70
THPC12[c]	3.24	3.76	3.63	3.56	3.41	11.30
THPC14[b]	2.14	2.19	2.24	2.20	2.16	7.29

[a]Ref. 30. [b]This work. [c]Ref. 31.

References

1 R. D. Shannon, *Acta Crystallogr., Sect. A*, 1976, **32**, 751.

2 G. W. Gokel, *Chem. Soc. Rev.*, 1992, 39.

3 R. D. Gandour, F. R. Fronczek, V. J. Gatto, C. Minganti, R. A. Shultz, B. D. White, K. A. Arnold, D. Mazzocchi, S. R. Miller and G. W. Gokel, *J. Am. Chem. Soc.*, 1986, **108**, 4078.

4 K. A. Arnold, L. Echegoyen, F. R. Fronczek, R. D. Gandour, V. J. Gatto, B. D. Gatto, B. D. White and G. W. Gokel, *J. Am. Chem. Soc.*, 1987, **109**, 3716.

5 J.-M. Lehn and J. P. Sauvage, *J. Am. Chem. Soc.*, 1975, **97**, 6700.

6 N. K. Dalley, R. M. Izatt and J. J. Christensen, *"Synthetic Multidentate Macrocyclic Compounds"*, Academic Press (New York), 1978.

7 C. J. Pederson and H. K. Frensdorff, *Angew. Chem.*, Int. Ed. Engl., 1972, **11**, 16.

8 B. G. Cox, J. Garcia-Rosas and H. Schneider, *J. Am. Chem. Soc.*, 1981, **103**, 1054.

9 U. Mayer and V. Gutmann, *Top. Curr. Chem.*, 1972, **27**, 113.

10 V. Gutmann, *"Coordination Chemistry in Non-Aqueous Solvents"*, Springer, New York, 1968.

11 R. H. Erlich, E. Roach and A. I. Popov, *J. Am. Chem. Soc.*, 1970, **92**, 4989.

12 W. J. Dewitte and A. I. Popov, *J. Soln. Chem.*, 1976, **5**, 231.

13 J.-M. Lehn, *Struct. Bonding* (Berlin), 1973, **16**, 1.

14 J.-M. Lehn, *Acc. Chem. Res.*, 1978, **11**, 49.

15 T. Rodopoulos, P.-A. Pittet and S. F. Lincoln, *J. Chem. Soc., Dalton Trans.*, 1993, 1055, 2079.

16 B. G. Cox, J. Garcia-Rosas and H. J. Schneider, *J. Am. Chem. Soc.*, 1981, **103**, 1384.

17 M.-F. Lejaille, M.-H. Livertoux and C. Guidon, *J. Bull. Soc. Chim. Fr.*, 1978, 1373.

18 H. J. Buschman, *Inorg. Chim. Acta*, 1986, **120**, 125.

19 M. Shamsipur and A. I. Popov, *Inorg. Chim. Acta*, 1980, **43**, 243.

20 R. D. Boss and A. I. Popov, *J. Inorg. Chem.*, 1986, **25**, 1747.

21 S. Kulstad and L. A. Malmsten, *J. Inorg. Nucl. Chem.*, 1980, **42**, 573.

22 B. G. Cox, P. Firman, H. Horst and H. Schneider, *Polyhedron*, 1983, **2**, 343.

23 B. G. Cox, H. Schneider and J. Stroka, *J. Am. Chem. Soc.*, 1978, **100**, 4746.
24 V. J. Gatto, K. A. Arnold, A. M. Viscariello, S. R. Miller and G. W. Gokel, *Tetrahedron Lett.*, 1986, **27**, 327.
25 V. J. Gatto, K. A. Arnold, A. M. Viscariello, S. R. Miller, C. R. Morgan and G. W. Gokel, *J. Org. Chem.*, 1986, **51**, 5373.
26 H. J. Buschman, *Inorg. Chim. Acta*, 1985, **102**, 95.
27 H. K. Frensdorff, *J. Am. Chem. Soc.*, 1971, **93**, 600.
28 P. Clarke, A. Abou-Hamdan, A. M. Hounslow and S. F. Lincoln, *Inorg. Chim. Acta*, 1988, **154**, 83.
29 I. Morolleau, J. P. Gisselbreacht, M. Gross, F. Arnaud-Neu and M. T. Schwing-Weill, *J. Chem. Soc. Dalton Trans.*, 1989, 367.
30 A. K. W. Stephens and S. F. Lincoln, unpublished material.
31 R. Dhillon and S. F. Lincoln, unpublished material.
32 R. D. Hancock, *Acc. Chem. Res.*, 1990, **23**, 253.

3. Aqueous Titrations

3.1 Protonation and Stability Constants of the Complexes of the Lariat Ethers BME-C21 and BME-C22

Schematic diagrams of the lariat ethers BME-C21 and BME-C22 studied, and the related ligands, C21, C22, C221, C222, BHE-C21 and BHE-C22 appear in Figure 3.1.

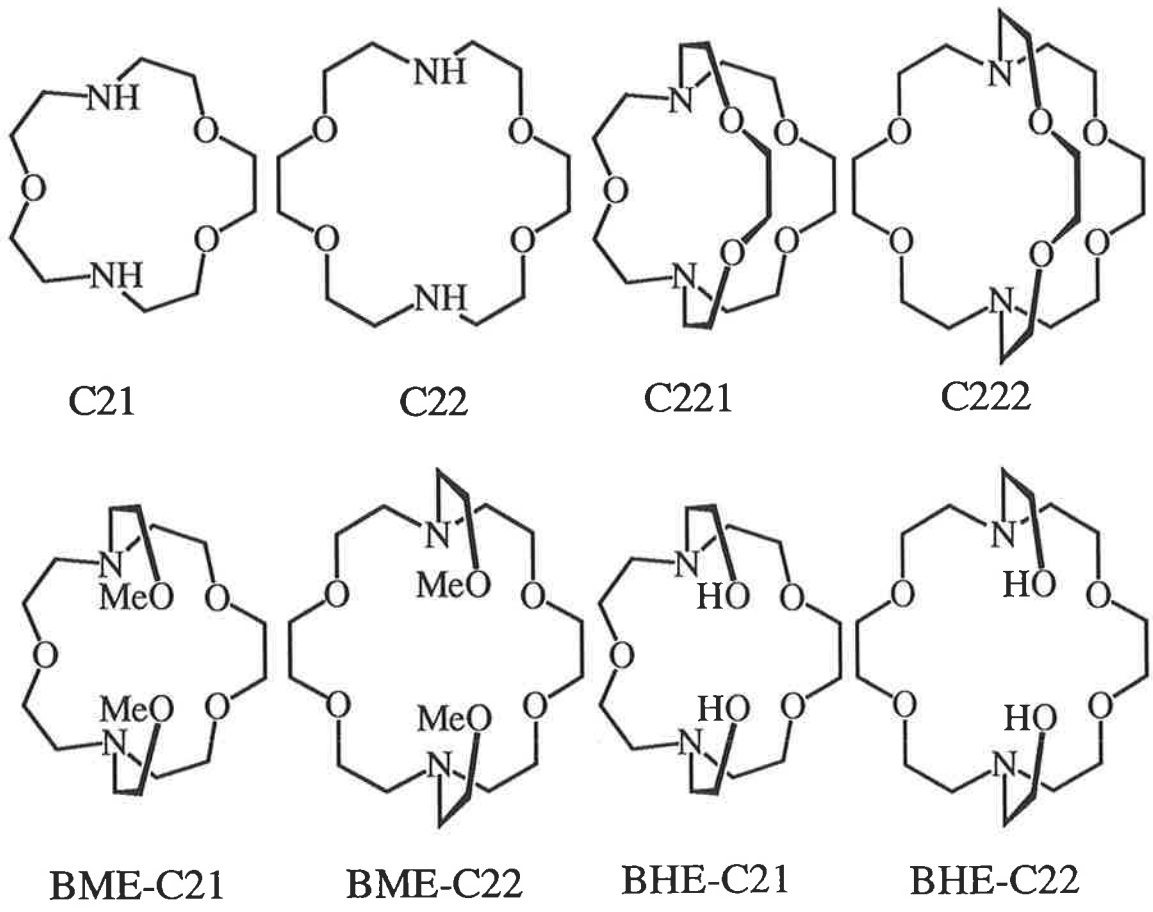

Figure 3.1 The diaza crown ethers, C21 and C22, the cryptands, C221 and C222, and the lariat ethers, BME-C21, BME-C22, BHE-C21 and BHE-C22.

3.1.1 Protonation Constants of BME-C21 and BME-C22

In water, the diaza crown ethers, lariat ethers and cryptands act as di-basic species, allowing protonation of both ring nitrogens. These protonation constants, K_1 and K_2 are defined as:

$$H^+ + L \underset{}{\overset{K_1}{\rightleftharpoons}} [LH]^+$$

$$K_1 = \frac{[LH^+]}{[H^+][L]} \qquad \textbf{3.1}$$

and $$H^+ + LH^+ \overset{K_2}{\rightleftharpoons} [LH_2]^{2+}$$

$$K_2 = \frac{[LH_2^{2+}]}{[H^+][LH^+]} \qquad \textbf{3.2}$$

where K_1 and K_2 are the stepwise protonation constants of the ligand, L, where L is a diaza macrocyclic ligand.

The equilibrium constants, K_{a1} and K_{a2} are defined as:

$$LH^+ \overset{K_{a1}}{\rightleftharpoons} L + H^+$$

$$K_{a1} = \frac{[L][H^+]}{[LH^+]} \qquad \textbf{3.3}$$

and $$LH_2^{2+} \overset{K_{a2}}{\rightleftharpoons} LH^+ + H^+$$

$$K_{a2} = \frac{[LH^+][H^+]}{[LH_2^{2+}]} \qquad \textbf{3.4}$$

where K_{a1} and K_{a2} are the acid ionisation or acid dissociation constants. The pK_a's of the ligand are defined as:

$$\log K_1 = -\log K_{a1} = pK_{a1} \qquad \textbf{3.5}$$

and $$\log K_2 = -\log K_{a2} = pK_{a2} \qquad \textbf{3.6}$$

The protonation constants of the lariat ethers BME-C21 and BME-C22, and related ligands, C21, C22, C221, C222, BHE-C21 and BHE-C22 are given in Table 3.1.

Table 3.1 The protonation constants of BME-C21, BME-C22 and the related ligands, C21, C22, C221, C222, BHE-C21 and BHE-C22.

Ligand	Cavity Size (Å)	pK_{a1}	pK_{a2}
C21[a]		8.76	8.04
C22[a]	~1.5[b]	9.08	7.94
C221[a]	1.1[b]	11.02	7.74
C222[a]	1.4[b]	10.00	7.53
BME-C21[c]		8.64 ± 0.05	7.16 ± 0.05
BME-C22[c]		8.42 ± 0.05	7.07 ± 0.05
BHE-C21[d]		8.79	7.57
BHE-C22[d]		8.60	7.20

[a]Ref. 1. [b]Ref. 2, 3. [c]This work. [d]Ref. 4.

For the diaza species, the nitrogen lone pair can adopt three main conformations, *endo-endo*, *endo-exo* and *exo-exo* (Figure 3.2).

When the diaza macrocyclic ligands are monoprotonated (pK_{a1}) it is anticipated that the ligand will adopt the *endo-endo* conformation, in which both nitrogen lone pairs are able to interact with the proton residing in the cavity.

The second protonation of the ligand leads to repulsion within the cavity between the two protonated nitrogens, particularly in the *endo-endo* configuration, which would probably lead to the *endo-exo* or *exo-exo* configuration becoming predominant for the diprotonated species. Thus, although it is anticipated that all conformations exchange rapidly between *endo* and *exo* in solution, the average structure would probably be *endo-exo* to minimise repulsion. In addition, there is a statistical effect, with the monoprotonated species only having one nitrogen which can be protonated. Hence, as a result of the extra repulsion for the diprotonated species and

also the statistical effect, there is a decrease in pK_{a2} compared with pK_{a1}. The difference between pK_{a1} and pK_{a2} is larger for the cryptands than for the crown and lariat ethers due to the cryptands adopting a more three dimensional structure, and hence shielding the proton from the solvent to a greater extent than for the crown and lariat ethers. The pK_{a1} values for the cryptands, C221 and C222 are much greater than those of the lariat ethers, BME-C21 and BME-C22. This can be attributed to the cryptand cavity shielding the proton more effectively from the solvent for the monoprotonated species than do the more flexible lariat ethers with a concomitant increase in pK_{a1} for the cryptands. The values of pK_{a2} for the cryptands and lariat ethers, however, are similar, with the greater electrostatic repulsion within the cavity leading to the *endo-exo* conformation becoming predominant for the cryptates. This leads to a similar interaction with the solvent for the second proton of the diprotonated species, resulting in similar pK_{a2} values for the cryptands and lariat ethers. In addition, there is a general decrease in the pK_a values in Table 3.1 upon increasing effective cavity size, particularly upon comparing the cryptand C221 with C222. Thus, as the cavity size increases the protons are more exposed to the solvent with a concomitant decrease in the pK_a's, particularly for the monoprotonated species with the two nitrogen lone pairs unable to optimally interact with the proton residing in the cavity due to their greater separation.

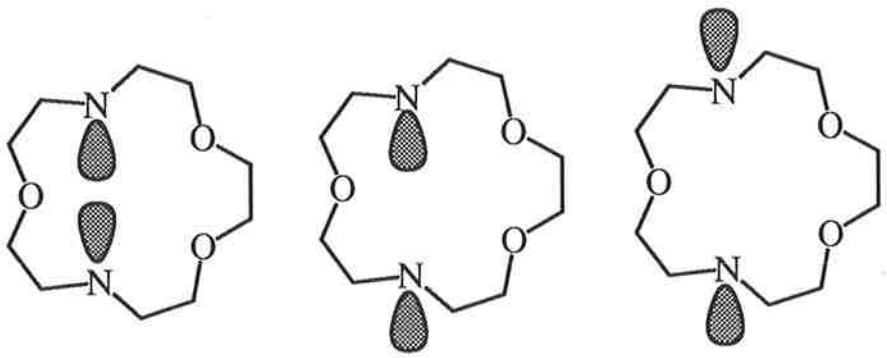

endo-endo *endo-exo* *exo-exo*

Figure 3.2 The crown ether C21 is used to demonstrate the three configurations which the nitrogen lone pairs may adopt. The *endo-endo* configuration is the most probable conformer, with both lone pairs of electrons directed into the centre of the intramolecular cavity. This maximises the interaction of a proton or cation with the nitrogen lone pairs.

3.1.2 Stability Constants of the Complexes of the Lariat Ethers BME-C21 and BME-C22

The stability constants, K_S, for the complexes of the lariat ethers BME-C21 and BME-C22 with a range of divalent metal ions are given in Table 3.2 along with those for the related ligands, BHE-C21, BHE-C22, C221, C222, C21 and C22.

K_S, the stability constant is given by:

$$L + M^{2+} \underset{}{\overset{K_S}{\rightleftharpoons}} [ML]^{2+}$$

where $K_S = \dfrac{[ML^{2+}]}{[L][M^{2+}]}$ **3.7**

for $M^{2+} = Mg^{2+}, Ca^{2+}, Sr^{2+}, Ba^{2+}, Mn^{2+}, Co^{2+}, Ni^{2+}, Cu^{2+}, Zn^{2+}, Cd^{2+}, Hg^{2+}$ and Pb^{2+}

and L = BME-C21 and BME-C22

There are a number of trends evident in Table 3.2, with the metal complexes placed in three groups. The alkaline metal complexes of Mg^{2+}, Ca^{2+}, Sr^{2+} and Ba^{2+}, the first row transition metal complexes of Mn^{2+}, Co^{2+}, Ni^{2+}, Cu^{2+} and Zn^{2+}, and the heavy metal complexes of Cd^{2+}, Pb^{2+} and Hg^{2+}.

3.1.2.1 Complexes of the Alkaline Earth Metal Ions, Mg^{2+}, Ca^{2+}, Sr^{2+} and Ba^{2+}

For the alkaline metal complexes of the lariat ether BME-C21, the stability sequence $Mg^{2+} < Ca^{2+} < Sr^{2+} > Ba^{2+}$ is observed. This suggests that the ligand BME-C21 is of optimal size for the complexation of Sr^{2+} (ionic radii of 1.21 Å for the 7-coordinate geometry [5]). However, in the high electron donating solvents, methanol and dimethylformamide, BME-C21 was found to be Na^+ selective (Chapter 2, Section 2.2.1) suggesting that in water (with a D_N of 33.0) the Ca^{2+} complex would be the most stable due to Ca^{2+} having a similar ionic radii to Na^+ (1.08 and 1.12 Å, respectively, for the 7-coordinate geometries [5]). The solvation energies of the alkaline earth metal ions vary to a greater extent than for the alkali metal ions, and this greater difference in solvation energy leads to Ca^{2+} becoming disfavoured in comparison with Sr^{2+}, with the Sr^{2+} complex becoming the most stable. The smaller ion, Mg^{2+} is too small to optimally fit the cavity and is also

disfavoured relative to Ca^{2+} on the basis of its high solvation energy, which leads to complexes of lower stability. Similarly, the low stability of the Ba^{2+} complex can be attributed to its large size which leads to less than optimal bonding distances within the complex, although the stability is close to that of the Sr^{2+} complex, with the Ba^{2+} complex favoured by a smaller solvation energy relative to Sr^{2+}. In contrast, the stability constants of the alkaline earth metal complexes of BME-C22 follow the sequence $Mg^{2+} < Ca^{2+} < Sr^{2+} < Ba^{2+}$, indicating that the larger cavity of the BME-C22 accommodates the larger Ba^{2+} (1.38 and 1.42 Å for the 7 and 8-coordinate geometries, respectively [5]) more optimally than it does the smaller ions, Mg^{2+}, Ca^{2+} and Sr^{2+}. From Table 3.2 it is observed the stability constants of the Sr^{2+} complexes for the ligands BME-C21 and BME-C22 are very similar. Thus, although the Sr^{2+} complex of BME-C22 may be expected to be less stable than that of BME-C21 due to the larger cavity size, the presence of the extra donor atom in BME-C22 counterbalances this size effect and hence the Sr^{2+} complexes of BME-C21 and BME-C22 are of similar stability.

3.1.2.2 Complexes of the First Row Transition Metal Ions, Mn^{2+}, Co^{2+}, Ni^{2+}, Cu^{2+} and Zn^{2+}

For complexes of the alkaline earth and transition metal ions with flexible ligands the Irving-Williams series [12,13] predicts the stability sequence $Ba^{2+} < Sr^{2+} < Ca^{2+} < Mg^{2+} < Mn^{2+} < Co^{2+} < Ni^{2+} < Cu^{2+} > Zn^{2+}$. The alkaline earth metal ions Mg^{2+}, Ca^{2+}, Sr^{2+} and Ba^{2+} are hard acids, and hence prefer oxygen donor groups to nitrogen donor groups. Thus, in aqueous solution the transition metal ions bind more strongly to the nitrogen donor atoms of the lariat ethers, BME-C21 and BME-C22 than do the harder alkaline metal ions. Hence, the greater stability predicted for the transition metal ions arises from their borderline hard character [14,15], higher charge density, and crystal field stabilisation energy (CFSE) [16]. However, from Table 3.2 it is observed that the alkaline metal ion complexes are not always less stable than their transition metal analogues. This arises from a combination of optimum size for complexation and the alkaline metal ions more readily adopting 7 and 8-coordinate complexes.

The stability of the complexes of both lariat ethers, BME-C21 and BME-C22 follow the sequence $Mn^{2+} > Co^{2+} > Ni^{2+} < Cu^{2+} > Zn^{2+}$, with the Mn^{2+} and Co^{2+} complexes relatively more stable than predicted from the Irving-Williams series. This stability sequence can be attributed to the

increase in ionic radii along the series $Mn^{2+} > Co^{2+} \approx Zn^{2+} > Ni^{2+}$ coinciding with an increase in stability along the same sequence for BME-C21 and BME-C22. Thus, as the ionic radii of the metal ions increase from Ni^{2+} (0.69 Å [5]) to Mn^{2+} (0.83 Å [5]) the metal ion is able to more optimally interact with the binding sites of the two ligands, BME-C21 and BME-C22. The decrease in the stability of $[M(BME\text{-}C22)]^{2+}$ in comparison with $[M(BME\text{-}C21)]^{2+}$ for $M^{2+} = Mn^{2+}$, Co^{2+}, Ni^{2+} and Zn^{2+}, results from the larger size of BME-C22. The $[Cu(BME\text{-}C21)]^{2+}$ and $[Cu(BME\text{-}C22)]^{2+}$ complexes are of higher stability than the other transition metal complexes probably as a result of the tetragonal distortion for d^9 Cu^{2+} [16]. The $[Cu(BME\text{-}C22)]^{2+}$ complex is of higher stability than the $[Cu(BME\text{-}C21)]^{2+}$ complex, possibly as a result of a more optimal interaction between the tetragonally distorted Cu^{2+} ion and the binding sites of BME-C22 compared to those of BME-C21.

3.1.2.3 Complexes of the Heavy Metal Ions, Cd^{2+}, Hg^{2+} and Pb^{2+}

The heavy metal ions, Cd^{2+}, Hg^{2+} and Pb^{2+}, tend to form the most stable complexes with the lariat ethers BME-C21 and BME-C22 (Table 3.2). In comparing the Zn^{2+} complexes of both ligands with their Cd^{2+} analogues, an increase in stability is observed for the Cd^{2+} complexes. The reason for this increase may be attributed to the more optimal fit of the larger Cd^{2+} (with the Zn^{2+} ion being too small), the greater softness of the Cd^{2+} leading to stronger bonds with the two ring nitrogen atoms, and Cd^{2+} more readily adopting a 7 or 8-coordinate geometry for BME-C21 and BME-C22, respectively. For the heavy metal complexes of BME-C21 and BME-C22 the stability of the complexes follow the sequence $Cd^{2+} < Pb^{2+} < Hg^{2+}$. The main factors in this sequence are the increase in softness along the sequence $Pb^{2+} < Cd^{2+} < Hg^{2+}$ [14,15], leading to stronger bonds with the soft ring nitrogen atoms in the diaza crown rings of the two lariat ethers, and also the decreasing solvation energies along the sequence $Cd^{2+} > Hg^{2+} > Pb^{2+}$ [17], leading to the formation of more stable complexes. The small difference between the stabilities of the heavy metal complexes of BME-C21 compared with those of BME-C22 indicates a higher preference for the ring nitrogens, over the harder oxygen binding sites with the heavy metal ions binding to the ring nitrogens very strongly leading to little variation between the stabilities of the two lariat ether complexes. Any decrease in stability for the complexes of BME-C21 compared to those of BME-C22 can then be attributed simply to a less optimal fit within the larger BME-C22 cavity.

Table 3.2 Stability constants of the divalent metal complexes of BME-C21 and BME-C22, and the related ligands, BHE-C21, BHE-C22, C221, C222, C21 and C22 in aqueous solution at 298.2 K with an ionic strength of 0.1 M Et_4NClO_4

	Ionic Radii[a]	log(K_S / dm^3 mol^{-1})							
M^{2+}	(Å)	BME-C21[b]	BME-C22[b]	BHE-C21[c]	BHE-C22	C221	C222	C21	C22
Mg^{2+}	0.72	< 2.0	< 2.0	~ 2	< 2.0[d]	< 2.0[e]	< 2.0[e]		< 0[i]
Ca^{2+}	1.00 (1.12)	2.8 ± 0.1	2.4 ± 0.1	4.86	4.08[d]	6.95[e]	4.57[h]		1.74[h]
Sr^{2+}	1.18 (1.26)	3.62 ± 0.05	3.64 ± 0.05	4.15	4.29[c]	7.35[e]	8.26[h]		2.57[h]
Ba^{2+}	1.35 (1.42)	3.45 ± 0.05	4.36 ± 0.05	3.99	5.33[c]	6.30[e]	9.7[h]		2.98[h]
Mn^{2+}	0.83	4.08 ± 0.05	2.78 ± 0.05	5.28	2.88[c]				
Co^{2+}	0.75	3.76 ± 0.05	2.68 ± 0.05	6.62	2.80[c]	5.40[f]	< 2.5[f]	5.05[f]	< 2.5[f]
Ni^{2+}	0.69	3.33 ± 0.05	2.32 ± 0.05	4.73	2.69[c]	4.28[f]	< 3.5[f]	3.73[f]	< 2.5[f]
Cu^{2+}	0.73	5.38 ± 0.05	5.89 ± 0.05	8.11	6.60[d]	7.56[f]	6.81[f]	7.17[f]	6.18[f]
Zn^{2+}	0.74	3.79 ± 0.05	2.58 ± 0.05	6.18	3.03[c]	5.41[f]	< 2.5[f]	5.19[f]	3.19[f]
Cd^{2+}	0.95 (1.10)	5.69 ± 0.05	4.72 ± 0.05	7.70	7.96[d]	10.04[f]	7.10[f]	6.46[f]	5.31[f]
Hg^{2+}	1.02 (1.14)	15.2 ± 0.1	14.1 ± 0.1	15.07	14.58[c]	19.97[g]	18.2[h]		17.85[h]
Pb^{2+}	1.19 (1.29)	8.12 ± 0.05	8.18 ± 0.05	8.91	9.20[d]	13.12[f]	12.72[f]	5.85[f]	6.90[f]

[a]Ref. 5. The first number refers to the ionic radius for the 6-coordinate geometry, the numbers in parentheses are for the 8-coordinate geometry. [b]This work. [c]Ref. 4. [d]Ref. 6. [e]Ref. 7. 0.05 M Et_4NBr [f]Ref. 8. [g]Ref. 9. [h]Ref. 10. 0.1 M Et_4NCl [i]Ref. 11. 0.1 M $NaNO_4$.

3.1.2.4 Effect of Pendant Arms on the Stabilities of the Lariat Ether Complexes in Aqueous Solution

Upon comparing the stabilities of the divalent metal complexes of the methoxyethyl pendant armed lariat ethers, BME-C21 and BME-C22 with their hydroxyethyl pendant armed analogues, BHE-C21 and BHE-C22 from Table 3.2 there is a general increase in stability for the complexes of BHE-C21 and BHE-C22. The methoxy groups have a greater inductive effect by comparison with the hydroxy groups, however this is apparently counterbalanced by the greater steric hindrance of the bulkier methoxy groups. As the stabilities of the complexes for BME-C21 and BME-C22 are less than those of BHE-C21 and BHE-C22, respectively, this suggests that the steric hindrance of the methoxyethyl pendant arms is the main reason for the decrease in stability. In addition, the hydroxy groups of BHE-C21 and BHE-C22 may hydrogen bond with water, however this appears to have an insufficient destabilising effect to decrease the stabilities of the BHE-C21 and BHE-C22 complexes below those of their methoxy analogues.

A general increase in stability for the cryptates of C221 and C222 compared to those of BME-C21 and BME-C22 is observed and can be attributed to the macrobicyclic effect [7,18-19], with the cryptands able to encapsulate the metal ions more effectively than can the more flexible BME-C21 and BME-C22 leading to cryptates of greater stability.

Upon comparing the stabilities of the complexes of the lariat ethers BME-C21 and BME-C22 with those of the diaza crown ethers, C21 and C22, respectively, the lower number of binding sites of the diaza crown ethers would be expected to lead to the formation of less stable complexes. This is reflected in the stabilities of the alkaline metal complexes of C22 in comparison with those of BME-C22. However, a number of first row transition and heavy metal complexes of C21 and C22 are higher in stability in comparison with those of the lariat ethers, BME-C21 and BME-C22. This can be explained by a combination of the greater steric hindrance induced by the methoxyethyl pendant arms of the lariat ethers and the greater flexibility of the crown ethers which may allow C21 and C22 to fold over the metal ions leading to optimal geometries for the metal ion. In addition, the secondary ring nitrogens of the crown ethers, C21 and C22 would be expected to have a greater inductive effect than the tertiary ring nitrogens of the lariat ethers, BME-C21 and BME-C22, possibly leading to the formation of stronger bonds between the ring nitrogens and the soft

transition and heavy metal ions.

3.2 Protonation and Stability Constants of the Complexes of the Tetraaza Macrocyclic Ligand TMEC14

A diagram showing the tetraaza macrocyclic ligands, cyclam, TMEC12, TMEC14 and THEC12 appears in Figure 3.3.

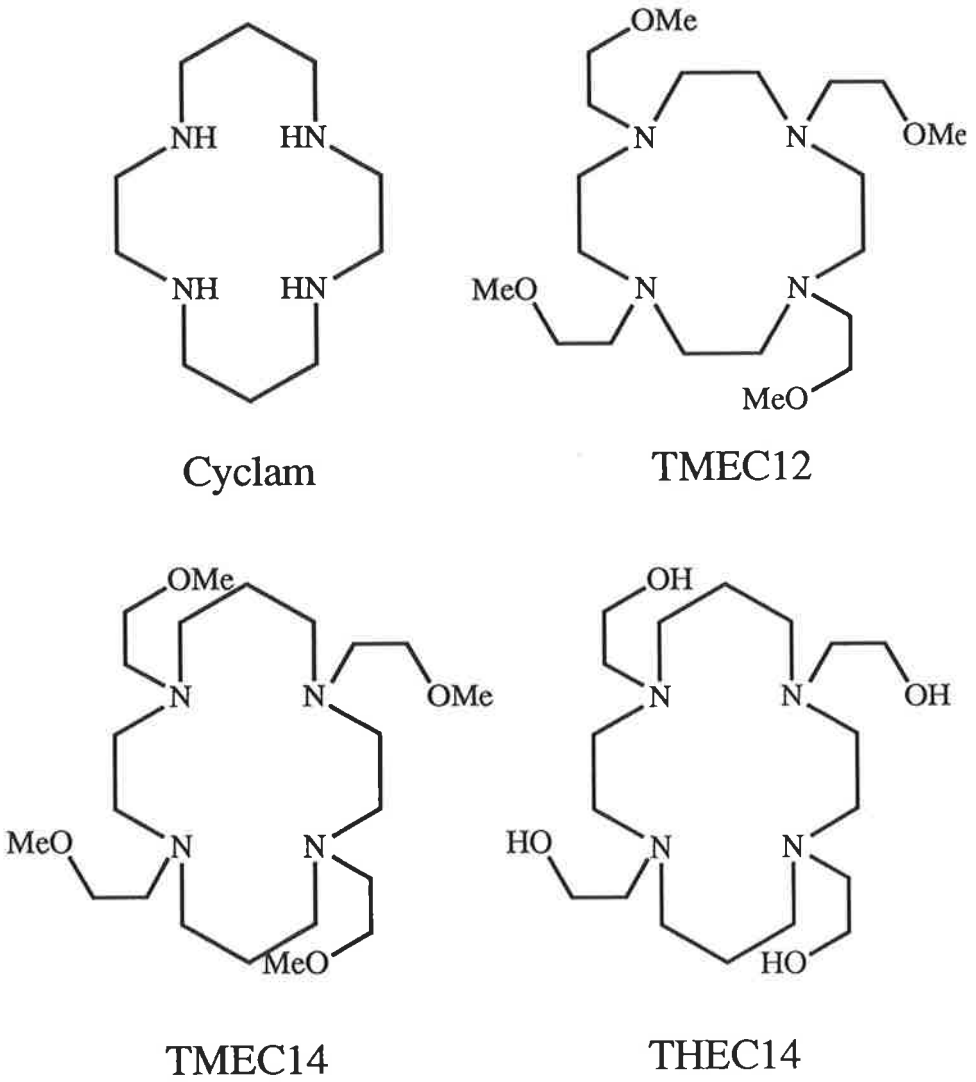

Figure 3.3 The tetraaza macrocyclic ligands, cyclam, TMEC12, TMEC14 and THEC14.

3.2.1 Protonation Constants of the Tetraaza Macrocyclic Ligand TMEC14

The tetraaza macrocyclic ligand, TMEC14 is a tetra-basic species, with four protonation constants, and two additional stepwise protonation constants, compared with the diaza species in Section 3.1. The two additional constants are defined as:

$$H^+ + LH_2^{2+} \overset{K_3}{\rightleftharpoons} LH_3^{3+}$$

where $K_3 = \dfrac{[LH_3^{3+}]}{[H^+][LH_2^{2+}]}$ **3.8**

and $$H^+ + LH_3^{3+} \overset{K_4}{\rightleftharpoons} LH_4^{4+}$$

where $K_4 = \dfrac{[LH_4^{4+}]}{[H^+][LH_3^{3+}]}$ **3.9**

leading to K_{a3} and K_{a4} defined as:

$$LH_3^{3+} \overset{K_{a3}}{\rightleftharpoons} LH_2^{2+} + H^+$$

where $K_{a3} = \dfrac{[LH_2^{2+}][H^+]}{[LH_3^{3+}]}$ **3.10**

and $$LH_4^{4+} \overset{K_{a4}}{\rightleftharpoons} LH_3^{3+} + H^+$$

where $K_{a4} = \dfrac{[LH_3^{3+}][H^+]}{[LH_4^{4+}]}$ **3.11**

and hence two additional pKa values:

$$\log K_3 = -\log K_{a3} = pK_{a3}$$ **3.12**

and $$\log K_4 = -\log K_{a4} = pK_{a4}$$ **3.13**

The protonation constants of the tetraaza macrocyclic ligand, TMEC14 and the related ligands, cyclam, TMEC12, THEC14 are given in Table 3.3.

For the tetraaza macrocyclic ligands (Figure 3.1) the pK_a values lie in the sequence:

$$pK_{a1} > pK_{a2} > pK_{a3} > pK_{a4}$$

As for the diaza macrocyclic ligands of the crown ethers, cryptands and lariat ethers (Section 3.1.1) each nitrogen lone pair may adopt either an *endo* or *exo* conformation. For the tetraaza macrocyclic ligands this leads to five possible conformations, *endo-endo-endo-endo*, *endo-endo-endo-exo*, *endo-endo-exo-exo*, *endo-exo-exo-exo*, and *exo-exo-exo-exo*. The

conformation which predominates will be the one which minimises repulsion and maximises the interaction between the nitrogen lone pairs and the proton(s). Hence, for the monoprotonated ligand all four nitrogen lone pairs are likely to be in the *endo* configuration. Then, as the number of protons increases the repulsion within the cavity also increases until some of the nitrogen lone pairs are forced into the *exo* configuration. In addition, there is a statistical effect, with the number of nitrogens which can be protonated reduced with progressive protonation. Thus, the increase in repulsion within the cavity and the statistical effect lead to a decrease in stability for the pK_a's in the sequence pK_{a1} > pK_{a2} > pK_{a3} > pK_{a4}.

Upon comparing the pK_a's for the tetraaza macrocyclic ligands in Table 3.3, a general decrease in stability is observed upon going from a flexible ligand such as cyclam to a less flexible ligand such as THEC14 and TMEC14 for pK_{a1} and pK_{a2}, but not for pK_{a3} and pK_{a4}. This may be attributed to the secondary amine groups of cyclam leading to higher pKa's by comparison with the tertiary amine groups in TMEC14 and THEC14. However, for pK_{a3} and pK_{a4} the repulsion within the cavity increases, leading to similar pK_a's for all three ligands. Another trend from Table 3.3 is the decrease in pK_{a3} and pK_{a4} upon going from a 14-membered ring ligand such as TMEC14 to a smaller 12-membered ring ligand such as TMEC12. This is a result of the greater repulsion within the 12-membered ring compared to the larger 14-membered ring for the 3rd and 4th protonated species, with a concomitant decrease in pK_{a3} and pK_{a4} for TMEC12.

Table 3.3 The protonation constants of TMEC14 and the related ligands, cyclam, THEC14 and TMEC12.

Ligand	pK_{a1}	pK_{a2}	pK_{a3}	pK_{a4}
Cyclam[a]	11.78	10.55	< 2.0	< 1.0
THEC14[b]	8.83	8.30	2.65	< 2.0
TMEC12[c]	10.92	8.04	2.17	< 2.0
TMEC14[d]	9.04 ± 0.05	7.87 ± 0.05	4.48 ± 0.05	2.29 ± 0.05

[a]Ref. 20, 21. 0.1 M $NaClO_4$ [b]Ref. 22. 0.1 M $NaClO_4$ [c]Ref. 23. [d]This work.

3.2.2 Stability Constants of the Complexes of the Tetraaza Macrocyclic Ligand TMEC14

The stability constants of a wide range of divalent metal complexes of TMEC14 in aqueous solution have been determined, and are given in Table 3.4 along with those for the related ligands, cyclam, TMEC12 and THEC14.

Table 3.4 Apparent stability constants for the complexation of TMEC14 and the related ligands, cyclam, TMEC12 and THEC14 with a range of divalent metal ions at 298.2 K, with 0.1 M NEt_4ClO_4.

	Ionic Radii[a]		log(K_s / dm^3 mol^{-1})		
M^{2+}	(Å)	Cyclam	TMEC12[g]	TMEC14[h]	THEC14
Mg^{2+}	0.72		2.47	< 2.0	1.86[j]
Ca^{2+}	1.00 (1.12)		5.47	3.22 ± 0.05	
Sr^{2+}	1.18 (1.26)		5.00	2.95 ± 0.05	
Ba^{2+}	1.35 (1.42)		4.72	2.89 ± 0.05	
Mn^{2+}	0.83		7.1	[i]	
Co^{2+}	0.75	12.71[b]	6.6	4.47 ± 0.05	6.10[j]
Ni^{2+}	0.69	20.3[c]	5.35	3.62 ± 0.05	7.45[k]
Cu^{2+}	0.73	27.15[d]	13.6	7.04 ± 0.05	15.69[j]
Zn^{2+}	0.74	15.0[e]	8.58	4.76 ± 0.05	6.43[j]
Cd^{2+}	0.95 (1.10)	11.23[f]	12.5	4.99 ± 0.05	9.38[j]
Hg^{2+}	1.02 (1.14)		18.57	15.1 ± 0.1	17.94[j]
Pb^{2+}	1.19 (1.29)	10.83[f]	14.87	5.78 ± 0.05	6.28[j]

[a]Ref. 5. The first number refers to the ionic radius for the 6-coordinate geometry, the numbers in parentheses are for the 8-coordinate geometry. [b]Ref. 24. 0.2 M $NaClO_4$ [c]Ref. 25. 0.5 M NaCl [d]Ref. 26. 0.2 M $NaClO_4$ [e]Ref. 27. 0.2 M $NaClO_4$ [f]Ref. 28. 0.1 M $NaNO_3$ [g]Ref. 23. [h]This work. [i]Unable to be determined due to formation of $Mn(OH)_2$ [j]Ref. 29. 0.1 M $NaNO_3$ [k]Ref. 30. 0.1 M $NaClO_4$

The apparent stability constant, K_S, is defined as:

$$TMEC14 + M^{2+} \underset{}{\overset{K_S}{\rightleftharpoons}} [M(TMEC14)]^{2+}$$

where $K_S = \dfrac{[M(TMEC14)^{2+}]}{[(TMEC14)][M^{2+}]}$

and $M^{2+} = Mg^{2+}, Ca^{2+}, Sr^{2+}, Ba^{2+}, Mn^{2+}, Co^{2+}, Ni^{2+}, Cu^{2+}, Zn^{2+}, Cd^{2+}, Hg^{2+}$ and Pb^{2+}

A number of trends are evident in Table 3.4 and are discussed with respect to the three groups, the alkaline metal complexes, the first row transition metal complexes, and the heavy metal complexes.

3.2.2.1 Complexes of the Alkaline Earth Metal Ions, Mg^{2+}, Ca^{2+}, Sr^{2+} and Ba^{2+}

For the alkaline metal complexes of TMEC14 the stability constants follow the sequence $Mg^{2+} < Ca^{2+} > Sr^{2+} > Ba^{2+}$ which suggests that Ca^{2+} (ionic radius of 1.12 Å for the 8-coordinate geometry [5]) is the optimal size for the complexation of TMEC14, and hence is probably the closest in size to the effective cavity size of TMEC14. The softer transition metal ions, Mn^{2+}, Co^{2+}, Ni^{2+}, Cu^{2+} and Zn^{2+}, have a preference for nitrogen donor atoms which leads to a general increase in stability of the complexes formed by comparison with those of the harder alkaline metal ions Mg^{2+}, Ca^{2+}, Sr^{2+} and Ba^{2+} as observed in Table 3.4.

3.2.2.2 Complexes of the First Row Transition Metal Ions, Mn^{2+}, Co^{2+}, Ni^{2+}, Cu^{2+} and Zn^{2+}

The stability constants of the first row transition metal complexes of TMEC14 follow the sequence $Co^{2+} > Ni^{2+} < Cu^{2+} > Zn^{2+}$, which is also observed for the lariat ethers in Section 3.1. This can be attributed to the increase in ionic radii along the sequence $Ni^{2+} < Cu^{2+} \approx Zn^{2+}$ leading to an increase in stability along the same sequence. Thus, as the size of the metal ion increases it is able to more optimally interact with the binding sites of TMEC14. The $[Cu(TMEC14)]^{2+}$ complex is highest in stability of the transition metal complexes as a result of the tetragonal distortion of d^9 Cu^{2+} [16].

3.2.2.3 Complexes of the Heavy Metal Ions, Cd^{2+}, Hg^{2+} and Pb^{2+}

The stabilities of the heavy metal complexes of TMEC14 follow the sequence $Zn^{2+} < Cd^{2+} < Pb^{2+} < Hg^{2+}$ (Table 3.4). In going from Zn^{2+} to Cd^{2+}, an increase in stability is observed due to a better fit of the metal ion size to the effective cavity size of TMEC14 and an increase in softness, and hence stronger bonding to the nitrogen ring atoms. The stability sequence $Cd^{2+} < Pb^{2+} < Hg^{2+}$ for the complexes of TMEC14 is related to the increasing softness, with Hg^{2+} binding to the four ring nitrogens more strongly than Pb^{2+} and Cd^{2+} leading to a large increase in stability. In general an increase in stability for the Pb^{2+} complex over the Cd^{2+} complex is observed despite the larger size of Pb^{2+} (ionic radii of 1.10 and 1.29 Å for the 8-coordinate geometries of Cd^{2+} and Pb^{2+}, respectively [5]). This increase in stability may be partly attributed to the 'inert pair effect' [31,32]. Initially, the $6s^2$ orbital of Pb^{2+} is stereochemically 'inactive'. The presence of multiple soft donor atoms such as nitrogens within a ligand can cause the $6s^2$ electrons to become 'active', leading to shorter Pb-N bond lengths by about 0.3 Å. Thus, as the effective ionic radius of Pb^{2+} becomes smaller, the charge density of Pb^{2+} increases, leading to the formation of a more stable complex.

3.2.2.4 The Size Effect of the 12- and 14-Membered Rings on the Stabilities of the Complexes Formed

The $[M(TMEC12)]^{2+}$ complexes are more stable than their $[M(TMEC14)]^{2+}$ analogues for all of the alkaline earth, transition and heavy metal ions, studied (Table 3.4). This is a result of the smaller 12-membered ring ligand, TMEC12 with four equal ($-CH_2CH_2-$) moieties being able to more optimally accommodate these metal ions in comparison with TMEC14. The smaller size of TMEC12 results in the metal ions being able to interact with more donor groups, and would probably lead to the formation of 8-coordinate complexes (Chapter 2, Section 2.4.3), whereas TMEC14, with its larger 14-membered ring cavity would most likely form 6-coordinate complexes due to the greater distance between the donor groups and optimal geometry of the ligand (Chapter 2, Section 2.4.3). A study by Hancock [33] using molecular mechanics calculations predicts that the smaller ligand, TMEC12 would have a preference for the larger heavy metal ions, and the larger TMEC14 would have a preference for the smaller transition metal ions. This prediction is supported, to a degree, by the

difference between the stabilities of the $[M(TMEC12)]^{2+}$ and $[M(TMEC14)]^{2+}$ complexes being much smaller for the transition metal ions, Co^{2+}, Ni^{2+}, Cu^{2+} and Zn^{2+} (2 to 3 orders of magnitude) compared with those for the larger heavy metal ions, Cd^{2+} and Pb^{2+} (8 to 9 orders of magnitude). However, the larger size and flexibility of TMEC14 compared with those of TMEC12 leads to all of the metal complexes of TMEC14 being less stable than those of TMEC12 (Table 3.4).

3.2.2.5 Effect of the Pendant Arms on the Stabilities of the Complexes of the Tetraaza Macrocyclic Ligands

A general increase in stability is observed for the complexes of THEC14 by comparison with those of TMEC14 from Table 3.4. The methoxy groups of TMEC14 have a stronger inductive effect than the hydroxy groups of THEC14, however this is often counterbalanced by the greater steric hindrance of the bulkier methoxy groups, particularly when there are four methoxyethyl pendant arms on a 14-membered ring as for TMEC14. In aqueous solution there also exists the possibility of hydrogen bonding between the solvent and the hydroxy groups of ligands such as THEC14, which would lead to a decrease in the stability of the complexes formed. However, it appears this does not effect the stabilities of the $[M(THEC14)]^{2+}$ complexes in aqueous solution to a great extent. Thus, in comparing the stabilities for the complexes of TMEC14 and THEC14 a combination of stronger inductive effect and greater steric hindrance must be taken into account, and in this case the steric hindrance appears to be the dominant factor, with the stabilities of the THEC14 complexes being the greater for all of the divalent metal ions in Table 3.4.

Upon comparing the stabilities of the complexes of the methoxyethyl pendant armed ligand, TMEC14 with those of cyclam for the metal ions in Table 3.4, a large increase in stability is observed for the complexes of cyclam. The ligand TMEC14 has four methoxyethyl groups on its 14-membered ring, and so upon complexing a metal ion there may be considerable steric hindrance between the methoxy groups. This leads to a destabilising effect on the resulting complex with a concomitant decrease in stability for the complexes of TMEC14 by comparison with those of cyclam. Also, the soft transition metal ions have a preference for nitrogen, and so the high stability of the complexes may be a result of the soft secondary ring nitrogens of cyclam having a greater inductive effect in comparison with the tertiary ring nitrogens of TMEC14. In addition, there

is the ability of flexible ligands such as cyclam and TMC (tetramethylcyclam) to fold over metal ions, adopting either 5 or 6-coordinate *trans*-V or *cis*-V complexes (Chapter 5, Figure 5.3 and 5.6) [34-42] with solvent molecules occupying the 5th and 6th sites. This may lead to complexes of much higher stability, with the transition metal ions able to adopt their favoured stereochemistries, although several transition metal complexes of cyclam in the *trans*-III configuration have been reported in the literature [39].

3.2.2.6 Protonated and Hydroxide Species in Aqueous Solution

The ligand TMEC14 was found to form other complex species in aqueous solution, in addition to the $[M(TMEC14)]^{2+}$ complex. Both protonated metal-ligand $[M(HTMEC14)]^{3+}$ and hydroxide metal-ligand $[M(OH)(TMEC14)]^{+}$ species were characterised using Superquad [37]. The stability constants for these species, and the $[M(TMEC14)]^{2+}$ complex are shown in Table 3.5.

The protonated species $[M(HTMEC14)]^{3+}$ for $M^{2+} = Co^{2+}$, Cu^{2+}, Cd^{2+} and Pb^{2+} are defined by K_H as:

$$M^{2+} + H^{+} + TMEC \xrightleftharpoons{K_H} [M(HTMEC14)]^{3+}$$

$$\text{where } K_H = \frac{[M(HTMEC14)^{3+}]}{[M^{2+}][H^{+}][(TMEC14)]}$$

It is envisaged that the tetraaza macrocycle, $[(HTMEC14)]^{+}$ would initially be bound to M^{2+} through the methoxyethyl pendant arms before interacting with the nitrogens in the macrocyclic ring. Upon continuing complexation, the $[M(HTMEC14)]^{+}$ complex deprotonates to form the $[M(TMEC14)]^{2+}$ complex.

Similarly, the hydroxide species $[M(OH)(TMEC14)]^{+}$ was found for $M^{2+} = Cu^{2+}$ and Pb^{2+} and is defined by K_{OH} as:

$$M^{2+} + OH^{-} + TMEC \xrightleftharpoons{K_{OH}} [M(OH)(TMEC14)]^{2+}$$

$$\text{where } K_{OH} = \frac{[M(OH)(TMEC14)]^{+}}{[M^{2+}][OH^{-}][(TMEC14)]}$$

For the hydroxide species it is envisaged that the solvated metal ion in the $[M(TMEC14)]^{2+}$ complex loses a proton from a bound water molecule, so producing a $[M(OH)(TMEC14)]^{+}$ species at higher pH.

Similar species have been reported in the literature for THEC14 with Co^{2+}, Ni^{2+}, Zn^{2+}, Cd^{2+} and Pb^{2+}, including a dihydroxide species $[Ni(OH)(THEC14)]_2$ [24,25]. A typical speciation curve, showing the formation of the protonated and hydroxide species with change of pH is shown in Figure 3.4 for $[Pb(TMEC14)]^{2+}$.

Table 3.5 Stability constants for the protonated and hydroxide species formed in aqueous solution for the ligand TMEC14, including $[M(TMEC14)]^{2+}$.

	$\log(K_S / dm^3\ mol^{-1})$		
M^{2+}	$[M(HTMEC14)]^{3+}$	$[M(TMEC14)]^{2+}$	$[M(OH)(TMEC14)]^{+}$
Co^{2+}	8.15 ± 0.05	4.47 ± 0.05	
Cu^{2+}	6.54 ± 0.05	7.04 ± 0.05	7.42 ± 0.05
Cd^{2+}	7.87 ± 0.05	4.99 ± 0.05	
Pb^{2+}	7.40 ± 0.05	5.78 ± 0.05	7.09 ± 0.05

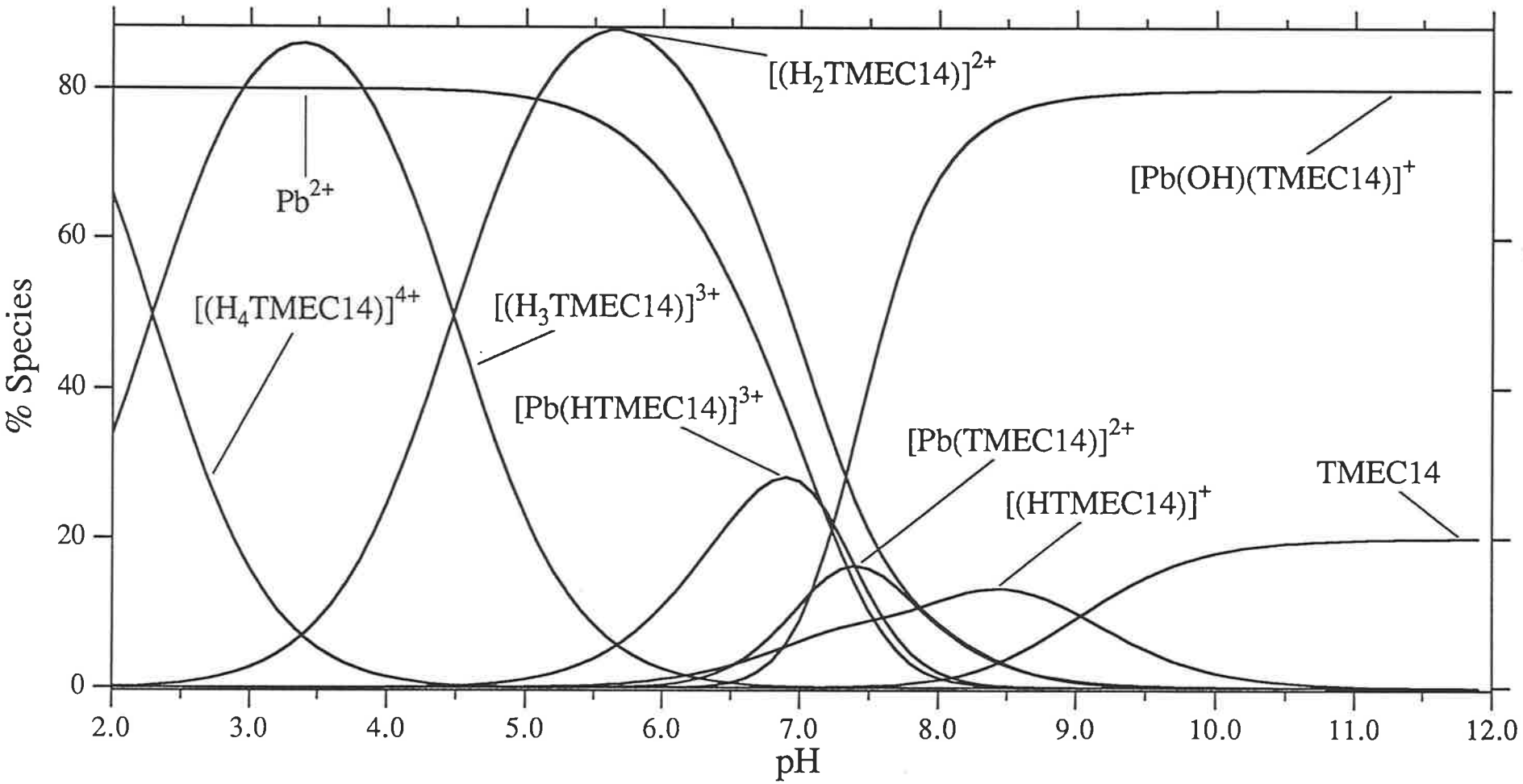

Figure 3.4 Speciation curves for Pb^{2+} complexes of TMEC14 at 298.2 K in 0.10 M NEt_4ClO_4 aqueous solution where percentages are expressed in terms of the total TMEC14 concentration being 100%. The total Pb^{2+} and TMEC14 concentrations are 8.76×10^{-4} M and 1.102×10^{-3} M, respectively.

References

1 F. Arnaud-Neu, B. Spiess and M. Schwing-Weill, *Helv. Chim. Acta*, 1977, **60**, 2633.

2 N. K. Dalley, R. M. Izatt and J. J. Christensen, *"Synthetic Multidentate Macrocyclic Compounds"*, Eds, Academic Press (New York), 1978.

3 C. J. Pederson and H. K. Frensdorff, *Angew. Chem.*, Int. Ed. Engl., 1972, **11**, 16.

4 T. Rodopoulos, PhD Dissertation, University of Adelaide, 1994.

5 R. D. Shannon, *Acta Crystallogr., Sect. A*, 1976, **32**, 751.

6 S. Kulstad and L. A. Malmsten, *J. Inorg. Nucl. Chem.*, 1981, **43**, 1299.

7 J.-M. Lehn, and J. P. Sauvage, *J. Am. Chem. Soc.*, 1975, **97**, 6700.

8 F. Arnaud-Neu, B. Spiess and M. J. Schwing-Weill, *Helv. Chim. Acta*, 1977, **60**, 2633.

9 F. Arnaud-Neu, B. Spiess and M. J. Schwing-Weill, *J. Am. Chem. Soc.*, 1982, **104**, 5641.

10 G. Anderegg, *Helv. Chim. Acta*, 1975, **58**, 1218.

11 R. D. Hancock, R. Bharan, M. S. Shaikjee, P. W. Wade and A. Hearn, *Inorg. Chim. Acta*, 1986, **112**, L23.

12 H. Irving and R. J. P. Williams, *Nature* (London), 1948, **162**, 746.

13 H. Irving and R. J. P. Williams, *J. Chem. Soc.*, 1953, 3192.

14 R. G. Pearson, *J. Am. Chem. Soc.*, 1963, **85**, 3533.

15 R. G. Pearson, *Coord. Chem. Rev.*, 1990, **100**, 403.

16 F. A. Cotton and G. Wilkinson, *"Advanced Inorganic Chemistry"*, 3rd Edn., Interscience (New York), 1980.

17 J. Burgess, *"Metal Ions in Solution"*, Ellis Horwood, Chichester, 1978.

18 J.-M. Lehn, *Struct. Bonding* (Berlin), 1973, **16**, 1.

19 J.-M. Lehn, *Acc. Chem. Res.*, 1978, **11**, 49.

20 E. Kimura, M. Shionoya, M. Okamoto and H. Nada, *J. Am. Chem. Soc.*, 1988, **110**, 3679.

21 M. Shionoya, E. Kimura and Y. Iitaka, *J. Am. Chem. Soc.*, 1990, **112**, 9237.

22 C. M. Madeyski, J. P. Michael and R. D. Hancock, *Inorg. Chem.*, 1984, **23**, 1487.

23 A. K. W. Stephens and S. F. Lincoln, unpublished material.

24 M. Kodama and E. Kimura, *J. Chem. Soc., Dalton Trans.*, 1980, 327.

25 A. Evers and R. D. Hancock, *Inorg. Chem.*, 1989, **160**, 245.

26 M. Kodama and E. Kimura, *J. Chem. Soc., Dalton Trans.*, 1977, 1473.

27 M. Kodama and E. Kimura, *J. Chem. Soc., Dalton Trans.*, 1978, 1081.

28 V. J. Thom, G. D. Hosken and R. D. Hancock, *Inorg. Chem.*, 1985, **24**, 3378.

29 C. M. Madeyski, J. P. Michael and R. D. Hancock, *Inorg. Chem.*, 1984, **23**, 1487.

30 R. W. Hay, M. P. Pujari, W. T. Moodie, S. Craig, D. T. Richens, A. Perotti and L. Ungaretti, *J. Chem. Soc., Dalton Trans.*, 1987, 2605.

31 R. D. Hancock, M. S. Shaikjee, S. M. Dobson and J. C. A. Boeyens, *Inorg. Chim. Acta*, 1988, **154**, 229.

32 R. D. Hancock, R. Bharan, P. W. Wade, J. C. A. Boeyens and S. M. Dobson, *Inorg. Chem.*, 1989, **28**, 187.

33 R. D. Hancock, *Acc. Chem. Res.*, 1990, **23**, 253.

34 R. W. Hay and C. You-Quan, *Inorg. Chim. Acta*, 1991, **180**, 147.

35 E. K. Barefield, A. Bianchi, E. J. Billo, P. J. Connolly, P. Paoletti, J. S. Summers and D. G. Van Derveer, *Inorg. Chem.*, 1986, **25**, 4197.

36 E. K. Barefield and F. Wagner, *Inorg. Chem.*, 1973, **12**, 2435.

37 K. Henrick, P. A. Tasker and L. F. Lindoy, *Prog. Inorg. Chem.*, 1985, **33**, 1.

38 B. S. Nakani, J. J. B. Welsh and R. D. Hancock, *Inorg. Chem.*, 1983, **22**, 2956.

39 N. W. Alcock, E. H. Curson, N. Herron and P. Moore, *J. Chem. Soc., Dalton Trans.*, 1979, 1987.

40 R. D. Hancock and M. P. Ngwenya, *J. Chem. Soc., Dalton Trans.*, 1987, 2911.

41 H. Miyamae, K. Yamauchi and M. Yamashita, *J. Chem. Soc., Dalton Trans.*, 1991, 2921.

42 P. Gans, *J. Chem. Soc., Dalton Trans.*, 1985, 1195.

4. ^{7}Li and ^{23}Na NMR Exchange Kinetics

4.1 Introduction

The formation of a complex in solution between a macrocyclic ligand and a metal ion involves a series of conformational and solvational changes for the ligand and metal ion. Initially, an encounter complex is formed between the macrocyclic ligand and the solvated metal ion. Metal to ligand bonds are then formed with partial desolvation of the metal ion and conformational changes in the macrocyclic ligand. Subsequent steps involve the further formation of metal to ligand bonds and progressive desolvation of the metal ion.

There are two possible mechanisms for the overall exchange process for alkali metal ions between the solvated and complexed states [1,2]:

(i) The first order unimolecular mechanism, in which the rate determining step is the decomplexation of the alkali metal ion. For this process, the rate of exchange is independent of the concentration of the solvated metal ion, M^+.

$$M^+ + \text{Ligand} \underset{k_d}{\overset{k_c}{\rightleftharpoons}} [M(\text{Ligand})]^+ \qquad 4.1$$

where k_c is the rate constant characterising the rate determining steps for the complexation process

k_d is the rate constant characterising the rate determining steps for the decomplexation process

and $\frac{k_c}{k_d} = K_S$ is the stability constant

with the exchange rate = $k_d[M(\text{Ligand})^+]$

The species lifetimes are given by:

$$\tau_c = \frac{1}{k_d} = \frac{\tau_s \chi_c}{\chi_s} \qquad 4.2$$

where χ_c and χ_s are the mole fractions of the metal ion, M^+, in the complexed and solvated environments, respectively, and:

τ_c is the mean lifetime of the complex

τ_s is the mean lifetime of the solvated metal ion, M^+

(ii) The second order bimolecular mechanism, in which the rate determining step involves the displacement of the complexed metal ion by another metal ion. For this process the rate of exchange is dependant on the concentration of the solvated metal ion, M^+.

$$*M^+ + [M(Ligand)]^+ \underset{k_b}{\overset{k_b}{\rightleftharpoons}} M^+ + [*M(Ligand)]^+ \qquad 4.3$$

where k_b is the rate constant for the bimolecular interchange

with the exchange rate = $k_b[M(Ligand)^+][M^+]$

The species lifetimes are given by:

$$\tau_c = \frac{1}{k_b[M^+]} = \frac{\chi_s}{\tau_s \chi_c} \qquad 4.4$$

Although the unimolecular exchange mechanism is predominant for most alkali metal macrocyclic complexes [3-11] the bimolecular exchange mechanism may become dominant in solvents of high dielectric constants (ε) such as acetonitrile (ε = 46.0 [12]) and propylene carbonate (ε = 46.6 [12]) [11,13-16].

The activation parameters, $\Delta H^{\ddagger}$ and $\Delta S^{\ddagger}$ are derived from the temperature variation of the observed lifetime, τ_c, through Equation 4.5 as discussed in Chapter 8 (Section 8.2).

$$k_d \text{ or } k_b = \frac{1}{\tau_c} = \frac{k_B T}{h} \exp\left(\frac{-\Delta H^{\ddagger}}{RT} + \frac{\Delta S^{\ddagger}}{R}\right) \qquad 4.5$$

where τ_c is the mean lifetime of the complex

k_d is the unimolecular and decomplexation rate constant

k_b is the bimolecular exchange rate constant

k_B is Boltzmann's constant

h is Plank's constant

$\Delta H^{\ddagger}$ is the enthalpy of activation

$\Delta S^{\ddagger}$ is the entropy of activation

Rearranging Equation 4.5 into its linear form yields:

$$\ln(T\tau_c) = \frac{-\Delta H^{\ddagger}}{R}\left(\frac{1}{T}\right) + \left[\ln\left(\frac{k_B}{h}\right) - \frac{\Delta S^{\ddagger}}{R}\right] \qquad 4.6$$

From Equation 4.6 it may be seen than a plot of $\ln(T\tau_c)$ versus $\frac{1}{T}$ yields a straight line of slope $\frac{-\Delta H^{\ddagger}}{R}$ and intercept $\left[\ln\left(\frac{k_B}{h}\right) - \frac{\Delta S^{\ddagger}}{R}\right]$

4.2 Exchange Kinetics for the Complexes of BME-C21 and BME-C22

The variable temperature ^{7}Li and ^{23}Na NMR spectra for $[Li(BME\text{-}C21)]^{+}$, $[Li(BME\text{-}C22)]^{+}$, $[Na(BME\text{-}C21)]^{+}$ and $[Na(BME\text{-}C22)]^{+}$ in the solvents acetonitrile, propylene carbonate, methanol, dimethylformamide and pyridine showed that several systems exchange within the NMR timescale and hence could be subjected to a lineshape analysis (Chapter 8). The $[Li(BME\text{-}C21)]^{+}$ exchange rates were within the ^{7}Li NMR timescale in the solvents, acetonitrile, propylene carbonate, methanol, dimethylformamide and pyridine, however the signal to noise ratio for the $[Li(BME\text{-}C21)]^{+}$ systems in the solvents acetonitrile and pyridine became too low at high temperature to be able to lineshape these systems. The $[Li(BME\text{-}C22)]^{+}$ exchange rates were in fast exchange in all five solvents. The $[Na(BME\text{-}C21)]^{+}$ exchange rates were within the ^{23}Na NMR timescale in the solvents acetonitrile, propylene carbonate and pyridine, but were in fast exchange in methanol and dimethylformamide. The $[Na(BME\text{-}C22)]^{+}$ exchange rates were within the ^{23}Na NMR timescale in the solvents, acetonitrile, methanol, dimethylformamide and pyridine, however the propylene carbonate system was in fast exchange.

4.2.1 Exchange Kinetics for $[Na(BME\text{-}C21)]^{+}$

The rates of Na^{+} exchange on $[Na(BME\text{-}C21)]^{+}$ have been determined in the solvents acetonitrile, propylene carbonate and pyridine,

and the results are given in Table 4.1 along with the compositions of each solution. The magnitudes and temperature variations of τ_c are very similar for each set of $[Na(BME\text{-}C21)]^+$ data indicating that the rate determining step is independent of the concentration of solvated Na^+ consistent with the operation of a monomolecular decomplexation process (Figure 4.1). Typical exchange modified 79.39 MHz ^{23}Na NMR spectra of Na^+ and $[Na(BME\text{-}C21)]^+$ in acetonitrile are shown in Figure 4.2. The kinetic parameters for the $[Na(BME\text{-}C21)]^+$ system at 298.2 K are given in Table 4.2, along with those for a number of related systems.

The higher stability of $[Na(BME\text{-}C21)]^+$ in acetonitrile is a result of the substantially higher k_c by comparison with the k_c characterising $[Na(BME\text{-}C21)]^+$ in propylene carbonate and pyridine. For acetonitrile, propylene carbonate and pyridine, as D_N increases, k_c decreases which suggests substantial desolvation in the rate determining steps for complexation. In contrast, k_d is essentially invariant with solvent suggesting that solvent plays only a minor role in the rate determining steps for the decomplexation of $[Na(BME\text{-}C21)]^+$. The kinetic parameters for $[Na(BME\text{-}C21)]^+$ in propylene carbonate and pyridine are similar despite the large difference in D_N from 15.1 to 33.1, respectively. This can be attributed to the steric effects between coordinated pyridine molecules resulting from their large size and also the nitrogen lone pair being delocalised into the aromatic ring leading to a weaker interaction with Na^+ than suggested by its D_N of 33.1 (Chapter 2, Section 2.3.2).

4.2.2 Exchange Kinetics for $[Na(BME\text{-}C22)]^+$

The rates of Na^+ exchange on $[Na(BME\text{-}C22)]^+$ have been determined in the solvents acetonitrile, methanol, dimethylformamide and pyridine, and the results are given in Table 4.3 along with the compositions of each solution. As for the $[Na(BME\text{-}C21)]^+$ systems, the $[Na(BME\text{-}C22)]^+$ systems are characterised by a monomolecular decomplexation process (Figure 4.3). Typical exchange modified 79.39 MHz ^{23}Na NMR spectra of Na^+ and $[Na(BME\text{-}C22)]^+$ in methanol are shown in Figure 4.4. The kinetic parameters for the $[Na(BME\text{-}C22)]^+$ system at 298.2 K are given in Table 4.2, along with those for a number of related systems.

For the $[Na(BME\text{-}C22)]^+$ complexes, k_c decreases with increasing D_N along the sequence acetonitrile, methanol and dimethylformamide. Thus, k_c decreases as the electron donating power of the solvent increases, consistent with the solvents competing more favourably for the metal ion in

comparison with the ligand and suggesting that solvent plays a substantial role in the rate determining steps for the complexation of $[Na(BME\text{-}C22)]^+$. The lower stability of $[Na(BME\text{-}C22)]^+$ in dimethylformamide is a result of the higher k_d by comparison with the k_d characterising $[Na(BME\text{-}C22)]^+$ in acetonitrile and methanol. The kinetic parameters for the $[Na(BME\text{-}C22)]^+$ system in pyridine are substantially lower than would be expected on the basis of its D_N of 33.1, similar to its $[Na(BME\text{-}C21)]^+$ analogue (Section 4.2.1). This is due to pyridine not solvating the hard acid Na^+ as well as would be expected on the basis of a D_N of 33.1 as a result of its soft base properties and steric crowding effects in solution (Chapter 2, Section 2.3.2) and this is reflected in the kinetic parameters for $[Na(BME\text{-}C22)]^+$ in pyridine which generally fall between those in acetonitrile and methanol.

The kinetic parameters for the $[Na(BME\text{-}C21)]^+$ and $[Na(BME\text{-}C22)]^+$ systems are given in Table 4.2. Upon comparing the $[Na(BME\text{-}C21)]^+$ and $[Na(BME\text{-}C22)]^+$ systems in acetonitrile and pyridine a number of trends become evident. Firstly, in acetonitrile the Na^+ complexes are both characterised by much larger k_c values than for the other solvents resulting in the large stability constants, K_S, observed for $[Na(BME\text{-}C21)]^+$ and $[Na(BME\text{-}C22)]^+$ in acetonitrile. In contrast, the two systems in pyridine have small k_d values, which result in the high K_S values for the Na^+ complexes in pyridine. The ligand, BME-C21, complexes Na^+ more strongly than the larger BME-C22 (Chapter 2, Section 2.3.4) and this is reflected in the kinetic parameters for $[Na(BME\text{-}C21)]^+$ and $[Na(BME\text{-}C22)]^+$ in acetonitrile and pyridine, with higher $\Delta H_d^{\ddagger}$ and lower k_d values observed for $[Na(BME\text{-}C21)]^+$. In addition, the $[Na(BME\text{-}C22)]^+$ systems are characterised by substantially greater k_c and k_d values in comparison with those of $[Na(BME\text{-}C21)]^+$ in the solvents acetonitrile and pyridine, indicating that BME-C22 is more flexible than the smaller BME-C21.

4.2.3 Exchange Kinetics for $[Li(BME\text{-}C21)]^+$

The rates of Li^+ exchange on $[Li(BME\text{-}C21)]^+$ have been determined in the solvents, propylene carbonate, methanol and dimethylformamide, and the results are given in Table 4.4 along with the compositions of each solution. As for $[Na(BME\text{-}C21)]^+$ and $[Na(BME\text{-}C22)]^+$, the $[Li(BME\text{-}C21)]^+$ systems operate through a monomolecular decomplexation process (Figure 4.5). Typical exchange modified 116.59 MHz ^{7}Li NMR spectra of Li^+ and $[Li(BME\text{-}C21)]^+$ in dimethylformamide are shown in Figure 4.6. The kinetic parameters for the $[Na(BME\text{-}C22)]^+$ system at 298.2 K are given in Table 4.2, along with those for a number of related systems.

Table 4.1 Sodium(I) exchange on $[Na(BME\text{-}C21)]^+$ in acetonitrile, propylene carbonate and pyridine. Solution composition and kinetic parameters[a]

soln.	solvent	$[Na^+_{solvated}]$ mol dm^{-3}	$[Na(BME\text{-})^+]$ mol dm^{-3}	k_d (331.0 K)[b] s^{-1}	k_d (298.2 K) s^{-1}	$\Delta H_d^{\ddagger}$ kJ mol^{-1}	$\Delta S_d^{\ddagger}$ J K^{-1} mol^{-1}
i	acetonitrile	0.0730	0.0298	783 ± 11	135 ± 4	41.0 ± 0.8	-66.4 ± 2.5
ii		0.0586	0.0442	768 ± 11	117 ± 3	44.9 ± 0.6	-55.0 ± 2.1
iii		0.0134	0.0894	778 ± 11	126 ± 4	43.7 ± 0.7	-58.6 ± 2.3
(i - iii)		-	-	775 ± 10	124 ± 3	43.2 ± 0.6	-60.0 ± 2.1
				k_d (336.3 K)[b]			
iv	propylene	0.0622	0.0397	771 ± 13	60.0 ± 3.2	56.0 ± 1.7	-26.1 ± 4.8
v	carbonate	0.0448	0.0571	768 ± 5	65.1 ± 1.2	53.2 ± 0.4	-32.5 ± 1.1
vi		0.0153	0.0866	787 ± 8	57.0 ± 2.3	51.6 ± 0.9	-34.9 ± 2.8
(iv - vi)		-	-	777 ± 11	60.0 ± 2.7	53.4 ± 0.8	-32.0 ± 2.5
				k_d (325.7 K)[b]			
vii	pyridine	0.0816	0.0262	437 ± 4	56.4 ± 1.3	59.1 ± 0.6	-18.3 ± 1.7
viii		0.0586	0.0460	439± 11	58.5 ± 3.5	56.7 ± 1.5	-21.0 ± 4.8
ix		0.0241	0.0805	469 ± 8	65.3 ± 1.8	54.2 ± 1.0	-27.1 ± 3.1
(vii - ix)		-	-	450 ± 8	61.8 ± 1.6	55.8 ± 0.9	-23.5 ± 2.8

[a]Errors represent one standard deviation from the least-squares fit of the experimental τ_c data by equation 4.5. [b]Temperature close to coalescence.

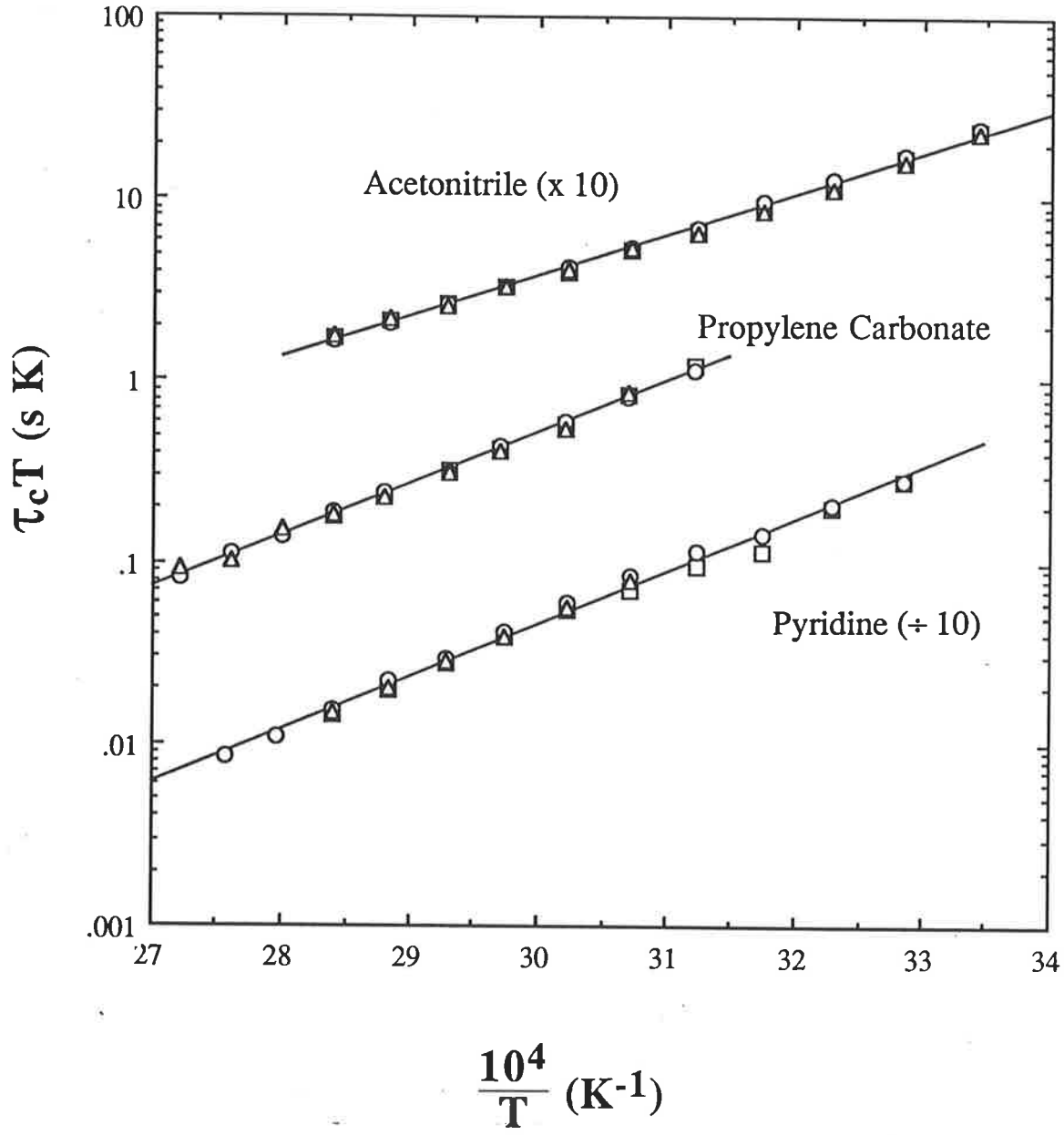

Figure 4.1 The temperature variation of τ_c for the Na^+-$[Na(BME\text{-}C21)]^+$ system in (a) acetonitrile (x 10), (b) propylene carbonate and (c) pyridine (÷ 10). Data points for solutions i-iii, the compositions of which are given in Table 4.1, are represented by triangles, circles and squares, respectively, for each system. The solid lines represent the best fits of the combined data by Equation 4.5 for each group of solutions.

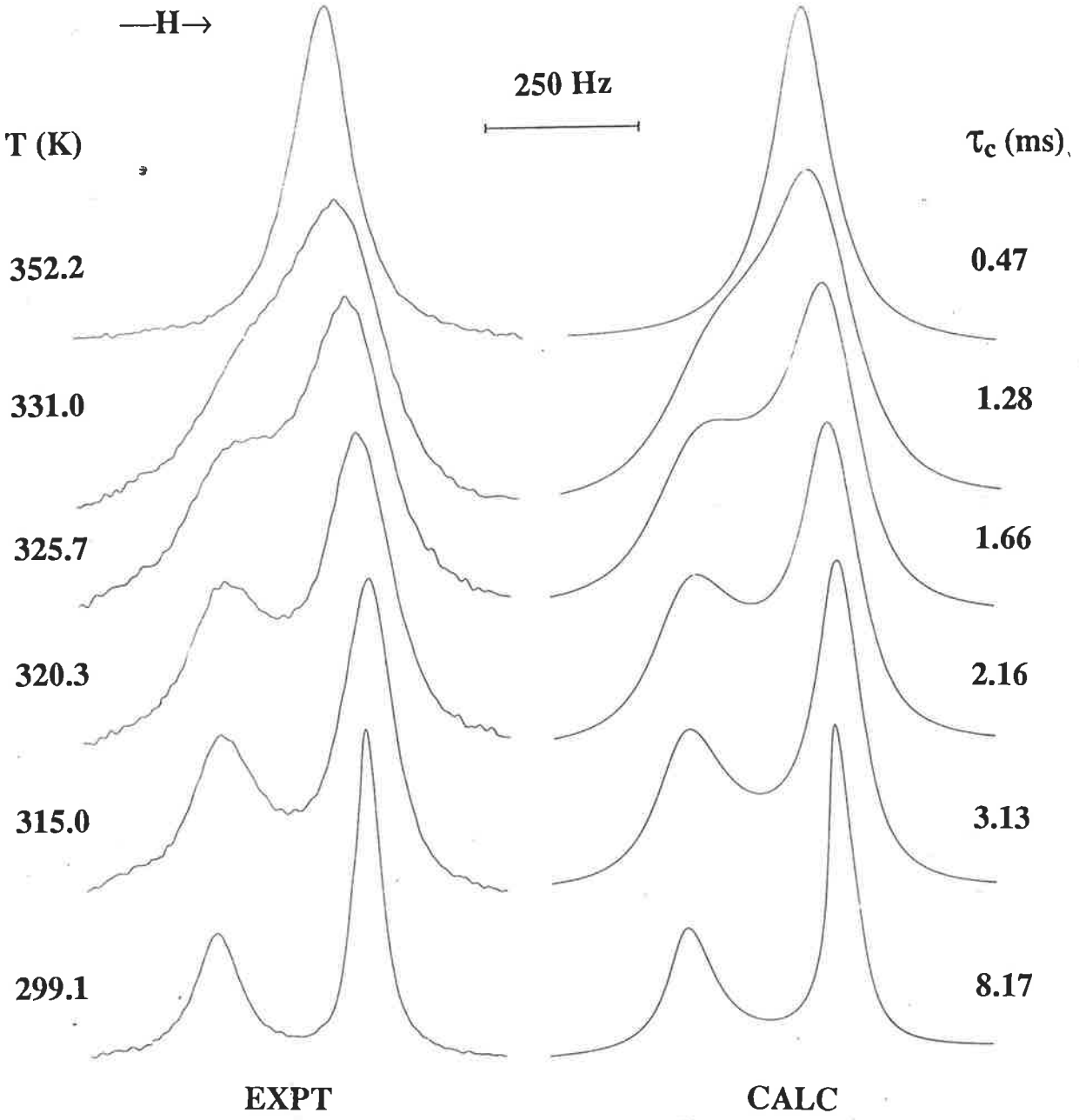

Figure 4.2 Typical exchange modified 79.39 MHz ^{23}Na NMR spectra of an acetonitrile solution of solvated Na^+ (0.0586 M) and $[Na(BME\text{-}C21)]^+$ (0.0442 M). Experimental temperatures and spectra appear to the left of the figure. Best fit calculated lineshapes and corresponding τ_c values appear to the right. The resonance of $[Na(BME\text{-}C21)]^+$ appears downfield from that of solvated Na^+.

[a][Na(BME-C22)]$^{+}$	acetonitrile	14.1	2154000	2650	37.5	-53.8	7.91
[a][Na(BME-C22)]$^{+}$	methanol	23.5	903	2430	59.9	20.8	4.57
[a][Na(BME-C22)]$^{+}$	dimethyl-formamide	26.6	529	25900	61.7	46.4	3.31
[a][Na(BME-C22)]$^{+}$	pyridine	33.1	12300	347	50.9	-26.5	6.55
[b][Na(BHE-C21)]$^{+}$	acetonitrile	14.1	20700	207	52.6	-24.1	7.00
[b][Na(BHE-C22)]$^{+}$	methanol	23.5	3058	4130	42.8	-32.0	4.87
[c][NaC221]$^{+}$	methanol	23.5	1700	0.0235			9.65
[c][NaC221]$^{+}$	dimethyl-formamide	26.6	180	0.25			7.93
[c][NaC222]$^{+}$	methanol	23.5	2700	2.87			7.9

[a]This work. [b]Ref 17. [c]Ref 18,19.

				k_d (320.3 K)[b]			
viii	pyridine	0.0764	0.0282	1540 ± 27	357 ± 13	48.0 ± 1.3	-32.6 ± 3.8
ix		0.0638	0.0408	1520 ± 22	321 ± 8	53.2 ± 1.1	-20.4 ± 3.7
x		0.0408	0.0638	1470 ± 18	331 ± 7	50.7 ± 1.0	-26.5 ± 3.4
xi		0.0253	0.0793	1500 ± 22	342 ± 9	51.8 ± 1.1	-28.6 ± 3.1
(viii - xi)		-	-	1510 ± 12	347 ± 7	50.9 ± 1.0	-26.5 ± 2 7
				k_d (256.9 K)[b]			
xii	dimethyl-	0.0775	0.0245	410 ± 10	24200 ± 240	62.8 ± 1.6	48.8 ± 3.2
xiii	formamide	0.0581	0.0439	388 ± 10	27300 ± 210	64.5 ± 1.7	51.2 ± 3.4
xiv		0.0326	0.0694	420 ± 16	25400 ± 310	59.8 ± 1.2	44.9 ± 4.5
(xii-xiv)		-	-	406 ± 9	25900 ± 200	61.7 ± 1.5	46.4 ± 3.0

[a]Errors represent one standard deviation from the least-squares fit of the experimental τ_c data by equation 4.5. [b]Temperature close to coalescence.

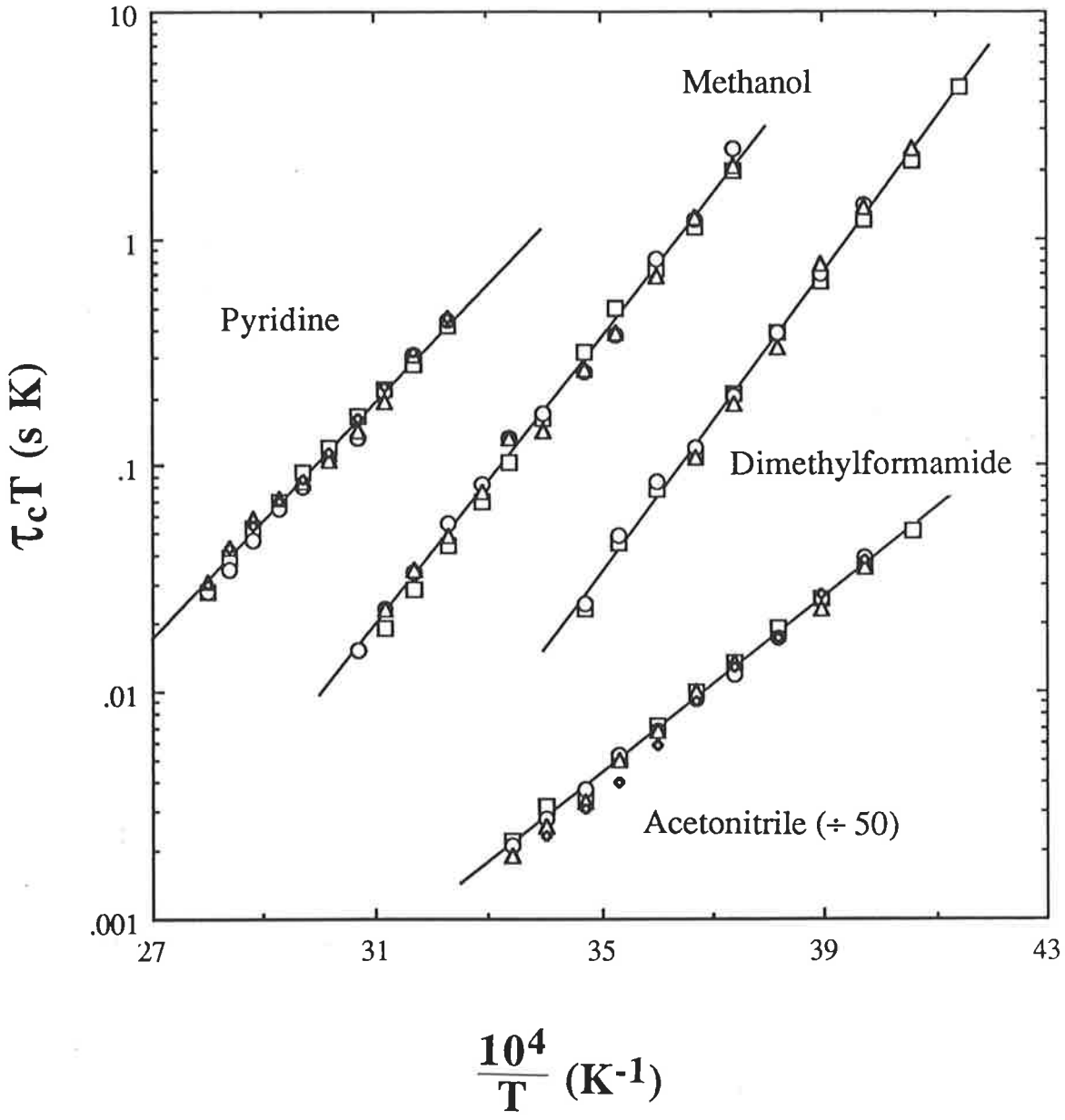

Figure 4.3 The temperature variation of τ_c for the Na^+-[Na(BME-C22)]$^+$ system in (a) pyridine, (b) methanol, (c) dimethylformamide and (d) acetonitrile (÷ 50). For pyridine and acetonitrile, data points for solutions i-iv, the compositions of which are given in Table 4.3, are represented by triangles, circles, squares and diamonds, respectively, for each system. For methanol and dimethylformamide, data points for solutions i-iii, the compositions of which are given in Table 4.3, are represented by triangles, circles and squares, respectively, for each system. The solid lines represent the best fits of the combined data by Equation 4.5 for each group of solutions.

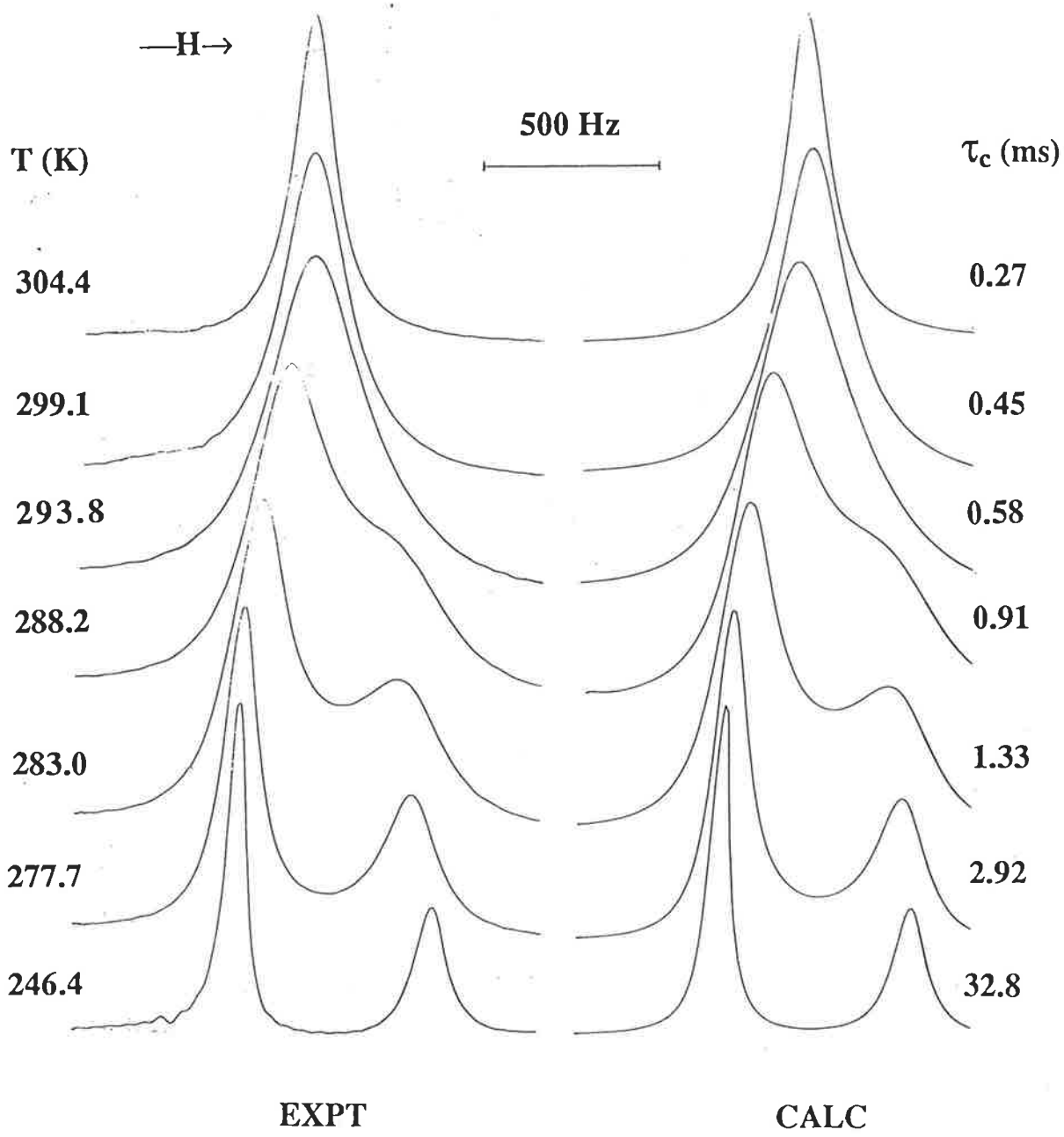

Figure 4.4 Typical exchange modified 79.39 MHz ^{23}Na NMR spectra of a methanol solution of solvated Na^+ (0.0463 M) and $[Na(BME\text{-}C22)]^+$ (0.0566 M). Experimental temperatures and spectra appear to the left of the figure. Best fit calculated lineshapes and corresponding τ_c values appear to the right. The resonance of $[Na(BME\text{-}C22)]^+$ appears upfield from that of solvated Na^+.

Table 4.4 Lithium(I) exchange on $[Li(BME\text{-}C21)]^{+}$ in dimethylformamide, methanol and propylene carbonate. Solution composition and kinetic parameters[a]

soln.	solvent	$[Li^{+}_{solvated}]$ mol dm^{-3}	$[Li(BME\text{-})^{+}]$ mol dm^{-3}	k_d (230.8 K)[b] s^{-1}	k_d (298.2 K) s^{-1}	$\Delta H_d^{\ddagger}$ kJ mol^{-1}	$\Delta S_d^{\ddagger}$ J K^{-1} mol^{-1}
i	dimethyl-	0.01441	0.00710	354 ± 10	31400 ± 200	35.9 ± 0.6	-38.5 ± 2.3
ii	formamide	0.01140	0.01011	331 ± 12	32500 ± 340	36.8 ± 0.8	-35.3 ± 3.2
iii		0.00774	0.01376	349 ± 15	34800 ± 480	36.9 ± 1.1	-34.3 ± 4.6
(i - iii)		-	-	346 ± 9	32600 ± 110	36.4 ± 0.5	-36.5 ± 2.0
				k_d (215.1 K)[b]			
iv	methanol	0.01333	0.00718	58.6 ± 2.1	2050 ± 47	20.7 ± 0.7	-112 ± 3
v		0.00984	0.01066	57.3 ± 0.7	1870 ± 36	18.3 ± 0.3	-122 ± 2
vi		0.00513	0.01538	57.0 ± 1.2	2100 ± 42	22.5 ± 0.5	-106 ± 3
(iv - vi)		-	-	59.1 ± 1.1	1970 ± 39	20.4 ± 0.4	-113 ± 2
				k_d (288.2 K)[b]			
vii	propylene	0.01370	0.00770	50.8 ± 0.5	87.5 ± 0.8	36.4 ± 0.3	-85.6 ± 0.8
viii	carbonate	0.00920	0.01220	45.8 ± 1.1	78.2 ± 1.5	35.7 ± 0.7	-88.2 ± 1.5
ix		0.00685	0.01455	42.9 ± 0.5	72.2 ± 0.7	34.6 ± 0.4	-92.2 ± 0.7
(vii - ix)		-	-	46.7 ± 0.8	79.7 ± 1.2	35.8 ± 0.6	-88.6 ± 1.2

[a]Errors represent one standard deviation from the least-squares fit of the experimental τ_c data by equation 4.5. [b]Temperature close to coalescence.

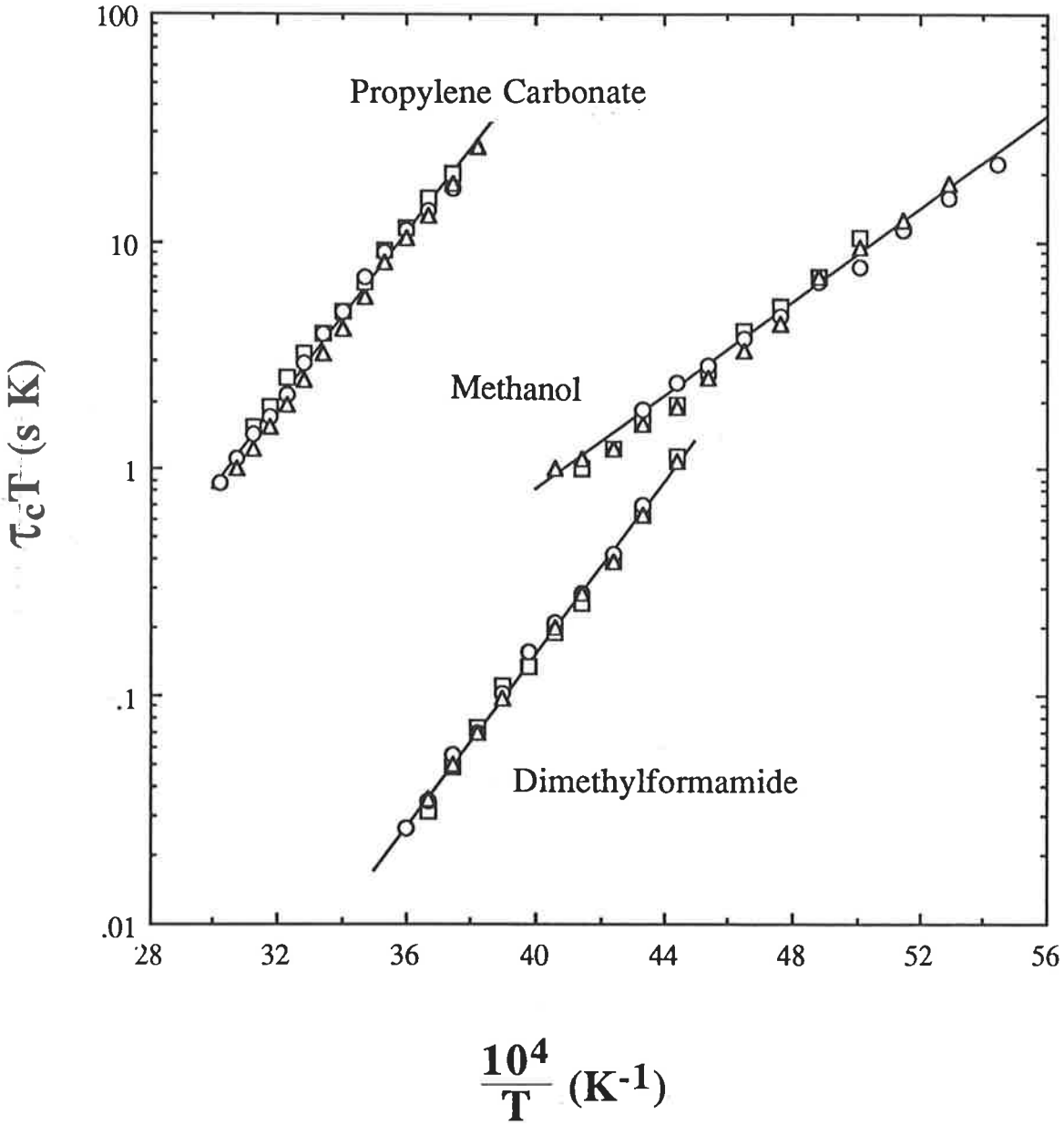

Figure 4.5 The temperature variation of τ_c for the Li^+-$[Li(BME\text{-}C21)]^+$ system in (a) propylene carbonate, (b) methanol and (c) dimethylformamide. Data points for solutions i-iii, the compositions of which are given in Table 4.4, are represented by triangles, circles and squares, respectively, for each system. The solid lines represent the best fits of the combined data by Equation 4.5 for each group of solutions.

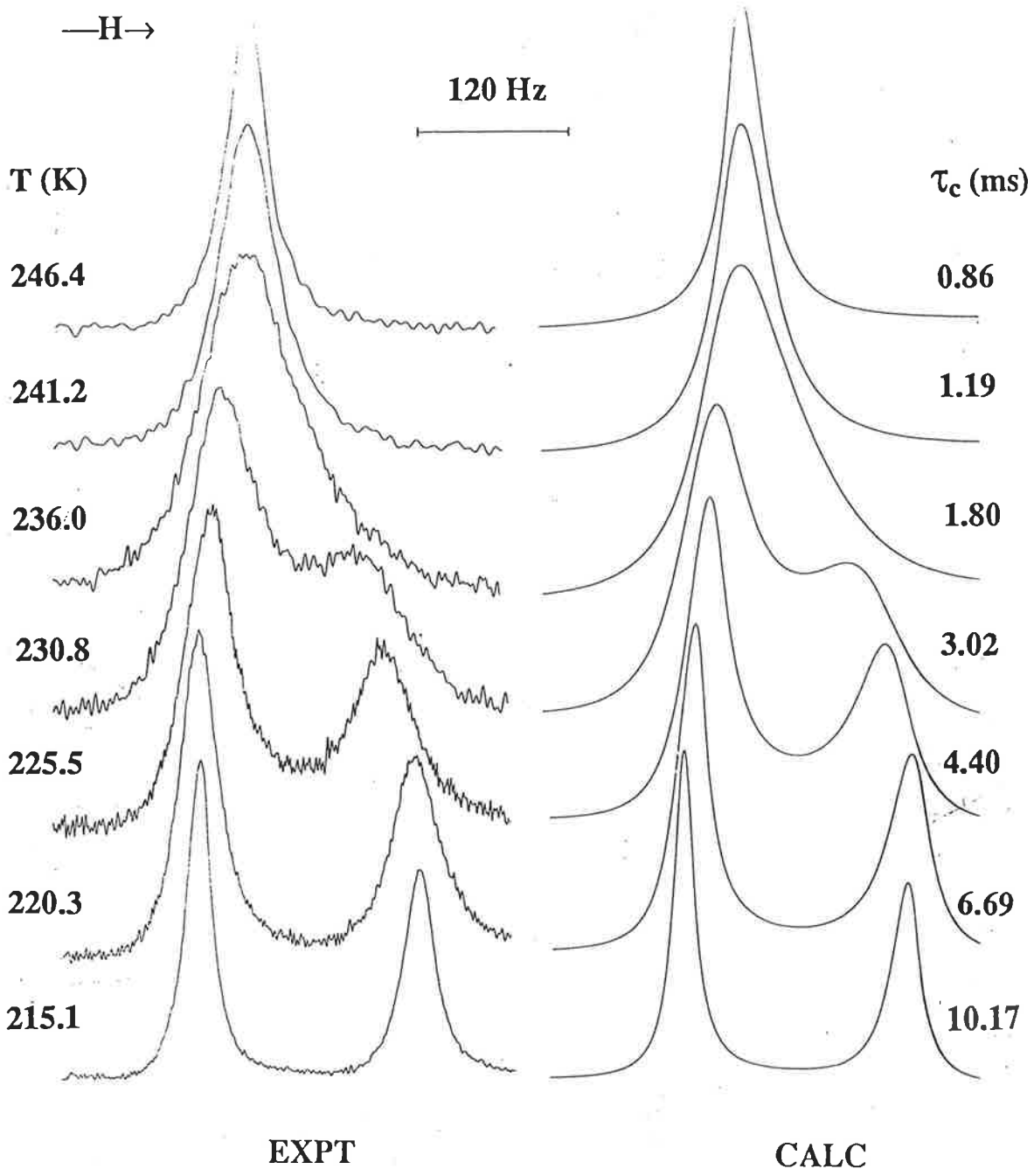

Figure 4.6 Typical exchange modified 116.59 MHz ^{7}Li NMR spectra of a dimethylformamide solution of solvated Li^+ (0.0114 M) and $[Li(BME\text{-}C21)]^+$ (0.0101 M). Experimental temperatures and spectra appear to the left of the figure. Best fit calculated lineshapes and corresponding τ_c values appear to the right. The resonance of $[Li(BME\text{-}C21)]^+$ appears upfield from that of solvated Li^+.

For the $[Li(BME\text{-}C21)]^+$ complexes, k_c decreases and k_d increases as D_N increases along the sequence, propylene carbonate, methanol and dimethylformamide. This indicates that as the electron donating power of the solvents increase they are able to compete more effectively for Li^+ in comparison with BME-C21 and suggests that solvents plays a major role in the rate determining steps for the complexation and decomplexation of $[Li(BME\text{-}C21)]^+$. The high K_S for $[Li(BME\text{-}C21)]^+$ in propylene carbonate is a result of the higher k_c and lower k_d values by comparison with those in methanol and dimethylformamide. The small $\Delta H_d^{\ddagger}$ observed in methanol by comparison with those observed in the other solvents is counterbalanced by a more negative $\Delta S_d^{\ddagger}$ than for the other solvents.

The kinetic parameters for the $[Li(BME\text{-}C21)]^+$ and $[Na(BME\text{-}C21)]^+$ systems are given in Table 4.2. Upon comparing the kinetic parameters of $[Li(BME\text{-}C21)]^+$ with those of $[Na(BME\text{-}C21)]^+$ in propylene carbonate, both the k_c and k_d values are similar for the two systems. This results in similar K_S values for the two complexes. The $[Li(BME\text{-}C21)]^+$ system in propylene carbonate is characterised by a substantially smaller $\Delta H_d^{\ddagger}$ by comparison with that for $[Na(BME\text{-}C21)]^+$ in propylene carbonate. This is probably a result of the inherent strain within the $[Li(BME\text{-}C21)]^+$ complex, due to the small size of the Li^+ ion.

4.2.4 Comparison of the Kinetic Parameters for a Number of Related Systems

The rates of metal ion exchange on BME-C21 and BME-C22, along with those of the related ligands, BHE-C21 and BHE-C22, and the cryptands, C221 and C222, are given in Table 4.2.

In acetonitrile, the higher k_c observed for the $[Na(BME\text{-}C21)]^+$ system, compared with that for the $[Na(BHE\text{-}C21)]^+$ system, results in the higher K_S for $[Na(BME\text{-}C21)]^+$. The greater k_d for the $[Na(BHE\text{-}C21)]^+$ and $[Na(BHE\text{-}C22)]^+$ systems by comparison with those for the $[Na(BME\text{-}C21)]^+$ and $[Na(BME\text{-}C22)]^+$ systems in acetonitrile and methanol, respectively, results from $[Na(BHE\text{-}C21)]^+$ and $[Na(BHE\text{-}C22)]^+$ being more labile than their methoxyethyl pendant armed analogues, $[Na(BME\text{-}C21)]^+$ and $[Na(BME\text{-}C21)]^+$, and suggests significant pendant arm involvement in the rate determining steps for decomplexation.

The k_c and k_d values for $[Li(BME\text{-}C21)]^+$ are smaller than those for $[Li(BHE\text{-}C21)]^+$ in methanol and dimethylformamide. This is consistent

with $[Li(BME\text{-}C21)]^+$ being less labile than $[Li(BHE\text{-}C21)]^+$ due to steric effects resulting from the two methoxy groups in BME-C21 and suggests that there is significant pendant arm involvement in the slowest reaction steps. The $\Delta H_d^{\ddagger}$ and $\Delta S_d^{\ddagger}$ for $[Li(BME\text{-}C21)]^+$ are smaller and more negative, respectively, by comparison with those of $[Li(BHE\text{-}C21)]^+$, which may be a result of the steric effects induced by the methoxyethyl pendant arms of BME-C21 upon the complexation of the small Li^+ ion.

A larger k_c and substantially smaller k_d lead to $[NaC222]^+$ being more stable than $[Na(BME\text{-}C22)]^+$ in methanol. This is a result of the cryptand C222 being able to encapsulate Na^+ to a greater extent than the more flexible BME-C22 resulting in a much lower k_d for C222. A similar relationship exists between $[LiC221]^+$ and $[Li(BME\text{-}C21)]^+$ in methanol, with $[LiC221]^+$ characterised by a larger k_c and substantially smaller k_d leading to $[LiC221]^+$ being more stable than $[Li(BME\text{-}C21)]^+$.

4.3 Exchange Kinetics for $[M(TMEC14)]^+$

The variable temperature ^{7}Li and ^{23}Na NMR spectra for $[Li(TMEC14)]^+$ and $[Na(TMEC14)]^+$ in the solvents acetonitrile, propylene carbonate, methanol, dimethylformamide and pyridine yielded only one system undergoing exchange within the NMR timescale which could be subjected to a lineshape analysis (Chapter 8, Section 8.2). The $[Li(TMEC14)]^+$ systems were in fast exchange in all solvents. The $[Na(TMEC14)]^+$ systems were in fast exchange in all solvents except acetonitrile. The kinetic parameters for Na^+ exchange on $[Na(TMEC14)]^+$ have been determined in acetonitrile and are shown in Table 4.5 along with the compositions of each solution. The magnitudes and temperature variations of τ_c are very similar for each set of $[Na(TMEC14)]^+$ data indicating that the rate determining step is independent of the concentration of solvated Na^+ consistent with the operation of a monomolecular decomplexation process (Figure 4.7). Typical exchange modified 79.39 MHz ^{23}Na NMR spectra of Na^+ and $[Na(TMEC14)]^+$ in acetonitrile are shown in Figure 4.8.

The kinetic parameters for $[Na(TMEC14)]^+$, along with those of the related systems, $[Na(TMEC12)]^+$ and $[Na(THEC12)]^+$ in acetonitrile are given in Table 4.6. For $[Na(TMEC12)]^+$ only K_S and an upper limit for k_d and k_c were determined, as the system was in slow exchange [17].

Firstly, comparing the kinetic parameters of $[Na(TMEC12)]^+$ with those of $[Na(THEC12)]^+$ from Table 4.6, $[Na(TMEC12)]^+$ has a smaller k_d and substantially higher k_c which result in $[Na(TMEC12)]^+$ being more stable than $[Na(THEC12)]^+$. This is probably a result of the greater inductive effect of the methoxy groups in TMEC12 compared to the hydroxy groups in THEC12.

Upon comparing the kinetic parameters of $[Na(TMEC14)]^+$ with those of $[Na(TMEC12)]^+$ from Table 4.6, $[Na(TMEC14)]^+$ is characterised by a smaller k_c and substantially higher k_d which results in $[Na(TMEC14)]^+$ being less stable than $[Na(TMEC12)]^+$. The large decrease in k_c and increase in k_d for $[Na(TMEC14)]^+$ compared with $[Na(TMEC12)]^+$ is a result of the greater size and flexibility of TMEC14 compared to TMEC12.

Table 4.5 Sodium(I) exchange on $[Na(TMEC14)]^+$ in acetonitrile.
Solution composition and kinetic parameters[a]

soln.	solvent	$[Na^+_{solvated}]$ mol dm^{-3}	$[Na(TMEC14)]^+$ mol dm^{-3}	k_d (251.6 K)[b] s^{-1}	k_d (298.2 K) s^{-1}	$\Delta H_d^{\ddagger}$ kJ mol^{-1}	$\Delta S_d^{\ddagger}$ J K^{-1} mol^{-1}
i	acetonitrile	0.0818	0.0192	1267 ± 9	9723 ± 210	25.0 ± 0.3	-84.6 ± 1.2
ii		0.0556	0.0455	1230 ± 13	9592 ± 250	25.3 ± 0.4	-84.0 ± 1.5
iii		0.0343	0.0667	1243 ± 11	9302 ± 240	24.6 ± 0.4	-86.7 ± 1.5
(i - iii)		-	-	1247 ± 7	9504 ± 150	25.0 ± 0.2	-85.1 ± 0.9

[a]Errors represent one standard deviation from the least-squares fit of the experimental τ_c data by equation 4.5. [b]Temperature close to coalescence.

Table 4.6 Kinetic parameters for Na^+ exchange on $[NaL]^+$ in acetonitrile

$[ML]^+$	$10^{-5}k_c$ (298.2 K) cm^{3}mol^{-1}s^{-1}	k_d (298.2 K) s^{-1}	$\Delta H_d^{\ddagger}$ kJ mol^{-1}	$\Delta S_d^{\ddagger}$ J K^{-1} mol^{-1}	K_s
$[Na(TMEC14)]^+$	1020	9504	25.0	-85.1	4.03
$[Na(TMEC12)]^+$	< 550000	< 41			9.13
$[Na(THEC12)]^+$	3588	78.5	49.2	-43.7	6.66

[a]This work. [b]Ref. 20. [c]Ref. 21. [d]Ref. 22.

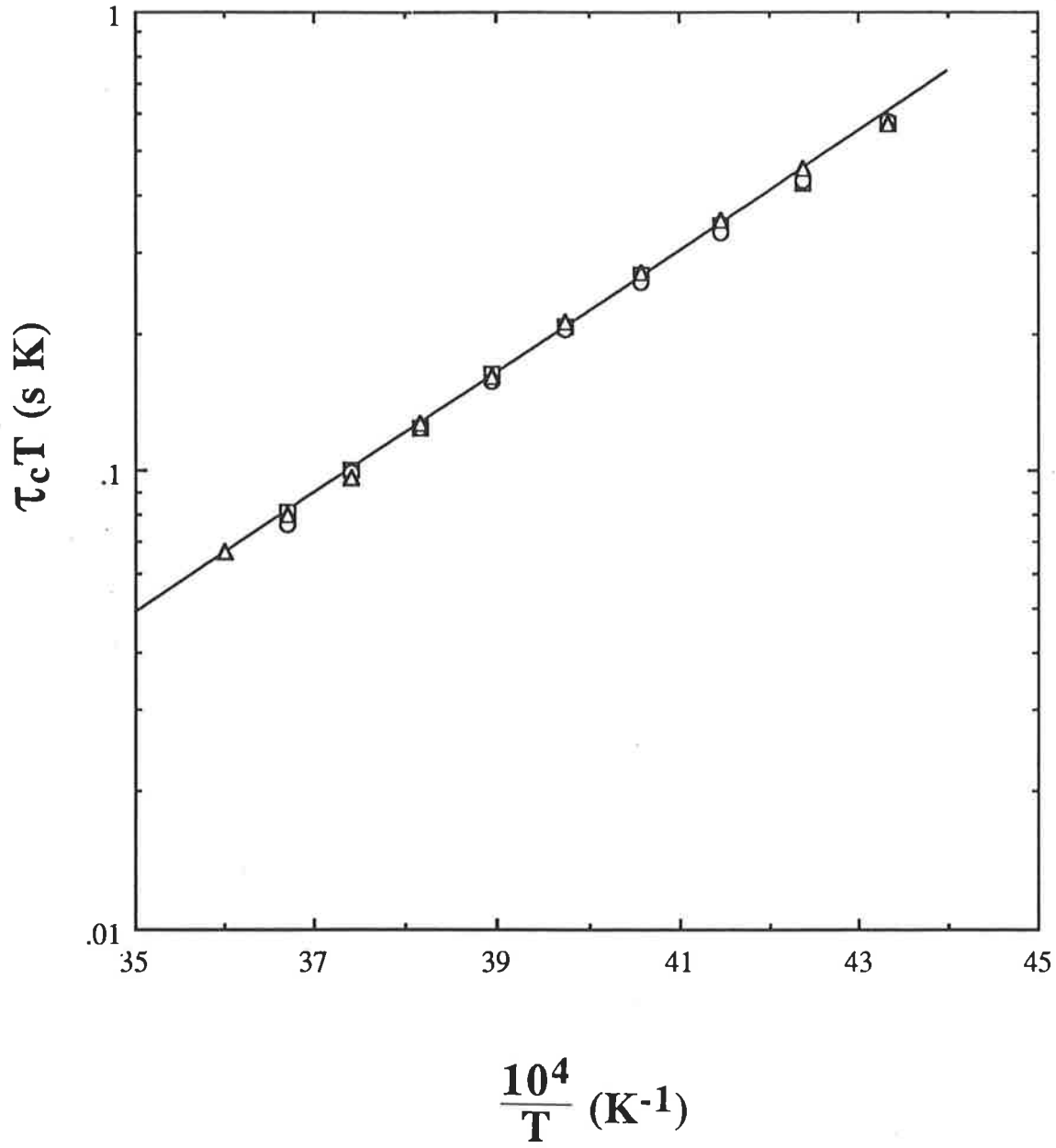

Figure 4.7 The temperature variation of τ_c for the Na^+-$[Na(TMEC14)]^+$ system in acetonitrile. The data points for solutions i-iii, the compositions of which are given in Table 4.5, are represented by triangles, circles and squares, respectively. The solid line represents the best fit of the combined data by Equation 4.5.

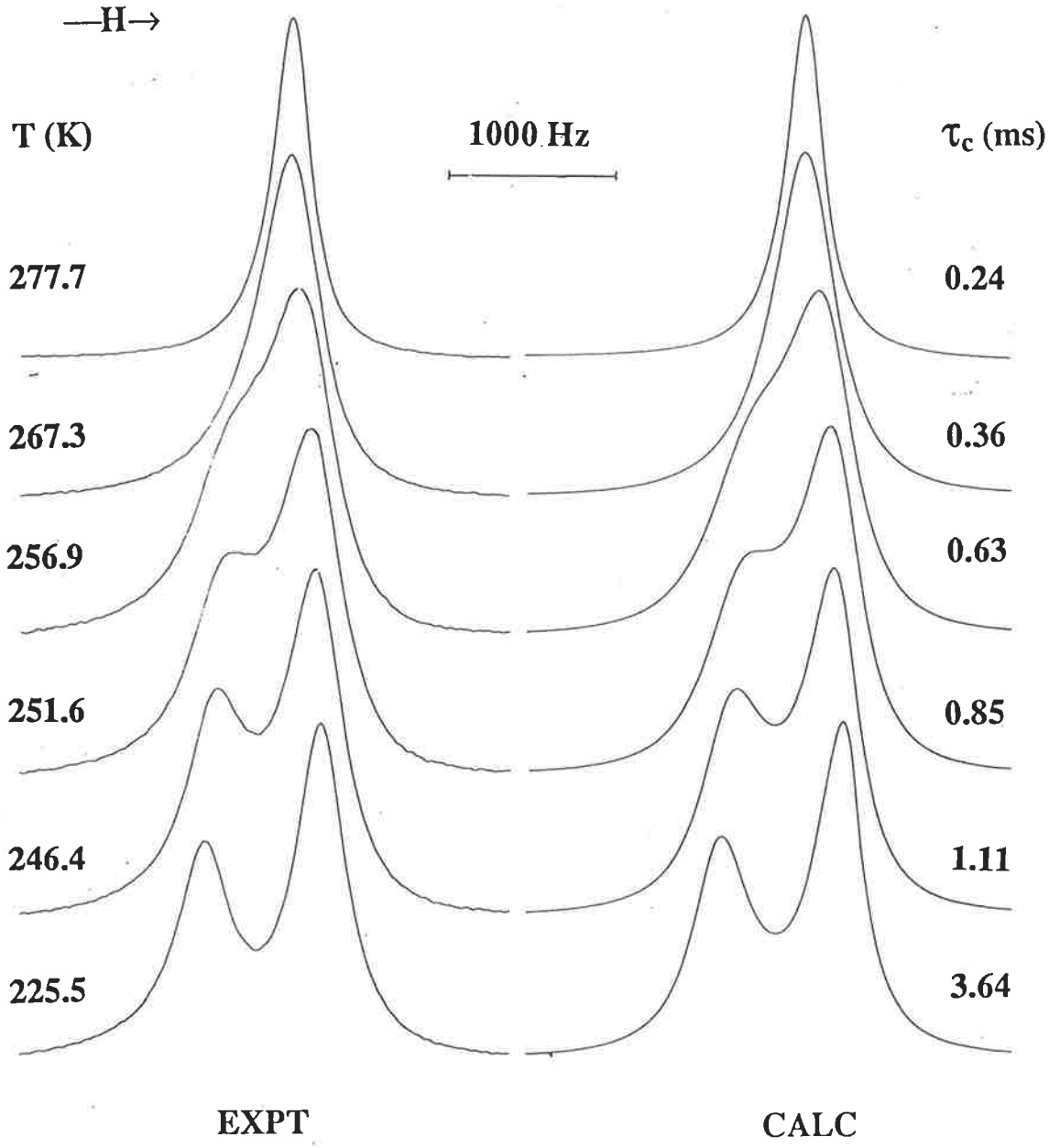

Figure 4.8 Typical exchange modified 79.39 MHz ^{23}Na NMR spectra of an acetonitrile solution of solvated Na^+ (0.0556 M) and $[Na(TMEC14)]^+$ (0.0455 M). Experimental temperatures and spectra appear to the left of the figure. Best fit calculated lineshapes and corresponding τ_c values appear to the right. The resonance of $[Na(TMEC14)]^+$ appears downfield from that of solvated Na^+.

References

1 E. Shchori, J. Jagur-Gradzinski, Z. Luz and M. Shporer, *J. Am. Chem. Soc.*, 1971, **93**, 7133.

2 E. Shchori, J. Jagur-Gradzinski and M. Shporer, *J. Am. Chem. Soc.*, 1973, **95**, 3842.

3 J. M. Ceraso, P. B. Smith, J. S. Landers and J. L. Dye, *J. Phys. Chem.*, 1977, **81**, 760.

4 S. F. Lincoln, I. M. Brereton and T. M. Spotswood, *J. Chem. Soc., Faraday Trans. 1*, 1985, **81**, 1623.

5 S. F. Lincoln, I. M. Brereton and T. M. Spotswood, *J. Am. Chem. Soc.*, 1986, **108**, 8134.

6 S. F. Lincoln and A. Abou-Hamdan, *Inorg. Chem.*, 1990, **29**, 3584.

7 S. F. Lincoln and A. K. W. Stephens, *Inorg. Chem.*, 1991, **30**, 462.

8 A. Abou-Hamdan and S. F. Lincoln, *Inorg. Chem.*, 1991, **30**, 3529.

9 P. Clarke, S. F. Lincoln and E. R. T. Tiekink, *Inorg. Chem.*, 1991, **30**, 2747.

10 M. Shamsipur and A. I. Popov, *J. Phys. Chem.*, 1986, **90**, 5997.

11 A. Delville, H. D. H. Stover and C. Detellier, *J. Am. Chem. Soc.*, 1987, **109**, 7293.

12 J. Burgess, *"Metal Ions in Solution"*, Ellis Horwood, Chichester, 1978.

13 B. O. Strasser and A. I. Popov, *J. Am. Chem. Soc.*, 1985, **107**, 7921.

14 M. Shamsipur and A. I. Popov, *J. Phys. Chem.*, 1988, **92**, 147.

15 H. P. Graves and C. Detellier, *J. Am. Chem. Soc.*, 1988, **110**, 6019.

16 B. G. Cox, N. Van Truong and H. Schneider, *J. Chem. Soc., Faraday Trans. 1*, 1984, **80**, 3285.

17 A. K. W. Stephens and S. F. Lincoln, unpublished material.

5. Intramolecular Exchange Kinetics using ^{13}C NMR

5.1 Introduction

A major effect of the attachment of pendant arms to tetraaza macrocyclic ligands, such as cyclam, is the increased denticity leading to the possibility of stereochemistries and intramolecular processes for the metal complexes which are absent for the unsubstituted parent ligands. Dynamic ^{13}C NMR studies have been used to characterise the rapid conformational exchange processes occurring in solution for a variety of pendant armed tetraaza macrocyclic complexes, primarily with the heavy metal ions [1-6].

This chapter seeks to explore and discuss the complexation and dynamic properties of some tetraaza macrocyclic ligand complexes with a range of alkali and divalent heavy metal ions. In particular the complexes of the ligands TMEC14 and THPC14 with the alkali metal ions, Li^+ and Na^+, and the heavy metal ions, Cd^{2+}, Hg^{2+} and Pb^{2+} will be discussed.

5.2 Assignment of the Structures of Some Heavy Metal Complexes of TMEC14 and (*S*)-THPC14 in d_4-MeOH

The ^{13}C NMR spectra in ^{12}C-d_4-methanol of $[Cd(TMEC14)]^{2+}$, $[Pb(TMEC14)]^{2+}$ and $[Hg(TMEC14)]^{2+}$ all exhibit six resonances at ambient temperature (Table 5.1).

Table 5.1 A comparison of room temperature (fast exchange) ^{13}C chemical shifts of the heavy metal complexes of TMEC14

Complex	Temp	δ^a					
	K	ppm	ppm	ppm	ppm	ppm	ppm
TMEC14	293.8	71.17	58.77	54.84	52.13	51.01	23.20
$[Cd(TMEC14)]^{2+}$	293.8	66.85	59.84	58.81	53.66	51.65	22.94
$[Hg(TMEC14)]^{2+}$	293.8	64.45	59.43	58.94	53.37	50.70	22.63
$[Pb(TMEC14)]^{2+}$	293.8	68.04	57.99	52.50	50.79	48.35	23.74
Intensity Ratio		2	2	2	2	2	1

[a]Referenced to d_4-^{13}C-methanol which was assigned a chemical shift of 47.05 ppm [7].

The ^{13}C NMR spectra of $[Cd(TMEC14)]^{2+}$ and $[Hg(TMEC14)]^{2+}$ show each of the six resonances at ambient temperature broaden and then split into two separate resonances at lower temperature (Table 5.2). The ^{13}C NMR spectra of $[Pb(TMEC14)]^{2+}$ also broadens at lower temperature, however poor solubility of the complex means no low temperature spectra were obtained.

Table 5.2 A comparison of the slow exchange ^{13}C chemical shifts of the heavy metal complexes of TMEC14 at 204.7 K

Complex	Temp	δ^a					
	K	ppm	ppm	ppm	ppm	ppm	ppm
$[Cd(TMEC14)]^{2+}$	204.7	76.85	69.96[b]	68.3[b]	64.01	61.98[b]	35.29
		76.49			63.12		30.56
$[Hg(TMEC14)]^{2+}$	204.7	76.82	69.88	68.87	63.47	61.05	35.30
		75.84	69.13	67.61	63.66	59.94	30.38

[a]Referenced to d_4-^{13}C-methanol which was assigned a chemical shift of 47.05 ppm [7]. [b]Broadened peak formed from two overlapping resonances.

The six observed ^{13}C resonances and their relative populations for the fast exchange spectra of $[M(TMEC14)]^{2+}$ arise from the six chemically different environments of the carbons within the ligand, TMEC14 (Figure 5.1). For TMEC14 the ^{13}C resonances at 71.17, 58.77 and 54.84 ppm are assigned to the methoxyethyl pendant arms (sites **a**, **b** and **c** in Figure 5.1), the resonances at 52.13 and 51.01 ppm are assigned to the ($-NCH_2-$) carbons of the ring (sites **d** and **e** in Figure 5.1) and the resonance at 23.20 ppm is assigned to the medial carbon of the ($-NCH_2CH_2CH_2N-$) moiety (site **f** in Figure 5.1) as deduced from the ^1H undecoupled ^{13}C spectrum of TMEC14. For $[Cd(TMEC14)]^{2+}$ and $[Pb(TMEC14)]^{2+}$ the resonances are assigned as site **a** at 66.85 and 68.04 ppm, site **b** at 59.84 and 57.99 ppm, site **c** at 58.81 and 52.50 ppm, site **d** at 53.66 and 50.79 ppm, site **e** at 51.65 and 48.35 ppm and site **f** at 22.94 and 23.74 ppm, respectively. For $[Hg(TMEC14)]^{2+}$ the resonances are assigned as site **a** at 64.43 ppm, site **c** at 59.41 ppm, site **b** at 58.92 ppm, site **d** at 53.34 ppm, site **e** at 50.68 ppm and site **f** at 22.61 ppm.

The ^{13}C spectra in ^{12}C-d_4-methanol of $[Cd(THPC14)]^{2+}$, $Pb(THPC14)]^{2+}$ and $[Hg(THPC14)]^{2+}$ all exhibit eleven resonances at ambient temperature (Table 5.3).

The ^{13}C spectra shows all eleven resonances simply broaden at lower temperature with the resonance for the medial carbon of the (-$NCH_2CH_2CH_2N$-) moiety remaining as a singlet.

The eleven observed ^{13}C resonances and their relative populations for the slow exchange spectra of $[M(THPC14)]^{2+}$ arise from the six chemically different environments of the carbons within the ligand, THPC14 (Figure 5.2). For THPC14 the ^{13}C resonances at 64.63 and 62.77 ppm are assigned to the 2-hydroxypropyl pendant arms (sites **a** and **b** in Figure 5.2), the resonances at 53.47 and 51.43 ppm are assigned to the (-NCH_2-) carbons of the ring (sites **c** and **d** in Figure 5.2), the resonance at 26.10 ppm is assigned to the medial carbon of the (-$NCH_2CH_2CH_2N$-) moiety (site **e** in Figure 5.2) and the resonance at 20.28 ppm is assigned to the methyl carbon of the 2-hydroxypropyl pendant arm (site **f** in Figure 5.2) as deduced from the ^{1}H undecoupled ^{13}C spectrum of THPC14. For $[Cd(THPC14)]^{2+}$, $[Pb(THPC14)]^{2+}$ and $[Hg(THPC14)]^{2+}$ the resonances are assigned as site **a** at 63.62, 65.78 and 65.11, and 63.94 and 63.36 ppm, site **b** at 63.28 and 62.75, 64.54 and 62.22, and 63.19 and 62.55 ppm, site **c** at 60.84 and 58.73, 54.66 and 54.13, and 60.88 and 60.51 ppm, site **d** at 55.04 and 53.79, 53.85 and 53.41, and 53.78 and 53.32 ppm, site **e** at 24.58, 24.70, and 24.55 ppm, site **f** at 21.75 and 21.21, 21.14 and 20.85, and 22.21 and 21.58 ppm, respectively.

Table 5.3 A comparison of room temperature ^{13}C chemical shifts of the heavy metal complexes of THPC14

Complex	Temp	δ^a					
	K	ppm	ppm	ppm	ppm	ppm	ppm
THPC14	293.8	64.63	62.77	53.47	51.43	26.10	20.28
$[Cd(THPC14)]^{2+}$	299.1	63.62[b]	63.28	60.84	55.04	24.58[c]	21.75
			62.75	58.73	53.79		21.21
$[Hg(THPC14)]^{2+}$	288.2	63.94	63.19	60.88	53.78	25.04[c]	22.21
		63.36	62.55	60.51	53.32		21.58
$[Pb(THPC14)]^{2+}$	299.1	65.78	64.54	60.88	53.78	24.55[c]	22.21
		65.11	62.22	60.51	53.32		21.58
Intensity Ratio		2	2	2	2	1	2

[a]Referenced to d_4-^{13}C-methanol which was assigned a chemical shift of 47.05 ppm [7]. [b]Broadened peak formed from two overlapping resonances. [c]Singlet.

Site **a** and **c** are pendant arm carbons
Site **b** are methoxy carbons
Site **d** are the 1,2-diaminoethane carbons
Site **e** are the 1,3-diaminopropane carbons
Site **f** are the medial carbons

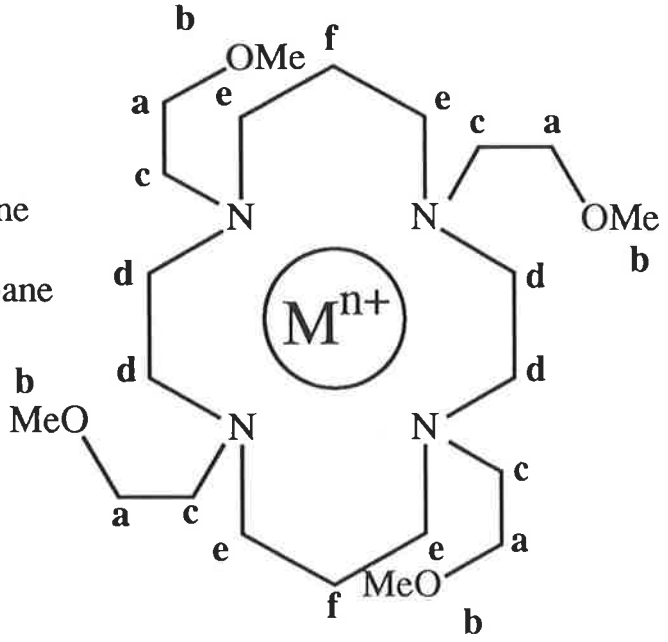

[M(TMEC14)]$^{n+}$

Figure 5.1 Structure and assignments of the ^{13}C resonances for the heavy metal complexes, [M(TMEC14)]$^{n+}$.

Site **a** are chiral carbons (*S*)
Site **b** are pendant arm carbons
Site **c** are the 1,2-diaminoethane carbons
Site **d** are the 1,3-diaminopropane carbons
Site **e** are the medial carbons
Site **f** are the methyl carbons

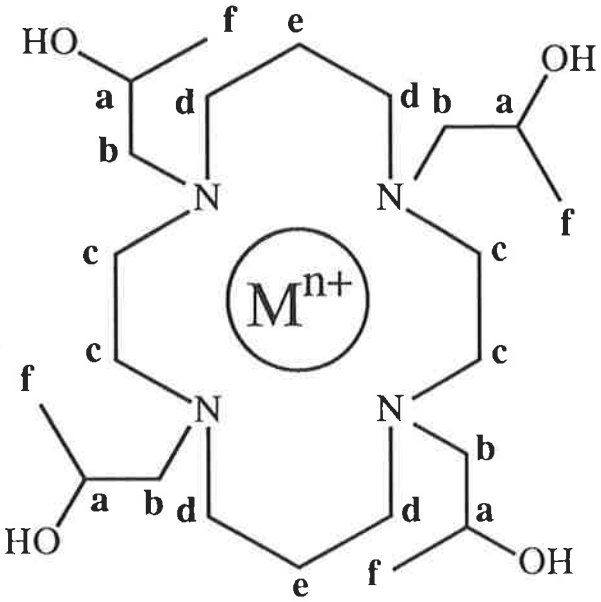

[M(THPC14)]$^{n+}$

Figure 5.2 Structure and assignments of the ^{13}C resonances for the heavy metal complexes, [M(THPC14)]$^{n+}$.

5.2.1 Assignment of the Structure of $[M(TMEC14)]^{2+}$ in Solution

The slow exchange NMR spectra were not obtained for $[Pb(TMEC14)]^{2+}$ due to poor solubility below 260 K. The solution structures of $[M(TMEC14)]^{2+}$, with $M^{2+} = Cd^{2+}$ and Hg^{2+}, may be deduced from the slow exchange ^{13}C NMR spectra from Table 5.2. The five possible configurations of the tetraaza ring with four coplanar nitrogens are shown in Figure 5.3. In order to generate the six symmetrical pairs of resonances observed, the medial carbons of the two (-$NCH_2CH_2CH_2N$-) moieties must be inequivalent, lying either within the plane of symmetry or on a C_2 axis. Such structures require the metal ion to be coordinated to four coplanar nitrogens and two methoxyethyl pendant arms from either end of a (-$NCH_2CH_2CH_2N$-) moiety.

Firstly, the *trans*-II configuration would produce an asymmetric structure with twenty-two inequivalent carbon resonances for the slow-exchange ^{13}C spectra. Therefore, this structure may be eliminated for $[M(TMEC14)]^{2+}$.

Examination of the four remaining configurations for $[M(TMEC14)]^{2+}$, *trans*-I, *trans*-III, *trans*-IV and *trans*-V, show each configuration could produce six doublet ^{13}C resonances.

For the *trans*-IV and *trans*-V configurations of $[M(TMEC14)]^{2+}$ the methoxyethyl pendant arms would be required to coordinate the metal ion from opposite sides of the ring, one above the plane and the other below. It would be expected that the torsional bond strain resulting from these skew-boat conformations would make them unstable and hence *trans*-IV and *trans*-V are unlikely configurations for $[M(TMEC14)]^{2+}$. This is further supported by the fact that no *trans*-IV configurations have been reported for ligands of the parent 1,4,8,11-tetraazacyclotetradecane ring (cyclam). The *trans*-V configurations reported in the literature [8,9] depend on a folded ring (*cis*-V) in which two nitrogens occupy the *trans*-coordination sites of an octahedral metal ion and the other two occupy the *cis*-coordination sites, with the remaining sites generally occupied by solvent molecules (in the absence of coordinating arms) as for *cis*-$[Ni(cyclam)(H_2O)_2]^{2+}$ [10]. In the *cis*-V configuration the two unoccupied *cis*-coordination sites would be attached to the methoxyethyl pendant arms, however this would lead to the two medial carbons of the (-$NCH_2CH_2CH_2N$-) moieties being equivalent. Hence, the *trans*-V configuration can be eliminated.

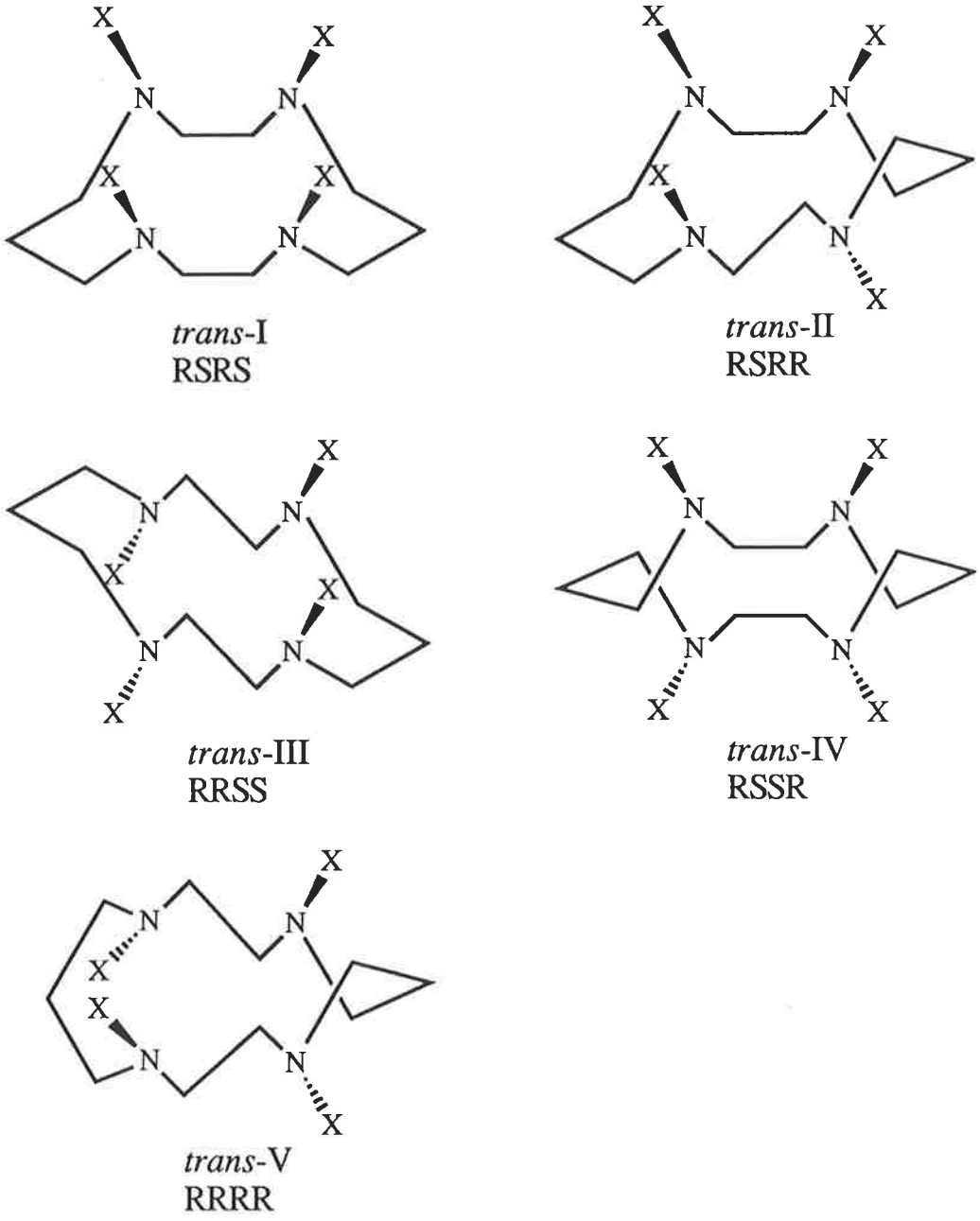

Figure 5.3 Possible configurational isomers of $[M(TMEC14)]^{2+}$ and $[M(THPC14)]^{2+}$ with X representing the methoxyethyl and (*S*)-2-hydroxypropyl pendant arms, respectively. For clarity M^{2+} is not shown but it is assumed to be bound at the centre of the plane by the four nitrogens and two pendant arms at either end of a ($-NCH_2CH_2CH_2N-$) moiety.

In the *trans*-I configuration, the methoxyethyl pendant arms may coordinate either attached to the same (-$NCH_2CH_2CH_2N$-) moiety or attached to diagonally opposite nitrogens and both would be equally likely to occur. Thus, the *trans*-I structure would result in either an additional peak for the equivalent medial carbons of the (-$NCH_2CH_2CH_2N$-) moiety, or simply one peak for the two equivalent medial carbons of the (-$NCH_2CH_2CH_2N$-) moiety. Since the slow-exchange ^{13}C NMR spectra does not reflect either case, the *trans*-I configuration can be eliminated.

Thus, the twelve resonance ^{13}C spectra of $[M(TMEC14)]^{2+}$ is best accounted for by the *trans*-III configuration in which the metal ion lies above the plane of the ring coordinated to the four ring nitrogens and two methoxyethyl pendant arms from above the plane of the ring (Figure 5.4). This structure is further supported from a number of similar *trans*-III complexes reported in the literature such as for $[M(THEC14)]^{2+}$, where M^{2+} = Pb^{2+}, Cd^{2+} and Hg^{2+}, and $[Ni(HTHEC14)]^{3+}$ [1-2,11].

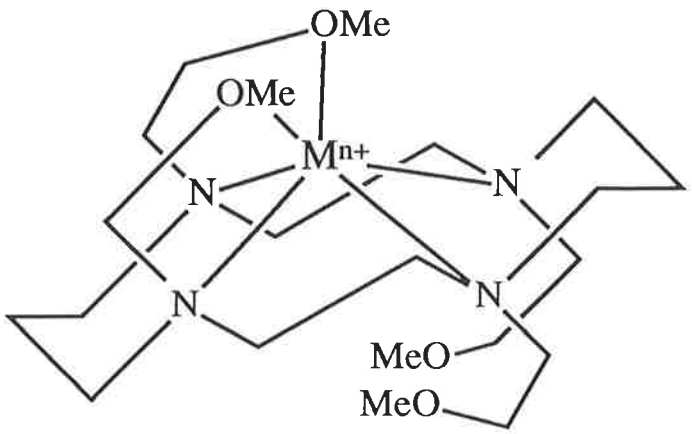

Figure 5.4 A diagram showing one of the possible *trans*-III isomers for the $[M(TMEC14)]^{n+}$ complex.

5.2.2 Assignment of the Structure of $[M(THPC14)]^{2+}$ in Solution

The ^{13}C spectra for $[M(THPC14)]^{2+}$ at ambient temperature for M^{2+} = Cd^{2+}, Hg^{2+} and Pb^{2+}, are shown in Figure 5.5.

The solution structure of $[M(THPC14)]^{2+}$, with M^{2+} = Cd^{2+}, Hg^{2+} and Pb^{2+}, can be deduced from the high temperature slow exchange NMR spectra, with the five possible conformations shown in Figure 5.3. The slow exchange NMR spectra clearly shows eleven resonances, with all six peaks split into two resonances except for the medial carbon of the (-$NCH_2CH_2CH_2N$-) moiety. Upon decreasing the temperature, all peaks simply broaden with the medial carbon remaining as a single resonance at 200 K. This implies that at ambient temperature (298.2 K) there is one fixed isomer, with the medial carbons of the (-$NCH_2CH_2CH_2N$-) moiety equivalent.

For the *trans*-II configuration, all carbons are inequivalent, and since the medial carbons of the (-$NCH_2CH_2CH_2N$-) moieties must be equivalent, the *trans*-II configuration can be eliminated.

The *trans*-III configuration would lead to an NMR spectra similar to those for $[M(TMEC14)]^{2+}$ for M^{2+} = Cd^{2+} and Hg^{2+}, with the medial carbon of the (-$NCH_2CH_2CH_2N$-) moiety becoming inequivalent, and so 12 resonances would be observed for the slow-exchange NMR spectra. Hence, the *trans*-III configuration can be eliminated.

The *trans*-IV configuration could coordinate the metal ion with two (*S*)-2-hydroxypropyl pendant arms in one of two ways. If both arms coordinated the metal ion from above the plane of the ring then there would be eleven resonances observed, with the medial carbons equivalent and the other five resonances split into two resonances. However, this implies that the two pendant arms coordinate from nitrogens separated by only a (-NCH_2CH_2N-) moiety, and is likely to result in steric hindrance. There is also the possibility for the two pendant arms to coordinate from opposite sides of the ring plane with the medial carbons equivalent, although this skew-boat configuration would be expected to be thermodynamically unstable. Thus, the *trans*-IV configuration is unlikely, and this is supported to a degree by the absence of reports of *trans*-IV configurations in the literature.

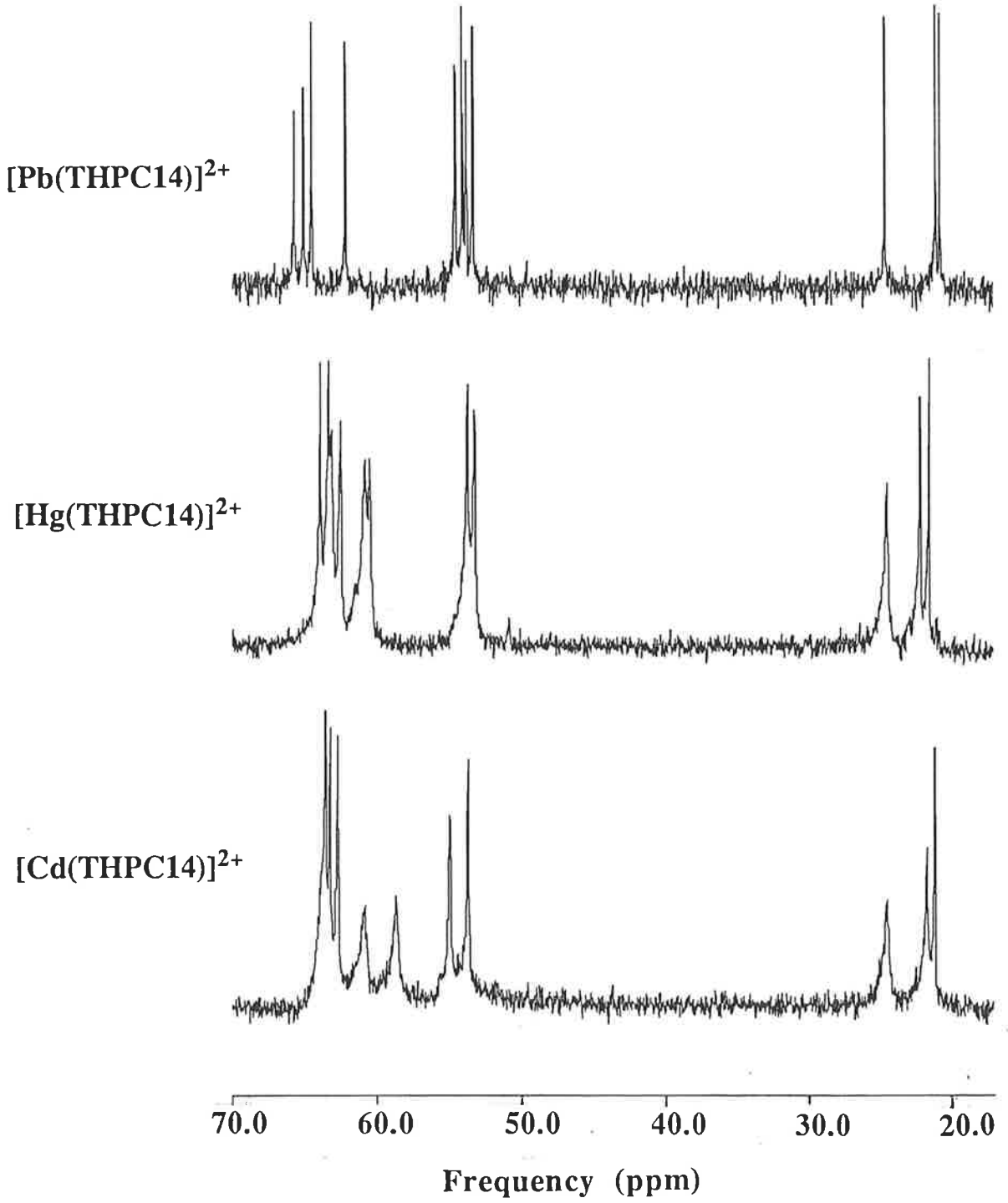

Figure 5.5 75.47 MHz, ^{13}C NMR spectra of $[Pb(THPC14)]^{2+}$, $[Hg(THPC14)]^{2+}$ and $[Cd(THPC14)]^{2+}$ at 298.2 K in ^{12}C-d_4-methanol. Some resolution was lost upon digitising the spectra.

The *trans*-I configuration would result in the desired NMR spectra only if the two pendant arms coordinated from diagonally opposite nitrogens. However the possibility exists for the four pendant arms to freely exchange, since all lie above the plane of the ring, and as the resonances for the other possible isomers are not observed in the NMR spectra this leads to the conclusion that the *trans*-I configuration is unlikely.

This leaves the *trans*-V (or *cis*-V) configuration as the most likely configuration, with the four ring nitrogens and two pendant arms coordinating from the same side of the ring plane in a six-coordinate complex, leaving two pendant arms uncoordinated (Figure 5.6). However, as reported in the literature [8,9], the *trans*-V configuration is generally folded to give *cis*-V and so the most likely configuration for the $[M(THPC14)]^{2+}$ complexes, for $M^{2+} = Cd^{2+}$, Hg^{2+} and Pb^{2+}, is *cis*-V. Thus, in solution the $[M(THPC14)]^{2+}$ complexes exist as one isomer in the *cis*-V configuration.

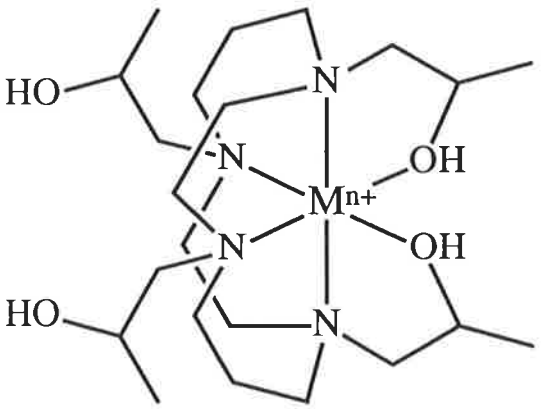

Figure 5.6 A diagram showing the folded *cis*-V configuration for the $[M(THPC14)]^{n+}$ complex.

5.2.3 Intramolecular Exchange of the Alkali Metal Complexes of $[M(TMEC14)]^+$ and $[M(THPC14)]^+$

The ^{13}C NMR spectra of the alkali metal systems, $[Na(TMEC14)]^+$ and $[Li(TMEC14)]^+$ in ^{12}C-d_4-methanol all exhibited 6 resonances at ambient temperature, similar to those observed for the heavy metal complexes of $[M(TMEC14)]^{2+}$ for $M^{2+} = Cd^{2+}$, Hg^{2+} and Pb^{2+}. At lower

temperature, all six resonances for the alkali metal systems simply broadened, however, with no intramolecular exchange observed.

The ^{13}C NMR spectra of the alkali metal systems $[Li(THPC14)]^+$ and $[Na(THPC14)]^+$ in ^{12}C-d_4-methanol also exhibited six resonances at ambient temperature, in contrast to the eleven resonances observed for the heavy metal systems of $[M(THPC14)]^{2+}$ for $M^{2+} = Cd^{2+}$, Hg^{2+} and Pb^{2+}. For the $[Li(THPC14)]^+$ system, all resonances simply broadened at lower temperature, with no intramolecular exchange observed. For the $[Na(THPC14)]^+$ system, however, the six resonances began to split into two resonances at low temperature (*ca* 210 K). The temperature variation of the $[Na(THPC14)]^+$ system is shown in Figure 5.7. At 200 K the resonance for the medial carbon of the (-$NCH_2CH_2CH_2N$-) moiety has split into two broad resonances, however the two resonances coalesce at too low a temperature (*ca* 210 K) for the system to be lineshaped with no slow exchange data able to be obtained. In addition, all six resonances observed at ambient temperature appear to be splitting into two separate resonances at lower temperature, suggesting that the $[Na(THPC14)]^+$ system adopts a 6-coordinate *trans*-III configuration, similar to the $[M(TMEC14)]^{2+}$ complexes (Section 5.2.1)

5.3 Intramolecular Exchange of $[M(TMEC14)]^{2+}$

The ^{13}C NMR spectra for $[Cd(TMEC14)]^{2+}$ and $[Hg(TMEC14)]^{2+}$ over a range of temperatures are shown in Figure 5.8 and 5.9, respectively.

As explained above (Section 5.2.2) the heavy metal complexes of $[M(TMEC14)]^{2+}$, where $M^{2+} = Cd^{2+}$ and Hg^{2+}, appear to undergo intramolecular exchange. The simplest mechanism for the six-coordinate intramolecular exchange for the *trans*-III geometry is the pair-wise exchange of pendant arms on either side of the plane of the ring, as shown in Figure 5.10. The transition state would be expected to be a reactive intermediate in which the metal ion is coordinated in an octahedral geometry within the plane of the ring to the four nitrogens and two pendant arms, one above the plane of the ring and the other below.

The mechanism shown in Figure 5.10 is identical to that for the related $[M(THEC14)]^{2+}$ systems, for $M^{2+} = Cd^{2+}$, Hg^{2+} and Pb^{2+}, which are also of six-coordinate *trans*-III geometry [1-2].

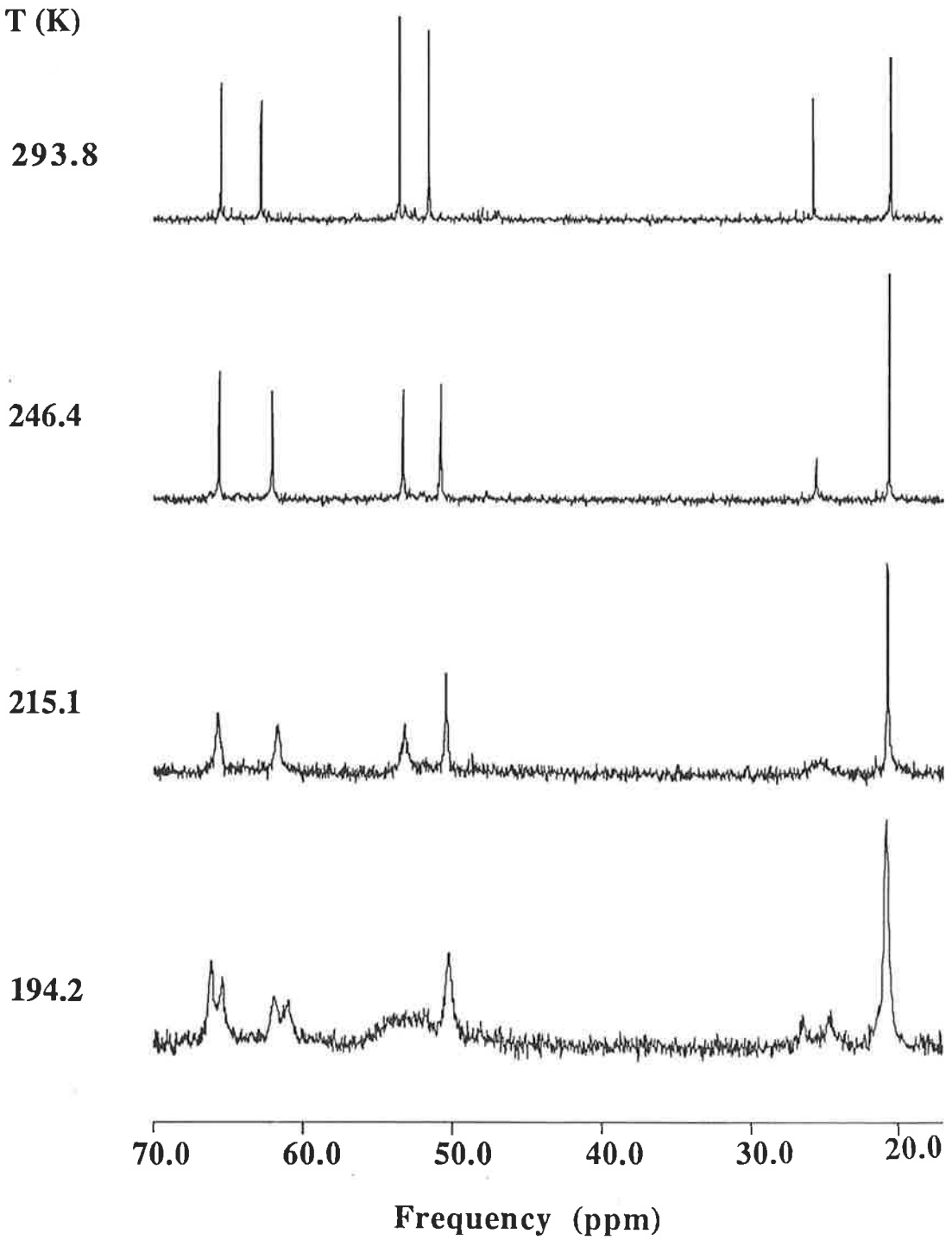

Figure 5.7 Temperature variation of the 75.47 MHz, ^{13}C NMR spectra of $[Na(THPC14)]^{2+}$ (0.102 M) in d_4-methanol. The broadening of the low field resonances arising from the 2-hydroxypropyl pendant arms is a consequence of the increase in solution viscosity with decreasing temperature. Some resolution was lost upon digitising the spectra.

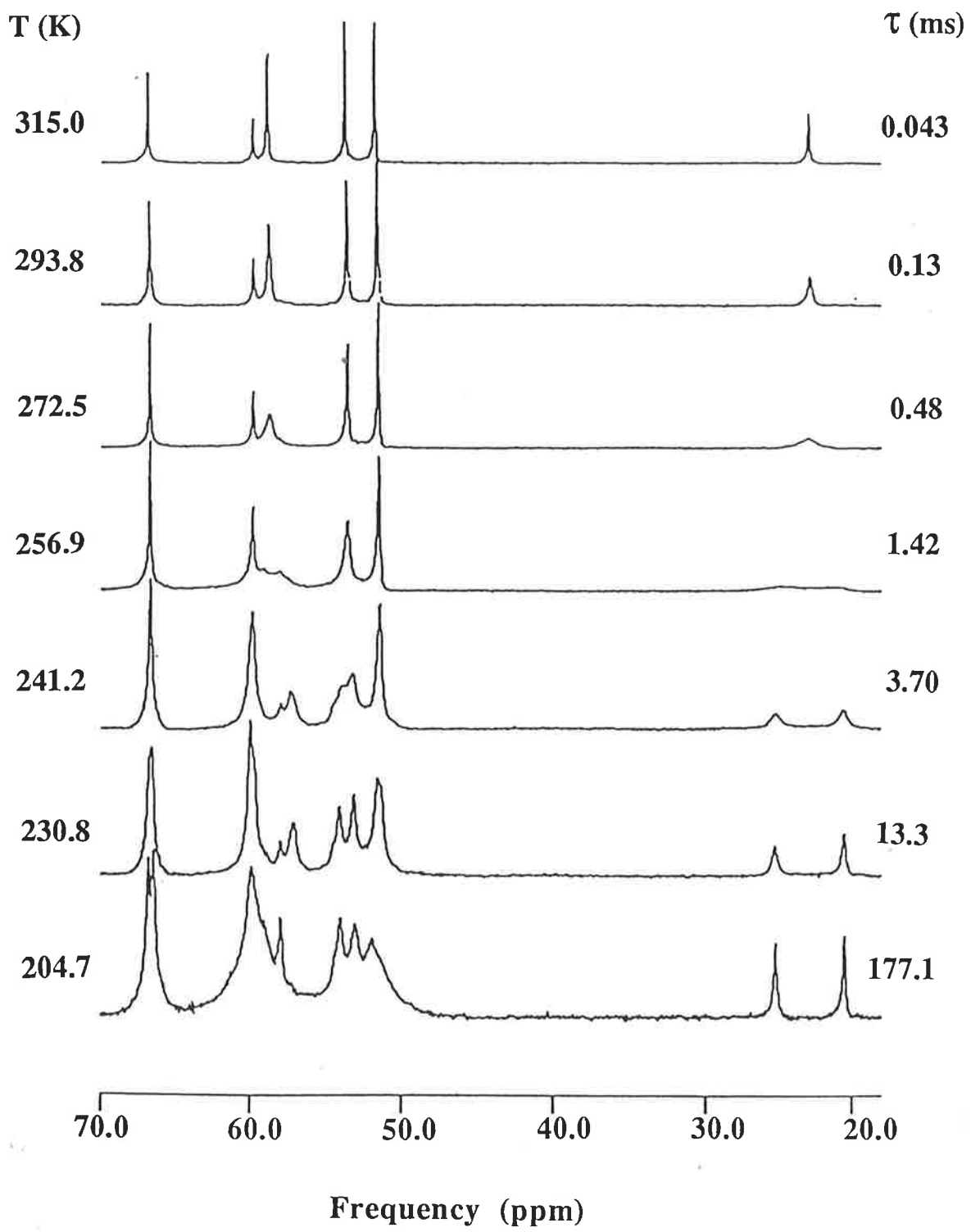

Figure 5.8 Temperature variation of the 75.47 MHz, ^{13}C NMR spectra of $[Cd(TMEC14)]^{2+}$ (0.210 M) in d_4-methanol. The values of the site lifetimes, τ, were derived from complete lineshape analyses of the exchange modified high field resonances arising from the medial carbons in the macrocyclic ring. The broadening of the low field resonances arising from the 2-methoxyethyl pendant arms is a consequence of the increase in solution viscosity with decreasing temperature. Some resolution was lost upon digitising the spectra.

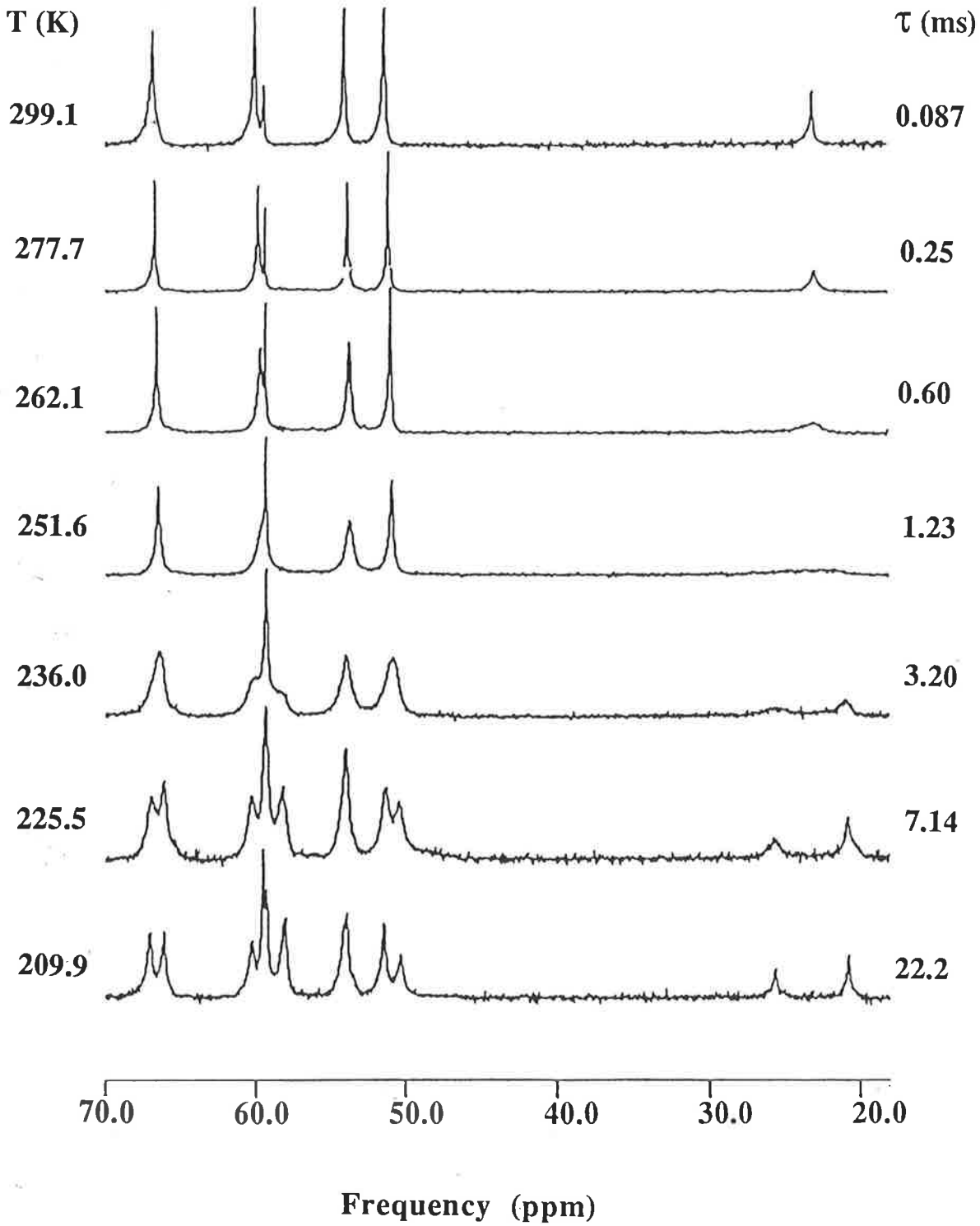

Figure 5.9 Temperature variation of the 75.47 MHz, ^{13}C NMR spectra of $[Hg(TMEC14)]^{2+}$ (0.105 M) in d_4-methanol. The values of the site lifetimes, τ, were derived from complete lineshape analyses of the exchange modified high field resonances arising from the medial carbons in the macrocyclic ring. The broadening of the low field resonances arising from the 2-methoxyethyl pendant arms is a consequence of the increase in solution viscosity with decreasing temperature. Some resolution was lost upon digitising the spectra.

The kinetic parameters derived from the variable temperature ^{13}C NMR for the coalescence of the medial carbon resonances for $[M(TMEC14)]^{2+}$ where $M^{2+} = Cd^{2+}$ and Hg^{2+} are given in Table 5.4. A plot of $T\tau$ versus 1/T for the $[Cd(TMEC14)]^{2+}$ and $[Hg(TMEC14)]^{2+}$ systems is shown in Figure 5.11. For the $[Hg(TMEC14)]^{2+}$ system the two medial carbon resonances at slow exchange are not of equal intensity. This may be a result of differences in the effectiveness of the Nuclear Overhauser Effect (NOE) at different sites [12].

The kinetic parameters for the intramolecular exchange of $[M(TMEC14)]^{2+}$ and the related complexes $[M(TMEC12)]^{2+}$ and $[M(THEC14)]^{2+}$ where $M^{2+} = Cd^{2+}$, Hg^{2+} and Pb^{2+} are given in Table 5.5.

The $[M(TMEC14)]^{2+}$ and $[M(THEC14)]^{2+}$ systems, where $M^{2+} = Cd^{2+}$, Hg^{2+} and Pb^{2+}, both adopt 6-coordinate *trans*-III configurations (Section 5.2.1) which is the most stable configuration for 14-membered ligands based on cyclam [13]. As the ring size decreases to 12-membered for TMEC12 the optimal geometry changes to *trans*-I. This leads to the $[M(TMEC12)]^{2+}$ complexes for $M^{2+} = Cd^{2+}$, Hg^{2+} and Pb^{2+} adopting 8-coordinate *trans*-I configurations, with the intramolecular exchange resulting from the two different enantiomers [3].

In contrast to the $[M(TMEC14)]^{2+}$ complexes, the $[M(THPC14)]^{2+}$ complexes for $M^{2+} = Cd^{2+}$, Hg^{2+} and Pb^{2+} adopt a 6-coordinate folded *trans*-V (*cis*-V) configuration (Section 5.2.2). The room temperature resonances of the $[Na(THPC14)]^{2+}$ complex appear to separate into two separate resonances at lower temperature as for the $[M(TMEC14)]^{2+}$ complexes, suggesting a 6-coordinate *trans*-III configuration (Section 5.2.1).

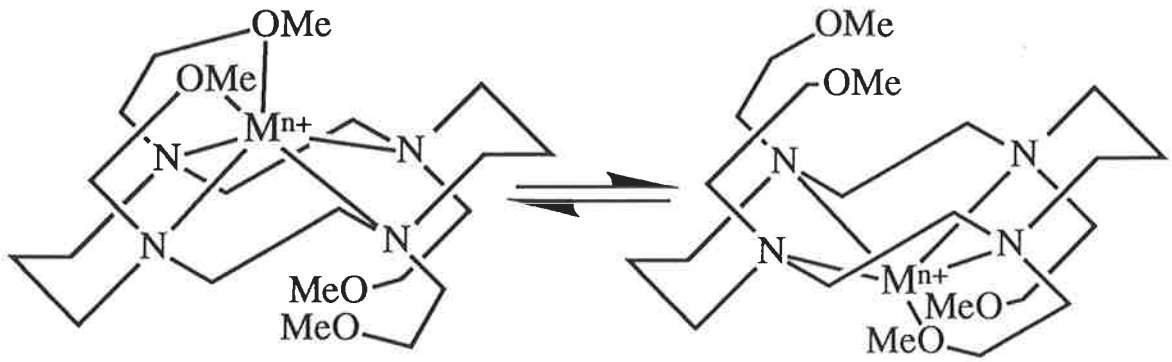

Figure 5.10 Proposed mechanism for the intramolecular exchange of $[M(TMEC14)]^{n+}$ showing the *trans*-III configuration.

Table 5.4 Kinetic parameters[a] for intramolecular exchange in the $[M(TMEC14)]^{2+}$ complexes

Complex	k (s^{-1}) (T)	k (s^{-1}) (298.2 K)	$\Delta H^{\ddagger}$ ($kJmol^{-1}$)	$\Delta S^{\ddagger}$ ($JK^{-1}mol^{-1}$)
$[Cd(TMEC14)]^{2+}$	689 ± 6 (256.9)	9690 ± 220	38.4 ± 0.3	-39.8 ± 1.3
$[Hg(TMEC14)]^{2+}$	628 ± 15 (246.4)	11090 ± 750	31.6 ± 0.6	-61.6 ± 2.9

[a]Errors represent one standard deviation for the fit of the experimental τ data to Equation 4.5.

Table 5.5 Kinetic parameters[a] for intramolecular exchange in the $[M(TMEC12)]^{2+}$, $[M(THEC14)]^{2+}$ and $[M(TMEC14)]^{2+}$ complexes

Complex	k (298.2 K)	$\Delta H^{\ddagger}$ ($kJmol^{-1}$)	$\Delta S^{\ddagger}$ ($JK^{-1}mol^{-1}$)
[b]$[Cd(TMEC12)]^{2+}$	4130	48.9	-11.7
[c]$[Cd(THEC14)]^{2+}$	34200	44.0	-10.6
[d]$[Cd(TMEC14)]^{2+}$	9690	38.4	-39.8
[b]$[Hg(TMEC12)]^{2+}$	4570	39.1	-43.9
[c]$[Hg(THEC14)]^{2+}$	3130	38.0	-50.6
[d]$[Hg(TMEC14)]^{2+}$	11090	31.6	-61.6
[b]$[Pb(TMEC12)]^{2+}$	570	44.1	-44.2
[c]$[Pb(THEC14)]^{2+}$	11200	45.4	-15.2

[a]Errors represent one standard deviation for the fit of the experimental τ data to Equation 4.5. [b]Ref 20. [c]Ref 18,19. [d]This work.

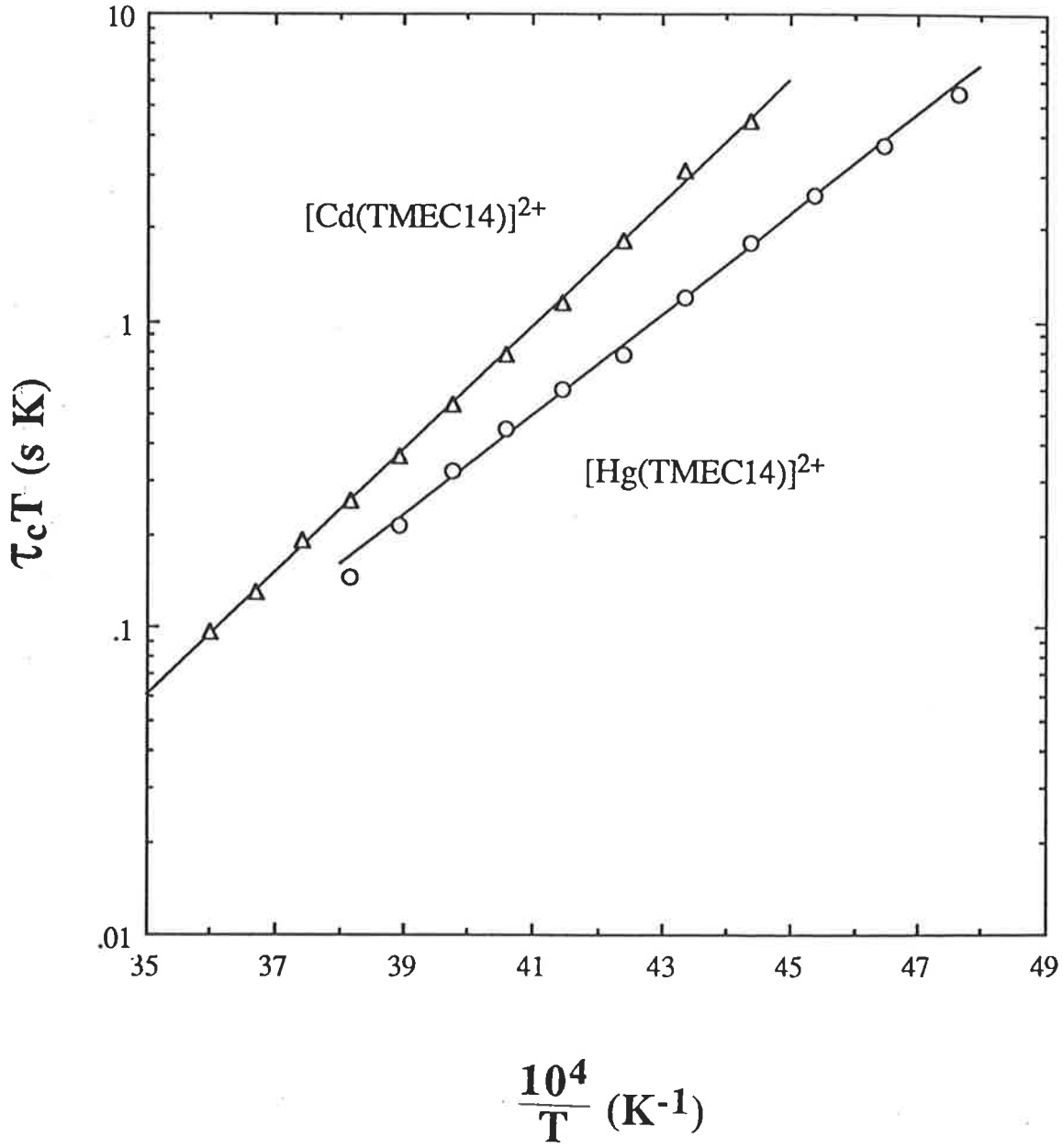

Figure 5.11 The temperature variation of τ for the intramolecular exchange of the $[Cd(TMEC14)]^{2+}$ (triangles) and $[Hg(TMEC14)]^{2+}$ (circles) systems in d_4-methanol. The solid line represents the best fit of the combined data by Equation 4.5.

References

1 P. Clarke, S. F. Lincoln and K. P. Wainwright, *Inorg. Chem.*, 1991, **30**, 134.

2 P. Clarke, A. M. Hounslow, R. A. Keough, S. F. Lincoln and K. P. Wainwright, *Inorg. Chem.*, 1990, **29**, 1793.

3 A. K. W. Stephens and S. F. Lincoln, unpublished material.

4 R. Dhillon and S. F. Lincoln, unpublished material.

5 N. W. Alcock, N. Herron and P. Moore, *J. Chem. Soc., Dalton Trans.*, 1978, 1282.

6 N. W. Alcock, E. H. Curson, N. Herron and P. Moore, *J. Chem. Soc., Dalton Trans.*, 1979, 1987.

7 E. Breitmaier, G. Haas and W. Voelter, *"Atlas of Carbon-13 NMR Data"*, Heyden (London), 1979, **1**.

8 N. W. Alcock, N. Herron and P. Moore, *J. Chem. Soc., Dalton Trans.*, 1979, 1486.

9 R. W. Hay and C. You-Quan, *Inorg. Chim. Acta*, 1991, **180**, 147.

10 E. K. Barefield, A. Bianchi, E. J. Billo, P. J. Connolly, P. Paoletti, J. S. Summers and D. G. Van Derveer, *Inorg. Chem.*, 1986, **25**, 4197.

11 R. W. Hay, M. P. Pujari, W. T. Moodie, S. Craig, D. T. Richens, A. Perotti and L. Ungaretti, *J. Chem. Soc., Dalton Trans.*, 1987, 2605.

12 F. A. Bovey, *"Nuclear Magnetic Resonance Spectroscopy"*, Academic Press (London), 1988, 271.

6. Experimental

6.1 Non-Aqueous Titrations

6.1.1 Materials

Acetonitrile (Ajax), dimethylformamide (BDH), methanol (CSR), propylene carbonate (Aldrich) and pyridine (BDH) were purified and dried as in the literature [1]. All solvents were stored under nitrogen, over Linde 3Å molecular sieves in the cases of acetonitrile and methanol, and over Linde 4Å molecular sieves for dimethylformamide, propylene carbonate and pyridine. $LiClO_4$ and $NaClO_4$ (Fluka) were used as received. $KClO_4$ (BDH) was recrystallised from water. $RbClO_4$ and $CsClO_4$ were prepared by treating RbCl and CsCl (BDH) with a slight excess of concentrated perchloric acid and then recrystallising the perchlorate salts from water until free from chloride and acid. $AgNO_3$ (Matthey-Garrett) and $AgClO_4$ (Aldrich) were used as provided. Tetraethylammonium perchlorate was prepared by addition of a slight excess of concentrated perchloric acid to tetraethylammonium bromide (BDH) and then recrystallised from water until free from bromide and acid. All perchlorate salts were vacuum dried at 353-363 K for 48 hours, and then stored over P_2O_5 under nitrogen.

6.1.2 Determination of Stability Constants in Non-Aqueous Solution

Stability constants were determined for the complex $[ML]^+$, for which L = BME-C21, BME-C22, TMEC14 and THPC14, and $M^+ = Li^+$, Na^+, K^+, Rb^+, Cs^+ and Ag^+, using potentiometric titrations. Solutions were prepared by volume under nitrogen in a dry box. All titrations were carried out at 298.2 K using water jacketed cells connected to a thermostatted water bath. Dry nitrogen was bubbled through the titration solution to prevent the ingress of oxygen and atmospheric moisture. The nitrogen stream was initially passed through a nitrogen bubbler containing dry solvent to prevent evaporation during the titration. A salt bridge was used to connect the working cell to the reference cell. All solutions were made up with 0.05 M Et_4NClO_4 to ensure the ionic strength remained constant. The reference cell consisted of a silver electrode inserted into a 0.01 M $AgNO_3$ or $AgClO_4$ solution.

6.1.3 Determination of Stability Constants using a Silver Electrode

The stability constants of all Ag^+ complexes were determined using direct titrations, in which a solution of 0.01 M ligand (L) was titrated by burette into 20 cm^3 of a 0.001 M $AgNO_3$ or $AgClO_4$ solution and the potential monitored using an Orion Research 720 digital analyser. The stability constants of the alkali metal complexes (except where their stability was higher than that for the corresponding $[AgL]^+$ complex - see below) were determined using competitive titration methods. This involved titrating 5 cm^3 of a solution of 0.01 M ligand solution (L) and 0.05 M metal ion solution (M^+) (burette) into 20 cm^3 of a 0.001 M $AgNO_3$ or $AgClO_4$ solution, and measuring the change in potential.

6.1.4 Determination of Stability Constants using a Sodium Selective Electrode

The stabilities of the complexes $[Li(BME\text{-}C21)]^+$, $[Na(BME\text{-}C21)]^+$ and $[Na(BME\text{-}C22)]^+$ in acetonitrile, and $[Na(BME\text{-}C21)]^+$, $[Na(BME\text{-}C22)]^+$, $[Li(BME\text{-}C21)]^+$ and $[Li(BME\text{-}C22)]^+$ in pyridine were greater than their silver analogues and hence were determined by direct titration using a Radiometer G502NA sodium ion selective electrode as has been previously described in literature [2-5]. The sodium selective electrode can also be used as a less sensitive lithium selective electrode for the direct titrations of the lithium complexes. The stability constants of the sodium and lithium complexes were determined by titrating 5 cm^3 of a solution of ligand (L) (burette) into 20 cm^3 of a 0.001 M $NaClO_4$ or $LiClO_4$ solution and measuring the change in potential.

6.1.5 Treatment of Data for Non-Aqueous Titrations

The systems were calibrated by titrating 5 cm^3 of 0.01 M $AgNO_3$ or $AgClO_4$ solution (burette) for the silver working electrode, and 5 cm^3 of 0.01 M $NaClO_4$ or $LiClO_4$ solution (burette) for the sodium selective electrode, into a 20 cm^3 solution of 0.05 M Et_4NClO_4.

The stability constants were determined from the data using the programs VISP [6] and STAB [6] as described in Chapter 7.

The electrode response for both the silver wire and sodium selective electrodes may be described by the pseudo Nernstian relationship:

$$E = E_0 + C\ln[M^+] \qquad \textbf{6.1}$$

where E_0 and C are determined by a plot of the potential, E (in mV), versus the natural logarithm of the metal ion concentration, $\ln[M^+]$. The values of E_0 and C vary with changing solvent, with C typically lying between 19.5 and 28.0 as previously quoted in the literature [7]. The silver electrode response means stability constants lie typically in the range of 10^2 - 10^{12} M^{-1}, with 10^2 - 10^7 M^{-1} being a typical range for the sodium ion selective electrode, though values up to 10^9 M^{-1} have been quoted in literature [4]. Generally, the stability constant of the metal complex $[ML]^+$ needs to be at least 10^1 M^{-1} less than that of the silver complex in order to be determined by the competitive potentiometric titration method.

6.2 Aqueous Titrations

6.2.1 Materials

Deionised water was ultrapurified using a MilliQ-Reagent system to produce water with a resistance of greater than 15 MΩ cm with which all solutions were prepared. The metal perchlorates of Li(I), Na(I), K(I), Rb(I), Cs(I) and Ag(I) were prepared as described in Section 6.1.1. The perchlorate salts of Mg(II), Mn(II), Co(II), Ni(II), Cu(II) and Zn(II) (Aldrich) were used as provided. The perchlorate salts of Ca(II), Sr(II), Ba(II), Cd(II) and Pb(II) were prepared by addition of a slight excess of concentrated perchloric acid to the corresponding metal carbonate (MCO_3) and then recrystallised from water until free from acid. All metal perchlorate salts were vacuum dried at 353-363 K for 48 hours and then stored over P_2O_5 under nitrogen. Mercuric perchlorate was prepared as a solution of 0.1 M $HgClO_4$ and 0.1 M $HClO_4$ (both due to the hazardous nature of mercuric salts and to prevent the formation of the red oxide which results at a pH of greater than 2) by addition of an excess of perchloric acid to mercuric oxide. All metal perchlorate solutions were standardised using EDTA titrations [8]. The Et_4NOH solution (autoburette) was standardised by titration with 1.0 M hydrochloric acid (CONVOL). All solutions were made up with 0.1 M Et_4NClO_4 to ensure that the ionic strength remained constant.

6.2.2 Determination of Stability Constants in Aqueous Solution

The stability constants of metal complexes in aqueous solution were determined using potentiometric titrations. The potential was measured with an Orion Ross Sureflow 81-72 BN combination electrode connected to an Orion SA720 potentiometer, using a Metrohm E665 Dosimat autoburette and interfaced to a Laser XT/3-8086. All titrations were carried out at 298.2 K using a water-jacketed cell connected to a thermostatted water bath. Nitrogen was bubbled into the solution to prevent oxygen and carbon dioxide from entering the solution (the presence of carbon dioxide may lead to the formation of a carbonic acid - carbonate buffer, which will effect the pH of the solution [9]) and the solutions stirred using a magnetic stirrer. The nitrogen stream was initially passed through a nitrogen bubbler containing ultrapurified water to prevent any evaporation during titrations. The system was calibrated by titrating 1 cm^3 of 0.101 M NEt_4OH (autoburette) with 10 cm^3 of a stock solution of 0.004 M $HClO_4$ in the case of the lariat ethers and 0.005 M $HClO_4$ in the case of TMEC14. The resulting data was fitted to the Nernst Equation:

$$E = E_o + \frac{RT}{F} \ln[H^+] \qquad \textbf{6.2}$$

where E is the observed potential (mV)

E_o is the standard potential for the electrode (mV)

R is the gas constant, 8.314 (J K^{-1} mol^{-1})

T is the temperature (K)

F is Faraday's constant, 9.6487 x 10^4 (C mol^{-1})

$[H^+]$ is the proton concentration

which at fixed temperature (298.2 K) then becomes:

$$pH = \frac{E_o - E}{59.15} \qquad \textbf{6.3}$$

where $pH = -\log [H^+]$

The program MacCalib [10] was used to calculate the endpoint (and hence the exact concentration of H^+ used), and the pK_w and E_o for each system. Diffusion correction parameters for the electrolyte, Et_4NClO_4,

were used as in the literature [11]. The system was recalibrated every five to six titrations. The protonation constants of the various ligands were calculated by titrating 1 cm^3 of 0.101 M Et_4NOH into 10 cm^3 of a solution which was 0.001 M in ligand and either 0.004 M in $HClO_4$ for the lariat ethers or 0.005 M in $HClO_4$ for TMEC14. The stability constants of the metal ion complexes were calculated by titrating 1 cm^3 of 0.1 M Et_4NOH into 10 cm^3 of a solution which was 0.001 M in ligand, 0.0005 - 0.0015 M in $M(ClO_4)_2$, and either 0.004 M in $HClO_4$ for the lariat ethers or 0.005 M in $HClO_4$ for TMEC14. The values of the pKa's and stability constants for the lariat ethers were calculated using Miniquad [10]. For the tetraaza macrocycle, TMEC14, Superquad [12] was used to determine the pKa values and the stability constants, including other species in solution (such as $[MLH]^{3+}$ and $[MLOH]^+$, see Chapter 3, Section 3.2.2.6). Titrations for protonation constants and stability constants were repeated at least three times, with the metal ion concentration also being varied between titrations for each metal complex.

6.3 NMR Spectroscopy

6.3.1 ^{23}Na and ^{7}Li NMR Measurements

For ^{23}Na and ^{7}Li NMR, solutions were prepared using 0.1 M $NaClO_4$ and 0.02 M $LiClO_4$, respectively. At least three different $[M^+]$ to $[ML]^+$ ratios were used for each system (typically 1:2, 1:1 and 2:1) with the total $[Na^+]$ and $[Li^+]$ remaining constant. All solutions were prepared under nitrogen to prevent the ingress of oxygen and water (moisture) from the air. The solutions were transferred to 5 mm NMR tubes (507PP) and were then degassed and sealed under vacuum. The sealed NMR tubes were coaxially mounted in a 10 mm NMR tube (513-1PP) containing either d_6-acetone (for temperatures less than 300 K) or D_2O (for temperatures higher than 300 K) as a lock solvent. ^{23}Na and ^{7}Li NMR measurements were carried out on a Bruker CXP-300 at 79.39 and 116.59 MHz, respectively. For ^{23}Na measurements, an average of 1000 - 6000 transients were accumulated in a 2048 point data base over a 10000 Hz spectral width prior to Fourier transformation. For ^{7}Li measurements, an average of 1000 - 6000 transients were accumulated in a 8192 point data base over a 1000 Hz spectral width prior to Fourier transformation. The temperature of the sample was controlled to within $\pm$ 0.3 K using a Bruker B-VT1000 variable temperature unit. The system was calibrated by monitoring the temperature dependence of the ^{1}H chemical shift of methanol (for temperatures below

300 K) and ethylene glycol (for temperatures above 300 K) [13]. For each new temperature, at least twenty minutes was allowed to ensure that the sample had reached thermal equilibrium. The accumulated transients were Fourier transformed and then transferred to a VAX 11-780 mainframe computer where the data was subjected to a full lineshape analysis [6,14]. Kinetic data were obtained from the lineshape analysis by fitting each experimental spectra to one calculated using theoretical data (non-broadened and non-exchanging linewidths and chemical shifts) taken from the purely solvated (free) and purely complexed (bound) spectra.

6.3.2 Materials for ^{13}C NMR Measurements

The heavy metal triflate salts $Cd(CF_3SO_3)_2$, $Pb(CF_3SO_3)_2$, $Hg(CF_3SO_3)_2$ and $Zn(CF_3SO_3)_2$ were prepared by addition of concentrated triflic acid (trifluromethanesulfonic acid) to an excess of the corresponding carbonate. Unreacted carbonate was gravity filtered off and the volume reduced until the triflate salt precipitated from solution at room temperature. The white salts were then collected by suction filtration, and dried under vacuum over P_2O_5 for 48 hours. For $Hg(CF_3SO_3)_2$ a slight excess of acid was used initially to prevent the formation of red HgO. All triflate salts were stored under nitrogen. The heavy metal complexes of TMEC14 and THPC14 were then made by addition of equimolar amounts of the respective ligand and the triflate salt in d_4-^{12}C-methanol (Aldrich). The solutions were then transferred to a 5 mm NMR tube (507PP).

6.3.3 ^{13}C NMR Measurements

^{13}C NMR was run on a Bruker CXP-300 spectrometer at 75.47 MHz using broad-band proton decoupling. An average of 2000 - 4000 transients was collected in an 8192 point data base over a 10000 Hz spectral width prior to Fourier transformation. The accumulated transients were Fourier transformed and then transferred to a VAX 11-780 mainframe computer where the data were subjected to a full lineshape analysis [6,14]. The temperature dependences of chemical widths and shifts in the absence of exchange were extrapolated from low temperatures where no exchange induced modification of the spectra occurred. Carbon-12 d_4-methanol was used to prevent the overlap of the ^{13}C signals arising from the complex and the lock solvent. Carbon-13 d_4-methanol was then used as an external reference and assigned a chemical shift of 47.05 ppm [15].

6.4 Preparation of the Lariat Ethers, BME-C21 and BME-C22

The synthesis of these lariat ethers uses methoxyethyl *p*-toluenesulfonate, which was synthesised from 2-methoxyethanol as described in the literature [16].

6.4.1 Preparation of Methoxyethyl *p*-Toluene Sulfonate

2-methoxyethanol (50 g, 0.657 moles, Ajax) was dissolved in pyridine (500 cm^3, BDH) and the solution cooled to 268 K in an ice-salt bath. *P*-toluenesulfonyl chloride (138 g, 0.724 moles, Fluka) was then added in portions and the suspension gently stirred by hand until all the tosyl chloride had dissolved. After keeping the solution at 273 K for a further 2 hours, water (50 cm^3) was added in portions (1 + 1 + 1 + 2 + 5 + 10 + 30 cm^3) at 5 minute intervals with stirring during which the temperature remained below 278 K. The solution was then diluted with water (500 cm^3). The aqueous pyridine solution was extracted with chloroform (3 x 500 cm^3) and the chloroform extracts washed successively with ice-cold dilute sulfuric acid (1%), deionised water, and saturated sodium bicarbonate solution. The chloroform solution was dried with anhydrous sodium sulfate, filtered and evaporated to dryness leaving a pale yellow oil. The oil was purified by vacuum distillation (414 K, 0.2 Torr) yielding a clear oil. Yield 113 g, 75%, ^{13}C ($CDCl_3$): δ 21.1 ($\underline{C}H_3$-Ar), 58.4 ($\underline{C}H_3$-0), 68.9 ($\underline{C}H_2$-0-CH_3), 69.4 ($\underline{C}H_2$-0-S), 127.6 (CH_3-$\underline{C}$), 129.5 ($\underline{C}$H-C-CH_3), 132.4 ($\underline{C}$H-C-S), 144.6 ($\underline{C}$-S).

6.4.2 Preparation of BME-C21

The lariat ether 1,7-bis(2-methoxyethyl)-4,10,13-trioxa-1,7-diazacyclopentadecane, BME-C21, was synthesised according to the literature [17].

To a 100 ml round bottomed flask containing ethanol (25 cm^3) was added 4,10,13-trioxa-1,7-diazacyclopentadecane (C21 Kryptofix) (2.0 g, 9.42 mmol, Merck), methoxyethyl *p*-toluene sulfonate (11.7 g, 56.5 mmol), and triethylamine (1.9 g, 19 mmol, BDH). The solution was refluxed for 10 hours and cooled to room temperature. The ethanol was then evaporated off and the resultant residue dissolved in water (150 cm^3) and washed with ether (4 x 100 cm^3) to remove the excess methoxyethyl *p*-toluenesulfonate. The water layer was made basic with triethylamine until the pH was greater than 11 and extracted with chloroform (3 x 100 cm^3). The chloroform

layer was evaporated and the residue distilled under vacuum (421 - 424 K, 0.01 Torr) to yield the product as a clear oil. Yield 1.4 g, 44%, ^{13}C ($CDCl_3$): δ 54.2 ($\underline{C}H_2$-O-CH_3), 54.5 (N-$\underline{C}H_2$-CH_2-O-CH_2-$\underline{C}H_2$-N), 55.2 ($\underline{C}H_2$-CH_2-O-CH_3), 58.3 ($\underline{C}H_3$-O), 69.0 (N-$\underline{C}H_2$-CH_2-O-CH_2-CH_2-O), 69.6 (N-CH_2-$\underline{C}H_2$-O-$\underline{C}H_2$-CH_2-N), 70.1 (N-CH_2-$\underline{C}H_2$-O-CH_2-CH_2-O), 70.6 (O-$\underline{C}H_2$-$\underline{C}H_2$-O).

6.4.3 Preparation of BME-C22

The preparation of the lariat ether 7,16-bis(2-methoxyethyl)-1,4,10,13-tetraoxa-7,16-diazacyclooctadecane, BME-C22, was taken from the literature [17] and is identical to that for BME-C21 except that C21 Kryptofix is replaced by 1,4,10,13-tetraoxa-7,16-diazacyclooctadecane (C22 Kryptofix) (Merck).

BME-C22 was purified by vacuum distillation at 438 - 441 K, at 0.01 Torr as a clear oil. Yield 1.3 g, 37%, ^{13}C ($CDCl_3$): δ 54.1 (N-$\underline{C}H_2$-CH_2-0-CH_3), 54.6 (N-$\underline{C}H_2$-CH_2-O-CH_2), 58.6 ($\underline{C}H_3$-O), 69.6 ($\underline{C}H_2$-O-CH_3), 70.5 (N-CH_2-$\underline{C}H_2$-O-CH_2), 70.9 (O-$\underline{C}H_2$-$\underline{C}H_2$-O).

6.5 Preparation of the Tetraaza Macrocyclic Ligands, Cyclam, TMEC14 and (*S*)-THPC14

6.5.1 Preparation of Cyclam

The preparation of 1,4,8,11-tetraazacyclotetradecane (cyclam) was taken from the literature [18].

1,3 diaminopropane, (445 g, 306 cm^3, 6 moles, Fluka) was placed in a two litre, three necked round bottom flask with a magnetic stirrer, addition funnel and thermometer. The diamine was cooled to 273 K and 1,2 dibromoethane (94 g, 61 cm^3, 0.5 moles, BDH) added drop-wise with vigorous stirring over 1 - 2 hours. The reaction mixture was then heated on a steam bath for 1 hour and concentrated by removal of excess 1,3-diaminopropane on a rotary evaporator. The concentrate was returned to the original reaction vessel, and pulverised potassium hydroxide (75 g) was added. The mixture was then heated with efficient stirring for 2 hours on a steam bath. After cooling to room temperature, the solids were removed by vacuum filtration and washed with several portions of ether to remove the adsorbed product. The ether washings and filtrate were combined and reduced on a rotary evaporator to a viscous oil which was then decanted

from the solid. The remaining solid was dissolved in water and extracted with ether to remove any remaining oil. The oil and ether layers were combined and rotory-evaporated leaving a viscous oil which was pale yellow. The linear tetramine, 1,5,8,12-tetraazadodecane was then distilled under vacuum (373 - 383 K, 0.1 Torr) using a 20 cm Vigreaux column. Yield 42 g, 48%.

Nickel(II) perchlorate (38.7 g, 0.15 moles) was dissolved in water (400 cm^3) in a two litre beaker and 1,5,8,12-tetraazadodecane (26 g, 0.15 moles) was added with stirring. The resultant red-brown solution was cooled to 278 K in an ice bath and 30% glyoxal solution (30 cm^3, 0.15 moles) was added with stirring. The beaker was removed from the ice-bath and allowed to stir overnight at room temperature. The solution was then cooled to 278 K (ice-bath) and treated with sodium tetrahydroborate (11 g, 0.3 moles, Ajax) in small portions over a 1 hour period to avoid severe frothing. During this addition the solution turned black (metallic nickel) and orange crystals ($[Ni(cyclam)]^{2+}$) formed. After addition of the tetrahydroborate the solution was removed from the ice-bath and heated to 353 K on a steam bath for about 40 minutes. The hot solution was then rapidly filtered through a pre-heated size 3 sinter to remove any nickel metal present (black powder) leaving the orange complex in solution.

The solution was then transferred to a one litre round bottomed flask fitted with a condenser and sodium cyanide (29 g, 0.6 moles, BDH) added. The solution was then refluxed for 2 hours and cooled to room temperature. Sodium hydroxide (15 g) was added to the solution and the water rotor-evaporated off until a semi-solid remained. Chloroform (100 cm^3) was added to the flask and the liquid drawn off. The remaining solid was treated twice with chloroform (100 cm^3 portions) and the aqueous layer separated and washed 5 - 7 times with chloroform (50 cm^3 portions). The chloroform extracts were combined, dried over sodium sulfate and evaporated to dryness. The yellowish solid remaining was recrystallised from chlorobenzene (800 cm^3) yielding white needles which were collected by suction filtration and washed with diethyl ether (50 cm^3). The product (cyclam) was then air-dried. A second crop was obtained by evaporation of the filtrate and treating similarly as above. Yield 4 g, 13%, ^{13}C ($CDCl_3$): δ 29.4 (CH_2-$\underline{C}H_2$-CH_2), 49.3 ($\underline{C}H_2$-CH_2-$\underline{C}H_2$), 50.6 (N-$\underline{C}H_2$-$\underline{C}H_2$-N).

6.5.2 Preparation of TMEC14

The synthesis of 1,4,8,11-tetrakis-(2-methoxyethyl)-1,4,8,11-tetraazacyclotetradecane (TMEC14) was modified from that of its twelve membered analogue (TMEC12) in the literature [19].

Cyclam (0.42 g, 2.1 mmol) and sodium hydroxide (0.34 g) were dissolved in 50% ethanol/water in a 100 ml round bottomed flask. 2-chloroethyl methyl ether (8.0 g, 84 mmol, Aldrich) was added and the solution refluxed under nitrogen for 7 days. A large excess of chloroethyl methyl ether was needed as it reacts slowly with sodium hydroxide to form the corresponding alcohol. Each day the pH of the solution was tested and an appropriate amount of NaOH added to keep the pH greater than 12 (approximately 0.2g/day). The solution was then cooled to room temperature, basified with sodium hydroxide (pH > 12) and water (40 cm^3) added. The resultant solution was then extracted with chloroform (3 x 100 cm^3), dried over sodium sulfate and evaporated leaving a pale yellow oil. Distillation under vacuum (445 - 448 K, 0.01 Torr) yielded the product as a clear oil. Yield 0.65 g, 72%, ^{13}C ($CDCl_3$): δ 23.1 (CH_2-$\underline{C}H_2$-CH_2), 50.9 ($\underline{C}H_2$-CH_2-$\underline{C}H_2$), 52.1 (N-$\underline{C}H_2$-$\underline{C}H_2$-N), 54.6 ($\underline{C}H_2$-CH_2-O-CH_3), 58.8 ($\underline{C}H_3$-O), 71.1 ($\underline{C}H_2$-O-CH_3).

6.5.3 Preparation of (*S*)-THPC14

The synthesis of 1,4,8,11-tetrakis-((*S*)-(-)-2-hydroxypropyl)-1,4,8,11-tetraazacyclotetradecane (THPC14) was modified from that of its twelve membered analogue (THPC12) in the literature [20].

Cyclam (0.5 g, 2.5 mmol) and (*S*)-(-)-propylene oxide (1 g, 1.2 cm^3, 17-mmol, Aldrich) were dissolved in dry ethanol (25 cm^3) and stirred for 4 days. The ethanol was evaporated off leaving a clear oil. The oil was then dissolved in boiling hexane and upon cooling yielded the product (THPC14) as fine white crystals. The crystals were collected, washed with a small amount of cold hexane and air dried. Yield 0.4 g, 44%, ^{13}C ($CDCl_3$): δ 20.3 ($\underline{C}H_3$), 26.1 (CH_2-$\underline{C}H_2$-CH_2), 51.4 ($\underline{C}H_2$-CH_2-$\underline{C}H_2$), 53.5 (N-$\underline{C}H_2$-$\underline{C}H_2$-N), 62.8 ($\underline{C}H_2$-CH-OH), 64.6 ($\underline{C}$H-OH).

References

1 D. D. Perrin, W. L. F. Aramaego and D. R. Perrin, *Purification of Laboratory Chemicals,* 2nd edn., Pergamon, Oxford, 1980.

2 T. Nakamura, Y. Yumoto and K. Izutsu, *Bull. Chem. Soc. Jpn.,* 1982, **55**, 1850.

3 T. Rodopoulos, P.-A. Pittet and S. F. Lincoln, *J. Chem. Soc., Dalton Trans.*, 1993, 1055, 2079.

4 J. Lucas and S. F. Lincoln, *J. Chem. Soc., Dalton Trans.*, 1994, 423.

5 J. Lucas and S. F. Lincoln, *Inorg. Chim. Acta.*, 1994, **219**, 217.

6 P. J. Clarke, PhD Dissertation, University of Adelaide, 1992.

7 J.-M. Lehn and J.-P. Sauvage, *J. Am. Chem. Soc.,* 1975, **97**, 6700.

8 I. Vogel, *"A Text Book of Quantitative Inorganic Analysis Including Elementary Instrumental Analysis"*, 3rd edn., Longmans, 1961.

9 A. E. Martel and P. J. Motekaitus, *"The Determination and Use of Stability Constants"*, VCH Publishers, 1988.

10 A. Sabatini, A. Vacca and P. Gans, *Talanta*, Pergamon Press, 1974, **21**, 53.

11 S. Kulstad and L. A. Malmsten, *J. Inorg. Nucl. Lett.,* 1980, **42**, 573.

12 P. Gans, *J. Chem. Soc., Dalton Trans.,* 1985, 1195.

13 D. S. Raiford, C. L. Fisk and E. D. Becker, *J. Anal. Chem.*, 1979, **51**, 2050.

14 S. F. Lincoln, *"Prog. React. Kinetics"*, 1977, **9**, 1.

15 E. Breitmaier, G. Haas and W. Voelter, *"Atlas of Carbon-13 NMR Data"*, Heyden (London), 1979, **1**.

16 R. S. Tipson, *J. Org. Chem.*, 1974, **9**, 235.

17 S. Kulstad and L. A. Malmsten, *J. Acta Chem. Scand.*, 1979, 469.

18 E. K. Barefield, F. Wagner, A. W. Herlinger and A. R. Dahl, *J. Inorg. Chem.*, 1972, **11**, 2273.

19 A. K. W. Stephens and S. F. Lincoln, *J. Chem. Soc., Dalton Trans.*, 1993, 2123.

20 R. Dhillon, K. Wainwright and S. F. Lincoln, unpublished material.

7. Experimental Methods for Potentiometric Titrations

7.1 Analysis of Potentiometric Titration Data in Aqueous Solution

The protonation constants, pK_{a1} and pK_{a2} for the lariat ethers BME-C21 and BME-C22 and those of the tetraaza macrocyclic ligand TMEC14, pK_{a1}, pK_{a2}, pK_{a3} and pK_{a4}, were calculated by taking the mean values of triplicated titrations of 10 cm^3 of a solution approximately 0.001 M in ligand, and either 0.004 M or 0.005 M in $HClO_4$ in the case of lariat ethers or the tetraaza macrocycle, respectively, with approximately 0.1 M NEt_4OH. The exact concentrations and calibration parameters used for the titrations are listed below in Table 7.1.

Table 7.1 A list of calibration parameters for all ligands used for aqueous titrations.

Ligand	[Ligand] (M)	[$HClO_4$] (M)	[NEt_4OH] (M)	pK_W	E_0 (mV)
BME-C21	0.000987	0.00396	0.101	13.74	394.9
BME-C22	0.00102	0.00403	0.101	13.80	401.3
TMEC14	0.000954	0.00530	0.105	13.77	429.6

The stability constants, K_S, of $[M(BME\text{-}C21)]^{2+}$, $[M(BME\text{-}C21)]^{2+}$ and $[M(TMEC14)]^{2+}$ where $M^{2+} = Mg^{2+}$, Ca^{2+}, Sr^{2+}, Ba^{2+}, Mn^{2+}, Co^{2+}, Ni^{2+}, Cu^{2+}, Zn^{2+}, Cd^{2+}, Pb^{2+} and Hg^{2+} are given in Tables 3.2 and 3.4 (Chapter 3), respectively.

Typical pK_a and metal-ligand titrations for the diaza lariat ethers are shown in Figures 7.1 and 7.2, respectively.

Typical pK_a and metal-ligand titrations for the tetraaza macrocycle, TMEC14, including MLH and MLOH species (Chapter 3, Section 3.2.2.6), are shown in Figures 7.3 and 7.4, respectively.

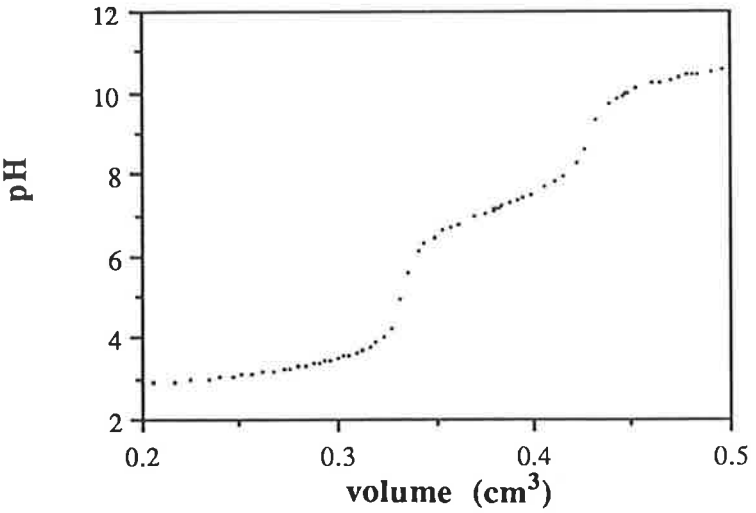

Figure 7.1 A typical titration curve used for the calculation of the protonation constants of the lariat ether BME-C21. Results calculated using the program Miniquad [1-3] for this titration were: log (K_1 / $dm^3\ mol^{-1}$) = 8.64 ± 0.01, log (K_2 / $dm^3\ mol^{-1}$) = 7.16 ± 0.01 (15.80 ± 0.01).

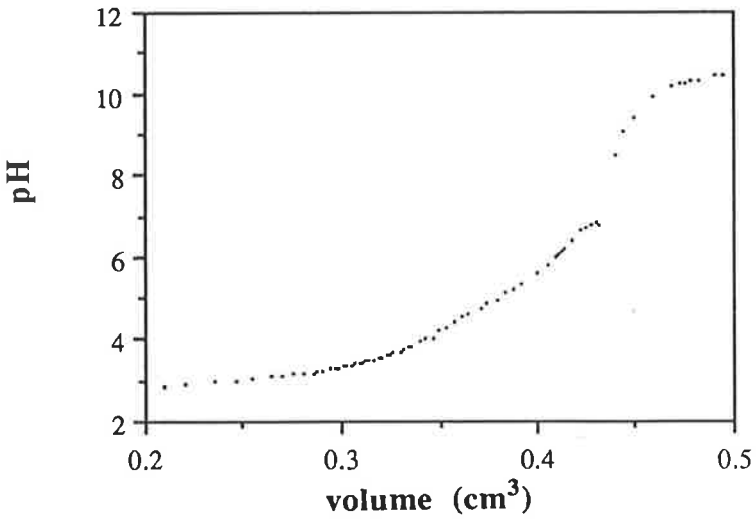

Figure 7.2 A typical titration curve used for the calculation of the stability constant of the complex $[Cu(BME\text{-}C21)]^{2+}$ Results calculated using the program Miniquad [1-3] for this titration were: log (K_{SCu} / $dm^3\ mol^{-1}$) = 5.35 ± 0.02. Precipitation of $Cu(OH)_2$ occurs at about 4.3 cm^3, and the following points are included only as a comparison with Figure 7.1 above.

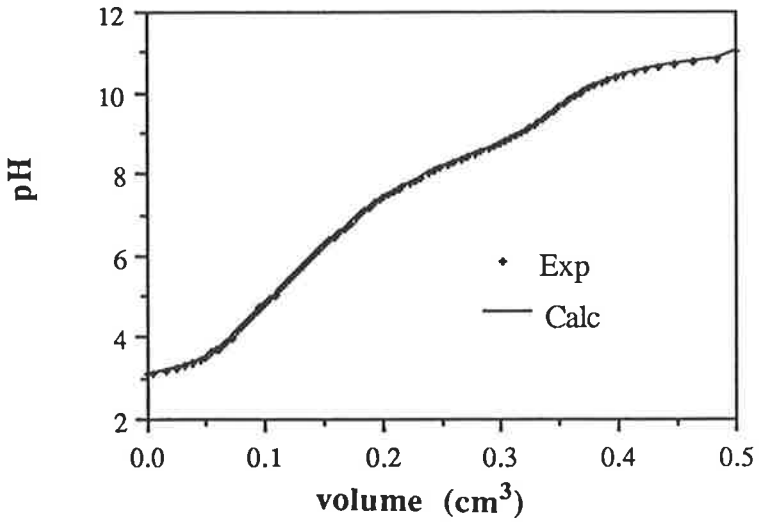

Figure 7.3 A typical titration curve used for the calculation of the protonation constants of the tetraaza macrocyclic ligand TMEC14. Results calculated using the program Superquad [4] for this titration were: log (K_1 / $dm^3\ mol^{-1}$) = 8.88 ± 0.03, log (K_2 / $dm^3\ mol^{-1}$) = 7.89 ± 0.01 (16.79 ± 0.02), log (K_3 / $dm^3\ mol^{-1}$) = 5.68 ± 0.01 (22.47 ± 0.02), and log (K_4 / $dm^3\ mol^{-1}$) = 2.47 ± 0.11 (24.94 ± 0.13).

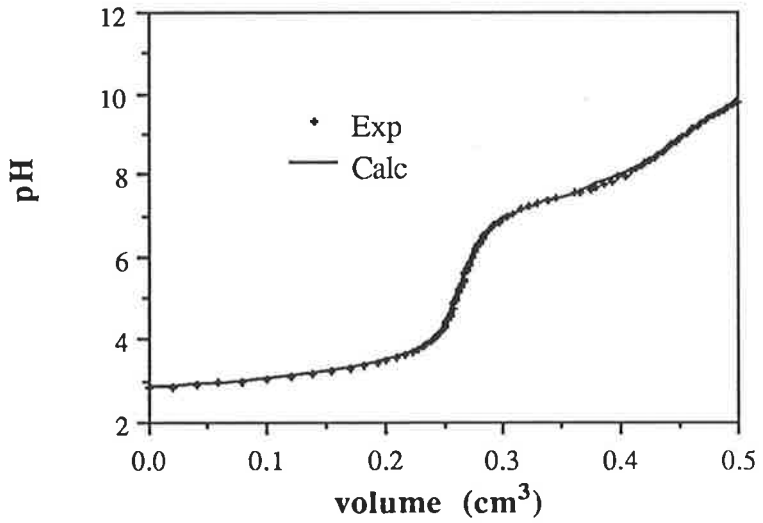

Figure 7.4 A typical titration curve used for the calculation of the stability constant of the complex $[Pb(TMEC14)]^{2+}$, with both $[Pb(HTMEC14)]^{3+}$ and $[Pb(OH)(TMEC14)]^{+}$ species present during the titration (Chapter 3, Section 3.2.2.6). Results calculated using the program Superquad [4] for this titration were: log (K_{SPb} / $dm^3\ mol^{-1}$) = 5.79 ± 0.02, log (K_{SHPb} / $dm^3\ mol^{-1}$) = 7.40 ± 0.01 (13.19 ± 0.01), log (K_{SOHPb} / $dm^3\ mol^{-1}$) = 7.07 ± 0.01 (-1.28 ± 0.01).

All aqueous stability constants were calculated by taking the mean of at least three titrations, with the metal to ligand ratio being varied between titrations (typically 2:1, 1:1 and 1:2).

The pK_a values and stability constants for the lariat ethers, BME-C21 and BME-C22, and the tetraaza macrocycle TMEC14 were determined as in Section 6.2.2 of Chapter 6 [1-4].

For the lariat ethers, only metal-ligand complexes of 1:1 ratio were found in solution, and no other species such as protonated (MLH) or hydroxide (MLOH) species were found.

For TMEC14 however, a number of other species were found in solution. There was evidence of the formation of both a hydroxide species, $[M(OH)(TMEC14)]^+$ where $M^{2+} = Cu^{2+}$ and Pb^{2+}, and a protonated species, $[M(HTMEC14)]^{3+}$ where $M^{2+} = Co^{2+}$, Cu^{2+}, Cd^{2+} and Pb^{2+} (Chapter 3, Section 3.2.2.6). For $[Mn(TMEC14)]^{2+}$ no apparent stability constant could be determined due to precipitation above a pH of 7 and the formation of manganese dioxide, MnO_2.

7.2 Analysis of Potentiometric Titration Data in Non-Aqueous Solution

The stability constants, K_S, of $[M(BME\text{-}C21)]^+$, $[M(BME\text{-}C22)]^+$, $[M(TMEC14)]^+$ and $[M(THPC14)]^+$ where $M^+ = Li^+$, Na^+, K^+, Rb^+, Cs^+, and Ag^+ are given in Tables 2.2, 2.3, and 2.5 (Chapter 2), respectively, and were calculated using either direct or competitive titrations. A silver wire electrode was used for all titrations, except for those in which the stability of the sodium or lithium complex was higher than that of its silver analogue, in which case a sodium selective electrode was used. (A sodium selective electrode can also be used as a less sensitive lithium selective electrode).

Direct titrations were performed as in Section 6.1 of Chapter 6, with K_S, the stability constant defined as:

$$M^+ + L \underset{}{\overset{K_S}{\rightleftharpoons}} [ML]^+$$

where $K_S = \frac{[ML^+]}{[M^+][L]}$ **7.1**

and $M^+ = Ag^+, Li^+$ and Na^+

Competitive titrations involved titrating the metal complex in the presence of Ag^+ using a silver electrode as described in Section 6.1 of Chapter 6. The metal ion, M^+ competes with Ag^+ for the ligand, L, and the stability constant K_{SM} could then be calculated using the equation:

$$K_{SM} = \frac{K_{SAg}}{K_{SE}} = \frac{[ML^+]}{[L][M^+]} \qquad \textbf{7.2}$$

for $M^+ = Li^+, Na^+, K^+, Rb^+$ and Cs^+

where K_{SE}, the equilibrium constant for the competitive metal complex is defined as:

$$[ML]^+ + Ag^+ \underset{}{\overset{K_{SE}}{\rightleftharpoons}} [AgL]^+ + M^+$$

and $K_{SE} = \frac{[AgL^+][M^+]}{[ML^+][Ag^+]}$ **7.3**

All non-aqueous stability constants were calculated by taking the mean of at least two titrations for both direct and competitive titrations using two FORTRAN-77 programs, VISP [5] and STAB [5]. The program VISP [5], which determines the stability constant, K_S, for a calculated titration curve by finding a best fit to the experimental data was used initially to check all concentrations and calibration parameters were correct. The stability constant calculated from the output of VISP [5] was then checked using the program STAB [5] which uses the linear solution method as described in literature [6]. A mathematical description for the derivation of K_S using both linear, and best-fit calculated methods, follows.

Typical titration data and output curves using VISP and STAB for direct titrations are shown in Table 7.2, and Figures 7.5 and 7.6, respectively. Typical titration data and output curves using VISP and STAB for competitive titrations are shown in Table 7.3, and Figures 7.7 and 7.8, respectively.

Table 7.2 Experimental and calculated results for the direct stability constant determination of $[Ag(TMEC14)]^+$ in acetonitrile, with log (K_S / $dm^3\ mol^{-1}$) = 8.46 ± 0.05.

Titre (cm^3)	EMF (exp) (mV)	EMF (the) (mV)	[TMEC14] (x 10^5) (M)	$\frac{[Ag^+_t]-[Ag^+]}{[Ag^+]}$ (M)
0.1	-58.0	-58.8		
0.2	-59.3	-60.0		
0.3	-60.8	-61.3		
0.4	-62.5	-62.7		
0.5	-64.6	-64.1		
0.6	-66.6	-65.6		
0.7	-68.5	-67.2		
0.9	-71.5	-70.7		
1.0	-73.6	-72.5		
1.1	-75.8	-74.5		
1.2	-77.8	-76.7		
1.3	-80.8	-79.0		
1.4	-82.4	-81.5		
1.5	-84.5	-84.3		
1.6	-87.8	-87.4		
1.7	-91.1	-90.8		
1.8	-95.3	-94.7		
1.9	-99.1	-99.3		
2.0	-105.9	-104.8		
2.1	-112.0	-111.7		
2.2	-121.2	-121.0		
2.3	-136.8	-135.3		
2.4	-182.6	-168.5		
2.5	-242.4	-267.0	0.999	1063
2.6	-278.7	-286.6	2.475	6248
2.7	-299.4	-304.0	3.973	10517
2.8	-312.0	-312.4	5.459	15128
2.9	-318.9	-318.8	6.932	19623
3.0	-321.6	-323.9	8.393	21668
3.1	-325.6	-328.2	9.841	25149
3.2	-329.2	-331.8	11.277	28745
3.3	-332.6	-335.0	12.701	32606
3.4	-336.2	-337.9	14.112	37270
3.5	-338.4	-340.5	15.512	40377
3.6	-340.7	-342.8	16.899	43911
3.7	-342.2	-345.0	18.275	46314
3.8	-344.5	-347.0	19.639	50369
3.9	-346.6	-348.8	20.992	54363
4.0	-348.9	-350.5	22.334	59126
4.1	-350.5	-352.2	23.664	62604
4.2	-352.3	-353.7	24.984	66799
4.3	-353.4	-355.1	26.293	69389
4.4	-355.1	-356.5	27.591	73757
4.5	-356.0	-357.8	28.878	76034
4.6	-357.4	-359.0	30.155	79900
4.7	-358.7	-360.2	31.421	83642
4.8	-359.5	-361.3	32.678	85899
4.9	-361.6	-362.4	33.924	92725
5.0	-362.8	-363.4	35.160	96701

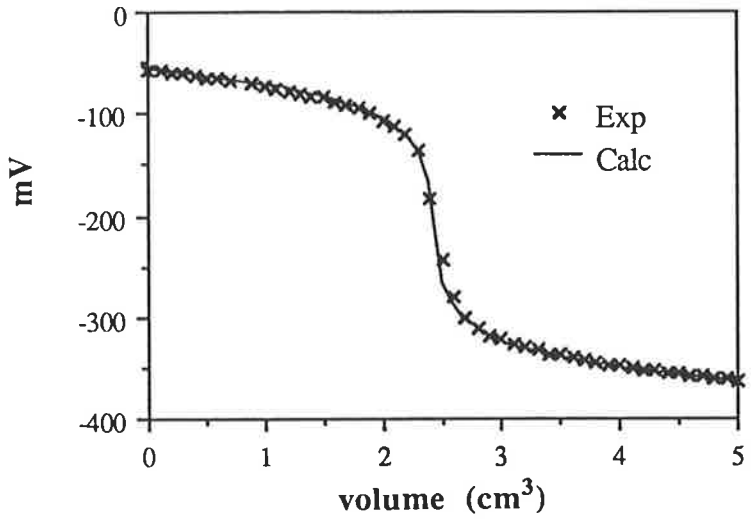

Figure 7.5 A plot of titration volume (cm^3) versus EMF (mV) for the experimental and calculated curves for the direct titration of TMEC14 with $AgClO_4$ in acetonitrile. Results calculated using the program VISP [5] for this titration were: log (K_{SAg} / $dm^3\ mol^{-1}$) = 8.45 ± 0.05.

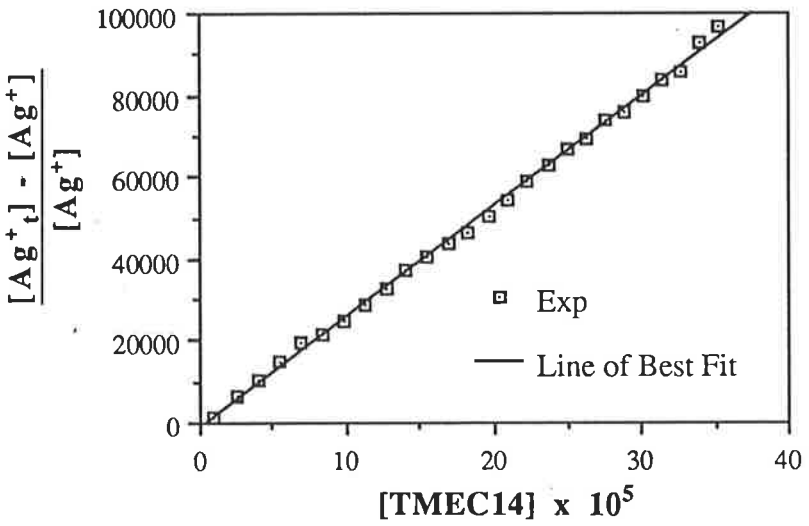

Figure 7.6 A plot of $\frac{[Ag^+_t] - [Ag^+]}{[Ag^+]}$ versus [TMEC14] for the experimental and theoretical line of best fit for the direct titration of TMEC14 with $AgClO_4$ in acetonitrile. Results calculated using the program STAB [5] for this titration were: log (K_{SAg} / $dm^3\ mol^{-1}$) = 8.46 ± 0.05.

Table 7.3 Experimental and calculated results for the competitive stability constant determination of $[Rb(THPC14)]^+$ versus Ag^+, with log (K_{SE} / dm^3 mol^{-1}) = 2.44 ± 0.05, which when subtracted from log (K_{SAg} / dm^3 mol^{-1}) = 5.43 ± 0.05 gave log (K_{SM} / dm^3 mol^{-1}) = 2.99 ± 0.05.

Titre	EMF (exp)	EMF (the)	$[Rb(THPC14)^+]$ (x 10^5)	$\left(\frac{[Ag^+t]-[Ag^+]}{[Ag^+]}\right)[Rb^+]$ (x 10^3)
(cm^3)	(mV)	(mV)	(M)	(M)
0.1	-117.9	-116.8		
0.3	-119.1	-119.2		
0.4	-120.7	-120.2		
0.5	-122.3	-121.4		
0.6	-123.4	-122.7		
0.7	-124.6	-124.0		
0.8	-125.8	-125.3		
0.9	-127.4	-126.7		
1.0	-128.8	-128.2		
1.1	-130.1	-129.7		
1.2	-131.7	-131.2		
1.3	-133.5	-133.1	0.002	0.25
1.4	-135.1	-134.6	0.016	0.30
1.51	-136.9	-136.6	0.078	0.37
1.6	-138.3	-138.3	0.103	0.43
1.71	-140.7	-140.5	0.155	0.53
1.81	-142.9	-142.6	0.179	0.63
1.9	-144.9	-144.6	0.216	0.74
2.0	-147.0	-146.9	0.290	0.87
2.1	-149.3	-149.3	0.360	1.03
2.2	-151.9	-151.8	0.418	1.22
2.3	-153.8	-154.4	0.560	1.39
2.41	-156.6	-157.3	0.668	1.65
2.5	-158.8	-159.8	0.779	1.89
2.6	-162.3	-162.6	0.845	2.30
2.7	-165.4	-165.4	0.961	2.72
2.82	-167.9	-168.6	1.187	3.13
2.91	-170.3	-171.0	1.337	3.56
3.01	-172.4	-173.5	1.537	3.99
3.1	-174.1	-175.7	1.730	4.37
3.2	-177.4	-178.0	1.893	5.14
3.3	-179.3	-180.1	2.116	5.68
3.4	-181.2	-182.1	2.341	6.26
3.5	-183.4	-184.0	2.559	6.98
3.6	-185.1	-185.7	2.793	7.62
3.71	-187.2	-187.5	3.046	8.45
3.8	-188.6	-188.9	3.261	9.08
3.9	-190.2	-190.3	3.499	9.83
4.0	-191.8	-191.6	3.737	10.64
4.1	-192.7	-192.8	3.989	11.19
4.2	-193.5	-194.0	4.242	11.71
4.3	-194.0	-195.0	4.499	12.11
4.4	-195.5	-196.0	4.734	13.02
4.5	-196.8	-197.0	4.973	13.88
4.6	-197.3	-197.9	5.224	14.33
4.7	-198.3	-198.8	5.465	15.08
4.8	-199.3	-199.6	5.705	15.87
4.9	-200.6	-200.4	5.938	16.89

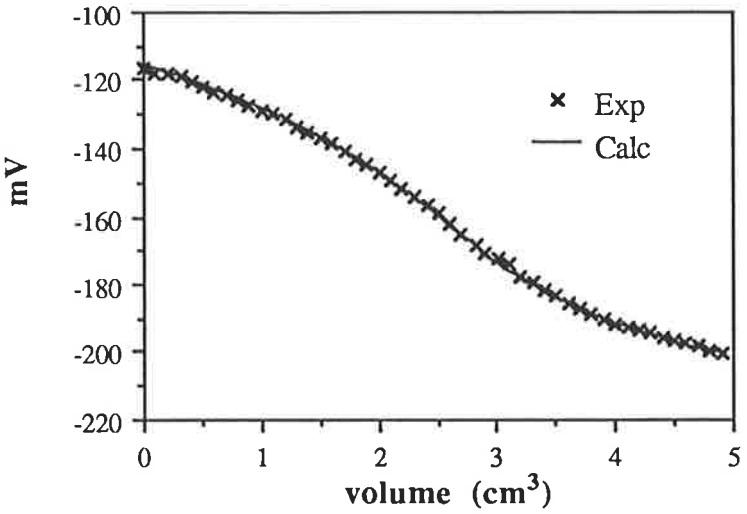

Figure 7.7 A plot of titration volume (cm^3) versus EMF (mV) for the experimental and calculated curves for the competitive titration of $[Ag(THPC14)]^+$ with $RbClO_4$ in acetonitrile. Results calculated using the program VISP [5] for this titration were: log (K_{SE} / $dm^3\ mol^{-1}$) = 2.43 ± 0.05, which when subtracted from log (K_{SAg} / $dm^3\ mol^{-1}$) = 5.43 ± 0.05 gave log (K_{SRb} / $dm^3\ mol^{-1}$) = 3.00 ± 0.05.

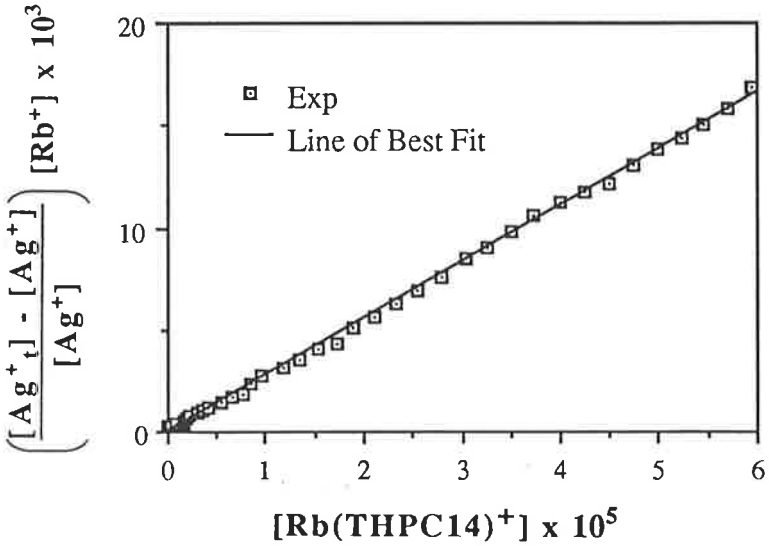

Figure 7.8 A plot of $\frac{([Ag^+_t] - [Ag^+])}{[Ag^+]}[Rb^+]$ versus $[Rb(THPC14)^+]$ for the experimental and theoretical line of best fit for the competitive titration of $[Ag(THPC14)]^+$ with $RbClO_4$ in acetonitrile. Results calculated using the program STAB [5] for this titration were: log (K_{SE} / $dm^3\ mol^{-1}$) = 2.44 ± 0.05, which when subtracted from log (K_{SAg} / $dm^3\ mol^{-1}$) = 5.43 ± 0.05 gave log (K_{SRb} / $dm^3\ mol^{-1}$) = 2.99 ± 0.05.

7.3 Mathematical Analysis of Titration Data using the Linear Solution (STAB) and Best Calculated Fit (VISP) Methods

7.3.1 Best Fit Calculated Method (VISP) for Direct Titrations

For direct titrations, VISP was used to calculate the best-fit titration curve for an experimental titration of potential (mV) versus volume (cm^3) with the calibration parameters, initial concentrations of free metal ion, M^+ (where $M^+ = Ag^+$, Li^+ and Na^+) and free ligand, L, and range and increments from which the best-fit curve was calculated included in the header file.

If $[M^+]_t$ and $[L^+]_t$ are used for the total or initial concentrations of metal ion and ligand, respectively, and $[M^+]$ is used to represent the solvated metal ion in solution, then K_S is given by:

$$K_S = \frac{[ML^+]}{[M^+][L]} \qquad 7.4$$

or $$K_S = \frac{[M^+]_t - [M^+]}{[M^+][L]} \qquad 7.5$$

but $$[L] = [L]_t - [Ag^+]_t + [Ag^+] \qquad 7.6$$

so substituting Equation 7.5 becomes:

$$K_S = \frac{[M^+]_t - [M^+]}{[M^+]([L]_t - [M^+]_t + [M^+])} \qquad 7.7$$

or expanding:

$$K_S = \frac{[M^+]_t - [M^+]}{[M^+][L]_t - [M^+][M^+]_t + [M^+]^2} \qquad 7.8$$

which upon rearranging becomes:

$$K_S[M^+]^2 + (K_S[L]_t - K_S[M^+]_t + 1)[M^+] - [M^+]_t = 0 \qquad 7.9$$

solving for $[M^+]$ gives:

$$[M^+] = \frac{K_S([M^+]_t-[L]_t)-1+\sqrt{K_S^2([L]_t-[M^+]_t)+2K_S([L]_t+[M^+]_t)+1}}{2K_S} \qquad 7.10$$

All terms in Equation 7.10 must be positive to have any real meaning.

Thus, using Equation 7.10 K_S is varied over a range with set increments until the sum of residuals is minimised, giving a best-fit value for K_S and also a theoretical plot which can be overlayed with the experimental one to determine goodness of fit (see Figure 7.5).

7.3.2 Best Fit Calculated Method (VISP) for Competitive Titrations

For competitive titrations, VISP was used to calculate the best-fit titration curve for an experimental titration of potential (mV) versus volume (cm^3) with the calibration parameters, initial concentrations of free silver, Ag^+, free ligand, L, and metal ion, M^+, and range and increments from which the best-fit curve was calculated included in the header file.

If $[Ag^+]_t$, $[L^+]_t$ and $[M^+]_t$ are used for the total or initial concentrations of silver, ligand and metal ion, respectively, and $[Ag^+]$ is used to represent the solvated silver in solution, then K_S is given by:

$$K_S = \frac{[AgL^+][M^+]}{[ML^+][Ag^+]} \qquad 7.11$$

or $$K_S = \frac{[Ag^+]_t - [Ag^+]}{[Ag^+]} \times \frac{[M^+]}{[ML^+]} \qquad 7.12$$

but $$[M^+] = [M^+]_t - [ML^+]_t + [Ag^+]_t - [Ag^+] \qquad 7.13$$

and $$[ML^+] = [ML^+]_t - [Ag^+]_t + [Ag^+] \qquad 7.14$$

so substituting Equations 7.13 and 7.14 into Equation 7.12 gives:

$$K_S = \frac{[Ag^+]_t - [Ag^+]}{[Ag^+]} \times \frac{[M^+]_t - [ML^+]_t + [Ag^+]_t - [Ag^+]}{[ML^+]_t - [Ag^+]_t + [Ag^+]} \qquad 7.15$$

or expanding:

$$K_S = \frac{[Ag^+]_t([M^+]_t-[ML^+]_t+[Ag^+]_t-2[Ag^+])+[Ag^+](-[M^+]_t+[ML^+]_t-[Ag^+])}{[Ag^+][ML^+]_t - [Ag^+][Ag^+]_t + [Ag^+]^2} \qquad 7.16$$

which upon rearranging becomes:

$$(K_S - 1)[Ag^+]^2 + (K_S[ML^+]_t - K_S[Ag^+]_t + 2[Ag^+]_t + [M^+]_t - [ML^+]_t)[Ag^+]$$

$$+ ([ML^+]_t - [M^+]_t - [Ag^+]_t)[Ag^+]_t = 0 \qquad 7.17$$

solving for $[Ag^+]$ gives:

$$[Ag^+] = \frac{(K_S - 2)[Ag^+]_t + (1 - K_S)[ML^+]_t - [M^+]_t + \sqrt{S}}{2(K_S - 1)} \qquad \textbf{7.18}$$

where $S = K_S^2([ML^+]_t - [Ag^+]_t) + K_S([M^+]_t(2[Ag^+]_t + [ML^+]_t)$

$$+ 2[ML^+]_t([Ag^+]_t - [ML^+]_t)) + ([ML^+]_t - [M^+]_t)^2 \qquad \textbf{7.19}$$

All terms in Equation 7.18 must be positive to have any real meaning.

Thus, using Equation 7.18 K_S is varied over a range with set increments until the sum of residuals is minimised, giving a best-fit value for K_{SE} and also a theoretical plot which can be overlayed with the experimental one to determine goodness of fit (see Figure 7.7). K_{SAg} and K_{SE} are then used to calculate K_{SM}, the stability constant of the competing metal ion from Equation 7.2.

7.3.3 Linear Solution Method (STAB) for Direct Titrations

For direct titrations, the value of K_S is given by:

$$M^+ + L \underset{}{\overset{K_S}{\rightleftharpoons}} [ML]^+$$

where $K_S = \frac{[ML^+]}{[M^+][L]}$ **7.20**

and $M^+ = Ag^+$, Na^+ and Li^+

substituting $[ML^+] = [M^+_t] - [M^+]$, Equation 7.20 becomes:

$$K_S = \frac{[M^+]_t - [M^+]}{[M^+][L]} \qquad \textbf{7.21}$$

or rearranging:

$$K_S[L] = \frac{[M^+]_t - [M^+]}{[M^+]} \qquad \textbf{7.22}$$

where [L], the free ligand concentration is given by:

$$[L] = [L]_t - [ML^+] \qquad \textbf{7.23}$$

or substituting $[ML^+] = [M^+]_t - [M^+]$, [L] becomes:

$$[L] = [L]_t - [M^+]_t + [M^+] \qquad \textbf{7.24}$$

From Equation 7.21 a plot of $\frac{[M^+]_t - [M^+]}{[M^+]}$ versus [L] yields a straight line of slope K_S.

Near the equivalence point, however [L] becomes very small, and thus the data points before equivalence are removed to minimise experimental error.

7.3.4 Linear Solution Method (STAB) for Competitive Titrations

For competitive titrations the value of K_S is given by:

$$[ML]^+ + Ag^+ \underset{}{\overset{K_S}{\rightleftharpoons}} [AgL]^+ + M^+$$

where $K_S = \frac{[AgL^+][M^+]}{[ML^+][Ag^+]}$ **7.25**

substituting $[AgL^+] = [Ag^+]_t - [Ag^+]$, Equation 7.25 becomes:

$$K_S = \frac{[Ag^+]_t - [Ag^+]}{[Ag^+]} \times \frac{[M^+]}{[ML^+]} \qquad \textbf{7.26}$$

or rearranging:

$$K_S[ML^+] = \frac{([Ag^+]_t - [Ag^+])[M^+]}{[Ag^+]} \qquad \textbf{7.27}$$

where $[ML^+] = [L]_t - [AgL^+] - [L]$ **7.28**

or substituting $[AgL^+] = [Ag^+]_t - [Ag^+]$, $[ML^+]$ becomes:

$$[ML^+] = [L]_t - [Ag^+]_t - [Ag^+] - [L] \qquad \textbf{7.29}$$

but $[M^+]_t > [L]_t$, so that for a stability constant of greater than 10^2, [L] becomes negligible and hence Equation 7.28 becomes:

$$[ML^+] = [L]_t - [Ag^+]_t - [Ag^+] \qquad \textbf{7.30}$$

and $$[M^+] = [M^+]_t - [ML^+] \qquad \textbf{7.31}$$

becomes $[M^+] = [M^+]_t - [L]_t + [Ag^+]_t + [Ag^+]$ **7.32**

A linear regression with a plot of $\frac{([Ag^+]_t - [Ag^+])[M^+]}{[Ag^+]}$ versus $[ML^+]$ yields a straight line of slope K_{SE}, the equilibrium constant for the competing metal complex versus that of the silver complex (Equation 7.3). K_{SAg} and K_{SE} can then be used to calculate K_{SM}, the stability constant of the competing metal ion from Equation 7.2.

References

1. A. Sabatini, A. Vacca and P. Gans, *Talanta*, 1974, **21**, 53.
2. P. Gans, A. Sabatini and A. Vacca, *Inorg. Chim. Acta*, 1977, **25**, 41.
3. M. Micheloni, A. Sabatini and A. Vacca, *Inorg. Chim. Acta*, 1977, **25**, 41.
4. P. Gans, *J. Chem. Soc., Dalton Trans.*, 1985, 1195.
5. P. J. Clarke, PhD Dissertation, University of Adelaide, 1992.
6. F. J. C. Rossotti and H. Rossotti, *"The Determination of Stability Constants"*, McGraw-Hill (New York), 1961, **5**.

8. Analysis of Chemical Exchange Systems using NMR Spectroscopy

8.1 Lineshape Analysis for Systems Undergoing Two-Site Exchange

Nuclear magnetic resonance spectroscopy (NMR) is a well established technique for the determination of chemical exchange rates from solution studies. In Chapter 4 of this study the intermolecular exchange of Li^+ and Na^+ between the solvated and complexed states were studied using ^7Li and ^{23}Na NMR, respectively. In Chapter 5, ^{13}C NMR was used to study the intramolecular exchange between two isomers of the heavy metal complexes of some pendant arm tetraaza macrocycles. NMR has been widely used to monitor both intermolecular and intramolecular chemical site exchange processes occurring in solution and there are many literature articles on the subject [1-15]. A mathematical basis with some spectroscopic theory is now needed to explain how the lineshape analysis was carried out to measure the kinetic processes for chemically exchanging sites in solution.

In a typical NMR experiment, a magnetic field, H_0, is applied to a sample along the z-axis causing the individual magnetic moments to precess about the z-axis at a frequency of ω_0, defined as the Larmor frequency. There is a net macroscopic magnetisation, $\boldsymbol{M}$, having only a z-component, M_z, with x and y components, M_x and M_y both being zero. When the direction of the nuclear spins are aligned with $\boldsymbol{M}$ the lowest energy state occurs.

If a smaller magnetic field, H_1, is now applied, with a vector rotating into the xy-plane at frequency ω, the total magnetic field now becomes:

$$\boldsymbol{H} = (H_1\cos\omega t, -H_1\sin\omega t, H_0) \qquad \textbf{8.1}$$

and $$\boldsymbol{M} = (M_x, M_y, M_z) \qquad \textbf{8.2}$$

with $\boldsymbol{M}$ rotated into the xy-plane, and M_x and M_y non-zero.

If M_0 is defined as the initial or equilibrium value of M_z prior to the application of H_1 ($\boldsymbol{M} = (0, 0, M_0)$) then the relaxation process in which M_z returns to M_0 is a first-order process characterised by T_1, the spin-lattice or longitudinal relaxation time. The decay of the magnetisation in the xy-plane to its equilibrium value of zero also follows a first order process and is characterised by T_2, the spin-spin or transverse relaxation time.

Bloch was the first to describe the time dependence of $\boldsymbol{M}$ for the stationary frame [16]:

$$\frac{dM_x}{dt} = \gamma(M_y H_0 + M_z H_1 \sin\omega t) - \frac{M_x}{T_2} \qquad \textbf{8.3}$$

$$\frac{dM_y}{dt} = \gamma(M_x H_0 + M_z H_1 \cos\omega t) - \frac{M_y}{T_2} \qquad \textbf{8.4}$$

$$\frac{dM_z}{dt} = \gamma(M_x H_1 \sin\omega t + M_y H_1 \cos\omega t) - \frac{(M_z - M_0)}{T_1} \qquad \textbf{8.5}$$

where γ is the gyromagnetic ratio.

Equations 8.4 and 8.5 may be simplified using a rotating frame of reference (x′, y′, z), which rotates at frequency ω about the x′-axis in the same direction as H_1 [12]:

$$\frac{dM_{xy}}{dt} = -\alpha M_{xy} - i\gamma H_1 M_0 \qquad \textbf{8.6}$$

$$\frac{dM_z}{dt} = \gamma v H_1 + \frac{M_0 - M_z}{T_1} \qquad \textbf{8.7}$$

where M_{xy} is the transverse magnetisation

$$\alpha = \frac{1}{T_2} - i(\omega_0 - \omega) \qquad \textbf{8.8}$$

and v is the component of $\boldsymbol{M}$ along y′, with direction perpendicular to that of H_0.

Thus, for field H_1, and frequency ω, the variation of M_z with time is dependent on v, the absorption mode lineshape, leading to the observed NMR absorption signal.

In general, the lineshape, v, (derived from the total lineshape for all frequencies, ω) gained from a pulsed Fourier transform experiment is equivalent to that gained from a continuous wave experiment and proof of this is given in Appendix ii [17-22]. Thus, the continuous wave method can now be pursued as it is more easily visualised.

Under continuous wave, adiabatic slow passage conditions, ω is varied through ω_0 such that $\boldsymbol{M}$ is constant with time. With $\frac{dM_{xy}}{dt}$ and $\frac{dM_z}{dt} = 0$, $H_1 << H_0$ such that $M_z \approx M_0$, and $M_{xy} \approx 0$, the absorption mode lineshape can be described as:

$$v = -M_0 \frac{\gamma H_1 T_2}{1 + T_2^2(\omega_0 - \omega)^2 + \gamma^2 H_1^2 T_1 T_2} \qquad \textbf{8.9}$$

where $M_0 = M_z$ at equilibrium.

When H_1 is small $\gamma^2 H_1^2 T_1 T_2$ becomes negligible and hence:

$$v = -M_0 \frac{\gamma H_1 T_2}{1 + T_2^2(\omega_0 - \omega)^2} \qquad \textbf{8.10}$$

This approximates a Lorentzian function with the half-height width at maximum intensity, $w_{\frac{1}{2}}$, described in terms of T_2:

$$w_{\frac{1}{2}} = \frac{1}{\pi T_2} \text{ (in Hertz)} \qquad \textbf{8.11}$$

The effects of site-exchange on the derivation of the absorption mode lineshape, v, and their incorporation into the Bloch equations [23-24] must now be considered.

The time required for a nuclear spin to transfer from site **a** to site **b** is assumed to be sufficiently small such that no nuclear precession occurs during the transfer. This results in a decrease in the transverse magnetisation of site **a** and a consequent increase in the magnetisation of site **b** at the same rate. Similarly transfer of nuclei from site **b** to site **a** will increase the complex magnetisation in site **a** and decrease that of site **b** at the same rate. These changes are characterised as:

$$\frac{dM_{xya}}{dt} = \frac{M_{xyb}}{\tau_b} - \frac{M_{xya}}{\tau_a} \qquad \textbf{8.12}$$

$$\frac{dM_{xyb}}{dt} = \frac{M_{xya}}{\tau_a} - \frac{M_{xyb}}{\tau_b} \qquad \textbf{8.13}$$

where τ_a and τ_b are the mean lifetimes of sites **a** and **b**, respectively, and are related by:

$$\frac{\chi_a}{\tau_a} = \frac{\chi_b}{\tau_b} \qquad \textbf{8.14}$$

where χ_a and χ_b are the populations of **a** and **b**, respectively.

Incorporation of their effects into the Bloch equations yields:

$$\frac{dM_{xya}}{dt} = -\alpha_a M_{xya} - i\gamma H_1 M_{0a} + \frac{M_{xyb}}{\tau_b} - \frac{M_{xya}}{\tau_a} \qquad \textbf{8.15}$$

$$\frac{dM_{xyb}}{dt} = -\alpha_b M_{xyb} - i\gamma H_1 M_{0b} + \frac{M_{xya}}{\tau_a} - \frac{M_{xyb}}{\tau_b} \qquad \textbf{8.16}$$

where $\alpha_a = \frac{1}{T_{2a}} - i(\omega_{0a} - \omega)$ **8.17**

and $\alpha_b = \frac{1}{T_{2b}} - i(\omega_{0b} - \omega)$ **8.18**

Equations 8.15 and 8.16 require that the average time for a transfer from site **a** to site **b** is much smaller than T_2.

For continuous wave, adiabatic slow passage conditions, M_z is essentially equal to M_0 such that:

$$M_{za} = M_{0a} = \chi_a M_0 \qquad \textbf{8.19}$$

and $M_{zb} = M_{0b} = \chi_b M_0$ **8.20**

with $\frac{dM_{xya}}{dt} = \frac{dM_{xyb}}{dt} = 0$ **8.21**

If chemical exchange is now incorporated into the total transverse magnetisation, $M_{xy} = M_{xya} + M_{xyb}$, and is described in terms of τ_a and τ_b then [12,13,25]:

$$M_{xy} = -i\gamma H_1 M_0 \frac{\tau_a + \tau_b + \tau_a\tau_b(\alpha_a\chi_b + \alpha_b\chi_a)}{(1 + \alpha_a\tau_a)(1 + \alpha_b\tau_b) - 1} \qquad \textbf{8.22}$$

The absorption intensity, v, at frequency ω (rads^{-1}) is proportional to the imaginary part of the complex magnetisation, M_{xy} and hence [1,12]:

$$\mathrm{Im}(M_{xy}) = v = -\gamma H_1 M_0 \frac{P\left[1 + \tau\left(\frac{\chi_b}{T_{2a}} + \frac{\chi_a}{T_{2b}}\right)\right] + QR}{P^2 + R^2} \qquad 8.23$$

where $\tau = \chi_b\tau_a = \chi_a\tau_b$ 8.24

$$\Delta\omega = \tfrac{1}{2}\left|\omega_{0a} + \omega_{0b}\right| - \omega \qquad 8.25$$

$$\delta\omega = \omega_{0a} - \omega_{0b} \qquad 8.26$$

$$P = \tau\left[\frac{1}{T_{2a}T_{2b}} - \Delta\omega^2 + \frac{\delta\omega^2}{4}\right] + \frac{\chi_b}{T_{2b}} + \frac{\chi_a}{T_{2a}} \qquad 8.27$$

$$Q = \tau\left[\Delta\omega - \frac{\delta\omega}{2}(\chi_a - \chi_b)\right] \qquad 8.28$$

$$R = \Delta\omega\left[1+\tau\left(\frac{1}{T_{2a}} + \frac{1}{T_{2b}}\right)\right] + \frac{\delta\omega}{2}\tau\left(\frac{1}{T_{2b}} - \frac{1}{T_{2a}}\right) + \frac{\delta\omega}{2}(\chi_a-\chi_b) \qquad 8.29$$

The complete lineshape can then be derived over a range of frequencies using Equation 8.23.

8.1.1 Kinetic Analysis for Systems in Slow Exchange

A system is in slow exchange when the inverse lifetimes for sites **a** and **b**, $\frac{1}{\tau_a}$ and $\frac{1}{\tau_b}$ are small compared to $\frac{1}{2\pi}\left|\omega_{0a} - \omega_{0b}\right|$ and hence the system consists of two distinct frequencies at ω_a and ω_b. For the continuous wave adiabatic slow passage experiment [26], if the observing frequency ω is close to ω_a, then M_{xyb} is effectively zero and Equation 8.22 becomes:

$$M_{xy} \approx M_{xya} \approx -i\gamma H_1 M_0 \frac{\chi_a\tau_a}{1 + \chi_a\tau_a} \qquad 8.30$$

and extracting the imaginary part gives:

$$\mathrm{Im}(M_{xy}) = v = -\gamma H_1 M_0 \frac{\chi_a T_{2a}'}{1 + (T_{2a}')^2(\omega_{0a} - \omega)^2} \qquad 8.31$$

where T_{2a}' is the apparent or observed transverse relaxation time of site **a** and:

$$\frac{1}{T_{2a}'} = \frac{1}{T_{2a}} + \frac{1}{\tau_a} \qquad \textbf{8.32}$$

Equation 8.30 describes a single exchange broadened resonance, centred at frequency ω_a with half-height width:

$$w_{\frac{1}{2}a}' = \frac{1}{\pi T_{2a}'} \qquad \textbf{8.33}$$

and similarly for site **b**:

$$\frac{1}{T_{2b}'} = \frac{1}{T_{2b}} + \frac{1}{\tau_b} \qquad \textbf{8.34}$$

and $$w_{\frac{1}{2}b}' = \frac{1}{\pi T_{2b}'} \qquad \textbf{8.35}$$

Expressing in a more convenient form:

$$\pi\,(w_{\frac{1}{2}a}' - w_{\frac{1}{2}a}) = \frac{1}{T_{2a}'} - \frac{1}{T_{2a}} = \frac{1}{\tau_a} \qquad \textbf{8.36}$$

and similarly for site B:

$$\pi\,(w_{\frac{1}{2}b}' - w_{\frac{1}{2}b}) = \frac{1}{T_{2b}'} - \frac{1}{T_{2b}} = \frac{1}{\tau_b} \qquad \textbf{8.37}$$

where $w_{\frac{1}{2}a}$ and $w_{\frac{1}{2}b}$ are the half-height line-widths of the **a** and **b** resonance lines, respectively, in the absence of exchange.

Thus τ_a and τ_b may be estimated from Equations 8.36 and 8.37 using the half-height widths, both in the absence of exchange, $w_{\frac{1}{2}a}$ and $w_{\frac{1}{2}b}$, and for the exchange broadened resonances, $w_{\frac{1}{2}a}'$ and $w_{\frac{1}{2}b}'$.

Also, the lifetime for site **b**, τ_b may be related to τ_a by the populations of both sites, χ_a and χ_b such that:

$$\tau_b = \frac{\tau_a \chi_b}{\chi_a} \qquad \textbf{8.38}$$

This simple relationship described above is valid when there is no appreciable overlap between the signals, however a number of affects such as solvent viscosity may induce broadening, and hence this method should only be used as an approximate indication of the exchange rates, or for estimating a minimum lifetime, τ_c ($\equiv \tau_a$) [1].

8.1.2 Kinetic Analysis for Systems at Intermediate Rates of Exchange

A system is at intermediate rates of exchange when the inverse lifetimes $\frac{1}{\tau_a}$ and $\frac{1}{\tau_b}$ are similar to $\frac{1}{2\pi}\left|\omega_{0a} - \omega_{0b}\right|$, with the spectrum observed as broad overlapping peaks. These broadened peaks coalesce at faster exchange rates to form a broad singlet.

Under the simplifying conditions, $\chi_a = \chi_b = \frac{1}{2}$, $\tau_a = \tau_b$, and $w_{\frac{1}{2}a}$ and $w_{\frac{1}{2}b}$ small compared to $(\omega_{0a} - \omega_{0b})$ then:

$$\frac{1}{T_{2a}} = \frac{1}{T_{2b}} = 0 \qquad \textbf{8.39}$$

and $$M_{za} = M_{zb} = \tfrac{1}{2}M_z \qquad \textbf{8.40}$$

Applying this to Equation 8.22 and taking the imaginary part gives:

$$v = \tfrac{1}{2}\gamma H_1 M_z \frac{\tau_a(\omega_{0a} - \omega_{0b})^2}{(\omega_{0a} + \omega_{0b} - 2\omega)^2 + \tau_a{}^2(\omega_{0a} - \omega)^2(\omega_{0b} - \omega)^2} \qquad \textbf{8.41}$$

for the absorption mode, or expressing in terms of frequencies, ν

(in Hz $= \frac{\omega}{2\pi}$) then:

$$f(\nu) = \tfrac{1}{2}\gamma H_1 M_z \frac{2\tau_a(\nu_a - \nu_b)^2}{[\nu - \frac{1}{2}(\nu_a + \nu_b)]^2 + \pi^2\tau_a{}^2(\nu_a - \nu)^2(\nu_b - \nu)^2} \qquad \textbf{8.42}$$

Equation 8.42 may be arranged into a dimensionless form as done by Harris in the literature [25] giving:

$$f(x) = \frac{2\tau_a}{[x^2 + \psi^2(x^2 - 1)^2]} \qquad \textbf{8.43}$$

where $x = \frac{\Delta\nu}{\psi}$ **8.44**

$$\psi = \pi\tau_a\nabla \quad \textbf{8.45}$$

$$\Delta\nu = \nu - \tfrac{1}{2}(\nu_a + \nu_b) \quad \textbf{8.46}$$

$$\nabla = \tfrac{1}{2}(\nu_a - \nu_b) \quad \textbf{8.47}$$

In this new form the NMR spectrum is described solely by the product ψ. Thus, under slow exchange conditions $\psi >> 1$, giving rise to two separate Lorentzian lines, at frequencies ν_a and ν_b. When the system is at intermediate rates of exchange, the two peaks coalesce when $\psi = \frac{1}{\sqrt{2}}$, giving a single broad Lorentzian peak at frequency $\frac{1}{2}(\nu_a + \nu_b)$. When the system approaches fast exchange the broad resonance narrows until the fast exchange limit is reached for $\psi << 1$, giving rise to a sharp Lorentzian peak at frequency $\frac{1}{2}(\nu_a + \nu_b)$.

Thus, for systems undergoing two-site chemical exchange, τ, the site lifetimes may be estimated when the two resonances characterising **a** and are seen to coalesce into a single broad resonance when $\psi = \frac{1}{\sqrt{2}}$

and hence $\tau = \tau_a = \tau_b = \frac{\sqrt{2}}{\pi(\nu_a - \nu_b)}$ **8.48**

Therefore, if ν_a and ν_b can be calculated in the absence of exchange then an accurate value for τ_c ($\equiv \tau_a$) can be found through complete lineshaping of the system using the full Equation 8.23 by comparison of observed and computed spectral lineshapes.

8.1.3 Kinetic Analysis for Systems in Fast Exchange

For a system in fast exchange the inverse lifetimes, $\frac{1}{\tau_a}$ and $\frac{1}{\tau_b}$ are much larger than $\frac{1}{2\pi}\left|\omega_{0a} - \omega_{0b}\right|$ and that system consists of only a single resonance. This single Lorentzian resonance is centred at a frequency at the population average of ω_a and ω_b or:

$$\omega_{av} = \chi_a\omega_{0a} + \chi_b\omega_{0b} \quad \textbf{8.49}$$

with the half-height width being similarly weighted and averaged yielding:

$$w_{\frac{1}{2}} = \frac{1}{\pi T_2} = \frac{\chi_a}{\pi T_{2a}} + \frac{\chi_b}{\pi T_{2b}} \qquad 8.50$$

If ω_{av} is now substituted into Equation 8.22 and exchange broadening introduced, then the imaginary part is defined as:

$$\mathrm{Im}(M_{xy}) = v = -\gamma H_1 M_0 \frac{T_2'}{1 + (T_2')^2(\chi_a\omega_{0a} + \chi_b\omega_{0b} - \omega)^2} \qquad 8.51$$

Substituting ω_{av} into Equation 8.36 leads to T_2' being defined as [26]:

$$\frac{1}{T_2'} = \frac{\chi_a}{T_{2a}} + \frac{\chi_b}{T_{2b}} + \chi_a^2\chi_b^2(\omega_{0a} - \omega_{0b})^2(\tau_a + \tau_b) \qquad 8.52$$

If the population weighted average ω_{av} is now considered, with similar weighting given to T_2 and τ, then Equation 8.53 applies:

$$\frac{1}{T_2'} = \frac{1}{T_{2av}} + \frac{1}{\tau_{av}} \qquad 8.53$$

$$T_{2av} = T_{2a}\chi_a + T_{2b}\chi_a \qquad 8.54$$

$$\tau_{av} = \tau_a\chi_a + \tau_b\chi_b \qquad 8.55$$

with the observed half-height width, $w_{\frac{1}{2}}'$, given by:

$$\pi w_{\frac{1}{2}}' = \pi\chi_a w_{\frac{1}{2}a} + \pi\chi_b w_{\frac{1}{2}b} + 4\pi^2\chi_a^2\chi_b^2\Delta\nu^2(\tau_a + \tau_b) \qquad 8.56$$

where:

$$\Delta\nu = \nu_a - \nu_b = 2\pi(\omega_{0a} - \omega_{0b}) \qquad 8.57$$

and $\nu_a = 2\pi\omega_{0a}$, $\nu_b = 2\pi\omega_{0b}$ (in Hertz) 8.58

Thus if the shift difference $(\nu_a - \nu_b)$, $w_{\frac{1}{2}a}$, $w_{\frac{1}{2}b}$, χ_a and χ_b are known in the absence of exchange then an upper limit for the lifetime, τ_c ($\equiv \tau_a$) may be calculated from Equation 8.56.

8.2 Calculation of Kinetic Parameters and Data

For the uncoupled two-site lineshape analysis of the ^{23}Na systems of BME-C21 in acetonitrile, propylene carbonate and pyridine, BME-C22 in acetonitrile, dimethylformamide, methanol and pyridine and TMEC14 in acetonitrile, the ^{7}Li systems of BME-C21 in dimethylformamide, methanol

and propylene carbonate and the ^{13}C systems of TMEC14 with Cd^{2+} and Hg^{2+} in d_4-^{12}C-methanol, all spectra were accumulated on a Bruker CXP-300 NMR spectrometer. The spectra were then transferred by serial mode to a Macintosh SE computer using the program KERMIT [27], converted from binary to floating decimal point files using NMR-SPEC [28] and finally transferred to a VAX 11-780 mainframe computer. The program LINSHP [12,29,30] was then used to perform a full lineshape analysis of the data files obtained as explained below.

The program LINSHP used a header file which included the frequencies of each resonance in the absence of exchange, ν_a and ν_b, the half-height widths of each resonance in the absence of exchange, $w^1_{\frac{1}{2}a}$ and $w^1_{\frac{1}{2}b}$, and χ_a and χ_b, the populations of sites **a** and **b**, respectively.

For the ^{23}Na and ^{7}Li NMR systems the parameters in the absence of exchange were taken from spectra of purely solvated Na^+ and Li^+ and fully complexed $[NaL]^+$ and $[LiL]^+$ solutions, respectively. For the ^{13}C NMR systems the parameters in the absence of exchange were obtained by extrapolating from the region of very slow exchange.

For all the NMR systems, spectra over a full range of temperatures were matched to the theoretically generated spectra at each temperature through a non-linear least squares analysis in which R (Equation 8.59) was varied until the difference between the calculated and experimental spectra was minimised.

$$R = \frac{1}{\tau_a \chi_b} = \frac{1}{\tau_b \chi_a} \qquad \textbf{8.59}$$

Examples of the theoretical versus experimental spectra over a full range of temperatures with τ_c ($\equiv \tau_a$) calculated for each temperature are shown in Figures 4.2, 4.4, 4.6 and 4.8 (Chapter 4).

Having obtained τ_c at each temperature the data was fitted to the Eyring Equation [31]:

$$k = \frac{1}{\tau_c} = \frac{k_B T}{h} \exp\left[\left(\frac{-\Delta H^{\ddagger}}{RT}\right) + \left(\frac{\Delta S^{\ddagger}}{R}\right)\right] \qquad \textbf{8.60}$$

where k_B = Boltzmann's constant, 1.381×10^{-23} J K^{-1}

h = Planck's constant, 6.603×10^{-34} J s

R = universal gas constant, 8.314 J K^{-1} mol^{-1}

$\Delta H^{\ddagger}$ = enthalpy of activation (kJ mol^{-1})

$\Delta S^{\ddagger}$ = entropy of activation (J K^{-1} mol^{-1})

T = temperature (K)

$\Delta H^{\ddagger}$, $\Delta S^{\ddagger}$ and k_d at coalescence and room temperature (298.2 K) were then calculated using the FORTRAN-77 program DATAFIT [32-34] on a VAX 11-780 computer which uses a non-linear, weighted least squares method. The errors quoted were the standard deviations calculated using the above program.

Using the linear form of the Eyring Equation [31]:

$$\ln(T\tau_c) = \left[\frac{\Delta S^{\ddagger}}{R} + \ln\left(\frac{h}{k_B}\right)\right] - \frac{\Delta H^{\ddagger}}{RT} \qquad \textbf{8.61}$$

A plot of $\ln(T\tau_c)$ versus $\frac{1}{T}$ yields a straight line of slope $\frac{\Delta H^{\ddagger}}{RT}$

and intercept $\left[\frac{\Delta S^{\ddagger}}{R} + \ln\left(\frac{h}{k_B}\right)\right]$. Examples of these $T\tau_c$ versus $\frac{1}{T}$ plots are shown in Figures 4.1, 4.3, 4.5 and 4.7 (Chapter 4).

References

1 I. O. Sutherland, *Ann. Reports NMR Spectros.*, 1971, **4**, 71.

2 J. I. Kaplan and G. Fraenkel, *"NMR of Chemically Exchanging Systems"*, Academic Press (New York), 1980.

3 S. Forsen and B. Lindman, *"Ion Binding in Biological Systems as Studied by NMR Spectroscopy"* - in *"Methods of Biochemical Analysis"*, Academic Press (New York), 1981, **27**, 289.

4 H. S. Gutowsky and C. H. Holm, *J. Chem. Phys.*, 1956, **25**, 1228.

5 T. S. Piper and G. Wilkinson, *J. Inorg. Nucl. Chem.*, 1956, **3**, 104.

6 A. Steigel, P. Diehl, E. Fluck and R. Kosfeld, *"NMR Basic Principles and Progress"*, (Eds.), 1978, **15**, 1.

7 J. Sandstrom, *"Dynamic NMR Spectroscopy"*, Academic Press, (London), 1982.

8 M. Oki, *"Applications of Dynamic NMR Spectroscopy to Organic Chemistry"*, VCH, 1985.

9 D. Gamliel, Z. Luz and S. Vega, *J. Chem. Phys.*, 1988, **88**, 25.

10 K. Orrell, V. Sik and D. Stephenson, *Prog. NMR Spec.*, 1990, **22**, 141.

11 C. L. Perrin and T. J. Dwyer, *Chem. Rev.*, 1990, **90**, 935.

12 S. F. Lincoln, *"Prog. React. Kinetics"*, 1977, **9**, 1.

13 H. S. Gutowsky, L. M. Jackman and F. A. Cotton, *"Time Dependant Magnetic Perturbations"* - in *"Dynamic Nuclear Magnetic Resonance Spectroscopy"*, (Eds.), Academic Press (New York), 1975, 1.

14 T. E. Bull, *J. Mag. Reson.*, 1972, **8**, 344.

15 A. Knuttel and R. S. Balaban, *J. Mag. Reson.*, 1991, **95**, 309.

16 F. Bloch, *Phys. Rev.*, 1946, **70**, 460.

17 R. K. Gupta, T. P. Pither and R. Wasyristen, *J. Mag. Reson.*, 1974, **13**, 383.

18 A. White, PhD Dissertation, University of Adelaide, 1987.

19 J. I. Kaplan, *J. Chem. Phys.*, 1972, **57**, 5615.

20 R. R. Ernst, *J. Chem. Phys.*, 1973, **59**, 989.

21 J. I. Kaplan, *J. Chem. Phys.*, 1973, **59**, 990.

22 T. C. Farrar and E. D. Becker, *"Pulse and Fourier Transform NMR"*, Academic Press, (New York), 1971.

23 E. L. Hahn and D. E. Maxwell, *Phys. Rev.*, 1952, **88**, 1070.

24 H. M. McConnell, *J. Chem. Phys.*, 1958, **28**, 430.

25 R. K. Harris, *"Nuclear Magnetic Resonance Spectroscopy"*, Pitman (London), 1983.

26 J. A. Pople, W. G. Schneider and H. J. Bernstein, *"High-Resolution Nuclear Magnetic Resonance"*, McGraw-Hill (New York), 1959.
27 W. Catchings, F. da Cruz, W. Shilit, M. Aebi and P. Placeway, Mackermit v. 0.98 (69), Colombia University, 1989. Info-kermit@cunixc.cc.colombia.edu.
28 J. R. Christie, NMR-Spec, v. 1.2, 1988.
29 E. H. Williams, PhD Dissertation, University of Adelaide, 1980.
30 P. J. Clarke, PhD Dissertation, University of Adelaide, 1992.
31 S. Gladstone, K. J. Laidler and Eyring, *"Theory of Rate Processes"*, McGraw-Hill (New York), 1941.
32 T. Kurucsev, *J. Chem. Educ.*, 1978, **55**, 128.
33 T. Kurucsev, Unpublished Material, University of Adelaide, 1990.
34 T. Pitha and R. N. Jones, *Can. J. Chem.*, 1966, **44**, 3031.

Appendix i:
The Gutmann Donor Number, D_N

The Gutmann donor number, D_N, where N refers to the nucleophilicity, is often used as a measure of solvent strength, and may be described as the ability of a solvent to donate electron density, and hence solvate a metal ion. In solution a ligand, L, competes with the solvent for a cation, M^+, in order to form a complex, $[ML]^+$. Hence, a measure of the ability of the solvent to compete for a metal ion becomes important for kinetic studies of this type. A measure of the electron donating power of each solvent which has been used with some success for the correlation of kinetic and equilibrium studies with varying solvent [1] is known as the Gutmann donor number, D_N [2,3]. D_N is defined as the enthalpy, $-\Delta H$ ($kJmol^{-1}$) for the formation of the 1:1 complex between antimony(V) chloride, $SbCl_5$ (as the electron acceptor) and a range of solvents, with 1,2-dichloroethane being used as the non-coordinating solvent.

$$SbCl_5 + Solvent \xrightarrow{ClCH_2CH_2Cl} [SbCl_5(Solvent)]$$

As D_N increases, the electron donating power of the solvent also increases, and thus the solvent competes more strongly for the metal ion in solution. Table i.1 shows a list of the Gutmann donor numbers, D_N, for the solvents used in this study.

The values of D_N for methanol and water of 23.5 and 33.0, respectively, have been suggested in literature [4,5] rather than 19.0 and 18.0, respectively, due to the intermolecular hydrogen bonding for the two solvents being disrupted when 1,2-dichloroethane is used as the non-coordinating solvent. In these studies NMR was used to measure the dependence of chemical shift on D_N.

Table i.1 A list of the Gutmann donor numbers, D_N, for a range of solvents used in this study.

Solvent	D_N[2,3]	D_N[4,5]
1,2-dichloroethane	0.0	
acetonitrile	14.1	
propylene carbonate	15.1	
methanol	19.0	23.5
N,N-dimethylformamide	26.6	
water	18.0	33.0
pyridine	33.1	

References

1. B. G. Cox, J. Garcia-Rosas and H. Schneider, *J. Am. Chem. Soc.*, 1981, **103**, 1054.
2. U. Mayer and V. Gutmann, *Top. Curr. Chem.*, 1972, **27**, 113.
3. V. Gutmann, *"Coordination Chemistry in Non-Aqueous Solvents"*, Springer, New York, 1968.
4. R. H. Erlich, E. Roach and A. I. Popov, *J. Am. Chem. Soc.*, 1970, **92**, 4989.
5. W. J. Dewitte and A. I. Popov, *J. Soln. Chem.*, 1976, **5**, 231.

Appendix ii:

Proof of the Equivalence of Pulsed Fourier Transform and Continuous Wave NMR

It may be shown that the free induction decay (FID) and the absorption mode lineshape, v, form a Fourier transform pair [1,2]. For Fourier transform NMR a short radio-frequency pulse (typically 10^{-4} - 10^{-6} seconds) of high energy, H_1, is directed along the x′-axis, for the rotating frame (x′, y′, z) which rotates around the z-axis at a frequency of ω. This pulse causes $\boldsymbol{M}$ to tilt towards the y′-axis generating a new transverse component for $\boldsymbol{M}$, M_{xy}. Immediately after the pulse, $\boldsymbol{M}$ begins to relax back to its initial or equilibrium position and align itself with the z-axis. This relaxation causes the M_{xy} component to undergo free induction decay (FID) and fall back to its initial zero intensity. Hence, solving the modified Bloch equations, 8.6 and 8.7, with $H_1 = 0$ then gives us the equation for the FID.

$$M_{xy} = C_1 e^{-\phi+t} + C_2 e^{-\phi-t} \qquad \textbf{ii.1}$$

where C_1 and C_2 are constants of integration and:

$$2\phi\pm = \left(\alpha_a + \frac{1}{\tau_a} + \alpha_b + \frac{1}{\tau_b}\right) \pm \sqrt{\left[\left(\alpha_a + \frac{1}{\tau_a} - \alpha_b - \frac{1}{\tau_b}\right)^2 + \frac{4}{\tau_a\tau_b}\right]} \qquad \textbf{ii.2}$$

with the Fourier transform of the FID given by:

$$FT = \int_0^\infty M_0 e^{-i(\omega-\omega_1)t}\, dt \qquad \textbf{ii.3}$$

$$= iM_0 \frac{[\tau_a + \tau_b + \tau_a\tau_b(\alpha_a\chi_b + \alpha_b\chi_a)]}{(1 + \alpha_a\tau_a)(1 + \alpha_b\tau_b) - 1} \qquad \textbf{ii.4}$$

where $\alpha_a = \frac{1}{T_{2a}} + i(\omega_{0a}-\omega)$ **ii.5**

and $\alpha_b = \frac{1}{T_{2b}} + i(\omega_{0b} - \omega)$ **ii.6**

with ω = the variable frequency

and ω_1 = the fixed pulse carrier frequency

The absorption mode lineshape, ν, is derived from the imaginary part of equation ii.4 and is identical to that obtained from the continuous wave NMR. Thus, the lineshape obtained for this simple case in which an uncoupled spin system undergoes chemical exchange is the same for the pulsed Fourier transform and the continuous wave experiments. This proof does not apply for more complex systems, however there are more complicated treatments described in the literature [3-6].

References

1. R. K. Gupta, T. P. Pither and R. Wasyristen, *J. Mag. Reson.*, 1974, **13**, 383.
2. A. White, PhD Dissertation, University of Adelaide, 1987.
3. J. I. Kaplan, *J. Chem. Phys.*, 1972, **57**, 5615.
4. R. R. Ernst, *J. Chem. Phys.*, 1973, **59**, 989.
5. J. I. Kaplan, *J. Chem. Phys.*, 1973, **59**, 990.
6. T. C. Farrar and E. D. Becker, *"Pulse and Fourier Transform NMR"*, Academic Press, New York, 1971.

Publications

"The Complexation of Bivalent Metal Ions by the Cryptand 4,7,13-tetraoxa-1,10-diazabicyclo[8.5.5]tricosane in Water and 95% Methanol / Water Solutions."

Paul A. Duckworth, Stephen F. Lincoln and Jeremy Lucas, *Inorg. Chim. Acta*, 1991, **188**, 55-59.

"The Complexation of Alkali Metal Ions by the Bibracchial Lariat Ether 1,7-bis(2-methoxyethyl)-4,10,13-trioxa-1,7-diazacyclo[2.1]pentadecane in Several Solvents. A Potentiometric Titration and Nuclear Magnetic Resonance Study."

Stephen F. Lincoln and Jeremy Lucas, *J. Chem. Soc., Dalton Trans.*, 1994, 423-427.

"Solution Studies of Monovalent Metal Complex Ions of the Bibracchial Lariat Ether 7,16-bis(2-methoxyethyl)-1,4,10,13-tetraoxa-7,16-diazacyclooctadecane."

Jeremy Lucas and Stephen F. Lincoln, *Inorg. Chim. Acta*, 1994, **219**, 217-220.